

NOTICE

When Government drawings, specifications, or other data are used for any purpose other than in connection with a definitely Government-related procurement, the United States Government incurs no responsibility or any obligation whatsoever. The fact that the Government may have formulated or in any way supplied the said drawings, specifications, or other data, is not to be regarded by implication, or otherwise as in any manner construed, as licensing the holder, or any other person or corporation; or as conveying any rights or permission to manufacture, use, or sell any patented invention that may in any way be related thereto.

This technical report has been reviewed and is approved for publication.

The Public Affairs Office has reviewed this report, and it is releasable to the National Technical Information Service (NTIS), where it will be available to the general public, including foreign nationals.

FOR THE COMMANDER



WALTER O. MAINE
Chief, Assessment and Instrumentation Division

Even though this report may contain special release rights held by the controlling office, please do not request copies from the Wright Laboratory, Armament Directorate. If you qualify as a recipient, release approval will be obtained from the originating activity by DTIC. Address your request for additional copies to:

Defense Technical Information Center
Cameron Station
Alexandria VA 22304-6145

If your address has changed, if you wish to be removed from our mailing list, or if your organization no longer employs the addressee, please notify WL/MNSA, 101 W. Eglin Blvd., Ste 326, Eglin AFB FL 32542-6810, to help us maintain a current mailing list.

Do not return copies of this report unless contractual obligations or notice on a specific document requires that it be returned.

REPORT DOCUMENTATION PAGE

Form Approved
OMB No 0704-0188

Public reporting burden for this collection of information is estimated to average 1 hour per response, including the time for reviewing instructions, searching existing data sources, gathering and maintaining the data needed, and completing and reviewing the collection of information. Send comments regarding this burden estimate or any other aspect of this collection of information, including suggestions for reducing this burden, to: Washington Headquarters Services, Directorate for Information Operations and Reports, 1215 Jefferson Davis Highway, Suite 1204, Arlington, VA 22202-4302, and to the Office of Management and Budget, Paperwork Reduction Project (0704-0188), Washington, DC 20503.

1. AGENCY USE ONLY (Leave blank)		2. REPORT DATE August 1993	3. REPORT TYPE AND DATES COVERED Final September 1992 - March 1993	
4. TITLE AND SUBTITLE Toward a Characterization of the Debris Cloud Created in a Hypervelocity Impact on a Thin Plate			5. FUNDING NUMBERS C: F49620-90-C-0076 PE: N/A PR: TA: WU:	
6. AUTHOR(S) William P. Schonberg			8. PERFORMING ORGANIZATION REPORT NUMBER	
7. PERFORMING ORGANIZATION NAME(S) AND ADDRESS(ES) University of Alabama Department of Civil and Environmental Engineering Huntsville AL 35899			10. SPONSORING / MONITORING AGENCY REPORT NUMBER WL-TR-93-7028	
9. SPONSORING / MONITORING AGENCY NAME(S) AND ADDRESS(ES) Wright Laboratory, Armament Directorate Assessment and Instrumentation Division Technology Assessment Branch (WL/MNSA) 101 W. Eglin Blvd., Ste 326 Eglin AFB FL 32542-6810			11. SUPPLEMENTARY NOTES Availability of report is specified on verso of front cover.	
12a. DISTRIBUTION / AVAILABILITY STATEMENT Approved for public release; distribution is unlimited.			12b. DISTRIBUTION CODE A	
13. ABSTRACT (Maximum 200 words) Semi-analytical lethality assessment models fall into one of two general categories: discrete particle models and expanding shell models. Discrete particle models account for and track only a small number of solid fragments in a debris cloud generated by a hypervelocity impact. They are best suited for impact scenarios in which melting and/or vaporization of the projectile and target materials do not occur. Expanding shell models assume that all of the debris cloud material is homogeneously distributed over a uniformly expanding spherical shell in those impact scenarios where melting and/or vaporization of the projectile and target materials do occur. A lethality assessment model that considers the creation and subsequent effects of debris clouds containing all three states of matter is needed. This report describes the results of an investigation into the composition of the material in a debris cloud generated by a hypervelocity projectile impact. The work completed represents the first step in a long-term research program whose overall objective is to develop a general model of the response of a target structure to a hypervelocity impact over the 4-16 kilometers per second impact regime.				
14. SUBJECT TERMS Hypervelocity Impact, Mie-Gruneisen, Hugoniot, Tillotson, Equation of State, Shock Waves, Debris Cloud			15. NUMBER OF PAGES 112	
17. SECURITY CLASSIFICATION OF REPORT UNCLASSIFIED			16. PRICE CODE	
18. SECURITY CLASSIFICATION OF THIS PAGE UNCLASSIFIED		19. SECURITY CLASSIFICATION OF ABSTRACT UNCLASSIFIED		20. LIMITATION OF ABSTRACT SAR

PREFACE

This program was conducted by the University of Alabama, Department of Civil and Environmental Engineering, Huntsville AL 35899 under Contract No. F49620-90-C-0076 with WL/MN, Eglin AFB FL 32542-6810. Mr. David M. Jerome, WL/MNSA, managed the program for the Wright Laboratory. The program was conducted during the period from September 1992 to March 1993.

The author would like to acknowledge the support of the AFOSR Summer Faculty Research Program. In addition, thanks is extended to Mr. Scott Mullin of the Southwest Research Institute and to Ms. Kathy Holian of the Los Alamos National Laboratory for their assistance with the implementation of the Tillotson equation of state. The guidance and assistance of Mr. Jerome during the course of the research program is also appreciated.

Accession For	
NTIS CR&I	<input checked="" type="checkbox"/>
DTIC TAB	<input type="checkbox"/>
Unannounced	<input type="checkbox"/>
Justification	
By	
Distribution	
Availability Codes	
Dist	Avail and/or Special
A-1	

DTIC QUALITY INSPECTED 5

TABLE OF CONTENTS

Section	Page
1.0 INTRODUCTION	1
2.0 LETHALITY ASSESSMENT MODEL REQUIREMENTS	3
3.0 DEBRIS CLOUD CHARACTERIZATION	7
3.1 Introductory Comments	7
3.2 Shock Loading and Release Analysis	7
3.2.1 Introductory Comments	7
3.2.2 Mie-Gruneisen Equation-of-State	10
3.2.3 Tillotson Equation-of-State	11
3.2.4 Modified Tillotson Equation-of-State	16
3.2.5 Discussion	20
3.3 Computing the Percentages of the Solid, Liquid, and Gaseous Debris Cloud Material	23
3.4 Computing the Masses of the Solid, Liquid, and Gaseous Debris Cloud Material	25
3.5 Debris Cloud Velocities	29
4.0 RESULTS AND DISCUSSION	32

TABLE OF CONTENTS (Concluded)

Section	Page
4.1 Introductory Comments	32
4.2 Material Characterization	33
4.3 Debris Cloud Velocities	37
5.0 SUMMARY AND RECOMMENDATIONS	39
6.0 REFERENCES	43
APPENDIX A -- DEBCLD Source Code	74
APPENDIX B -- Sample Input Files	92
APPENDIX C -- Sample Output Files	97

LIST OF FIGURES

Figure	Page
1. Generic Hugoniot and Release Isentrope	51
2a. Tillotson Equation-of-State with Mixed Phase Formulation and $E < E_s$	52
2b. Tillotson Equation-of-State with Mixed Phase Formulation and $E_s < E < E_s'$	53
2c. Tillotson Equation-of-State with Mixed Phase Formulation and $E_s' < E$	54
3a. Modified Tillotson Equation-of-State with $E = (E_s)^+$	55
3b. Modified Tillotson Equation-of-State with and $E_s < E < E_s'$	56
3c. Modified Tillotson Equation-of-State with $E = E_s'$	57
4. Low Energy Impact Shock Loading and Release Curves (H ... Hugoniot, MG ... Mie-Gruneisen EOS Release Isen- trope, T ... Tillotson EOS Release Isentrope)	58
5. High Energy Impact Shock Loading and Release Curves (H ... Hugoniot, MG ... Mie-Gruneisen EOS Release Isen- trope, T ... Tillotson EOS Release Isentrope)	59

LIST OF FIGURES (Continued)

Figure	Page
6. Moderate Energy Impact Shock Loading and Release Curves (H ... Hugoniot, MG ... Mie-Gruneisen EOS Release Isentrope, T ... Tillotson EOS Release Isentrope, MT ... Modified Tillotson EOS Release Isentrope)	60
7. Close-up of Moderate Energy Impact Shock Loading and Release Curves (H ... Hugoniot, MG ... Mie-Gruneisen EOS Release Isentrope, T ... Tillotson EOS Release Isentrope, MT ... Modified Tillotson EOS Release Isentrope)	61
8. Final Specific Volume vs. Impact Velocity (MG ... Mie-Gruneisen EOS Values, T ... Tillotson EOS Values, MT ... Modified Tillotson EOS Values)	62
9. Wave Patterns in a Projectile and an Impacted Target [28] ...	63
10. Debris Cloud Velocities [30]	64
11. Debris Cloud Material Composition Using the Mie-Gruneisen EOS, Aluminum-on-Aluminum Impact	65
12. Debris Cloud Material Composition Using the Tillotson EOS, Aluminum-on-Aluminum Impact	66
13. Debris Cloud Material Composition Using the Modified Tillotson EOS, Aluminum-on-Aluminum Impact	67
14. Projectile Material Mass Distribution, Aluminum-on-Aluminum Impact	68

LIST OF FIGURES (Concluded)

Figure	Page
15. Target Material Mass Distribution, Aluminum-on-Aluminum Impact	69
16. Target Hole Diameter Prediction Comparison, Aluminum-on-Aluminum Impact, L/D=2.0, T/D=0.1	70
17. Target Hole Diameter Prediction Comparison, Aluminum-on-Aluminum Impact, L/D=2.0, T/D=0.5	71
18. Target Hole Diameter Prediction Comparison, Aluminum-on-Aluminum Impact, L/D=0.1, T/D=0.1	72
19. Target Hole Diameter Prediction Comparison, Aluminum-on-Aluminum Impact, L/D=0.1, T/D=0.5	73

LIST OF TABLES

Table	Page
1. Material Mechanical Properties	47
2. Material Thermal Properties	48
3. Values of V_s for Materials Considered	49
4. Debris Cloud Velocities: Comparison with Experiment and 1-D Hydrocode Predictions	50

1.0 INTRODUCTION

The Air Force Armament Directorate at Eglin Air Force Base has undertaken a program to evaluate the effectiveness of kinetic energy weapons (KEWs) against ballistic missiles. This program, which is part of the Lethality and Target Hardening (LTH-5) Program of the Strategic Defense Initiative, has focused on the response of ICBM boosters and post-boost vehicles to KEW impacts. The evaluation and selection of the systems to advance from the conceptual phase of design to demonstration/validation, engineering/manufacturing development, production, and deployment requires the assessment of candidate weapons effectiveness against a threat spectrum.

The response of a target to a KEW impact can be said to consist of two basic and distinct types of response: 'local response' and 'global response'. Local response is primarily due to the intense loading associated with a hypervelocity impact. For KEW impacts, material damage occurs very quickly (on the order of microseconds) and is limited to an area near the impact site. At sufficiently high impact velocities, shatter, melting, and/or vaporization of the materials can occur. For an aluminum-on-aluminum impact, the projectile and target materials will begin to shatter, melt, and vaporize at impact velocities of approx. 3.2, 5.6, and 10.4 km/sec, respectively [1,2].

Global response can refer to any one of a number of global phenomena that occur over a longer period of time (on the order of milliseconds), under less intense loads, and over a larger area of the target structure. In KEW impacts, one or more debris clouds are created during the initial impact on the outer wall of a target. These debris clouds spread out as they move through target voids and eventually impact an inner wall or in-

terior component of the target structure. Depending on the impact velocity and the relative material properties of the projectile and target, these debris clouds can contain solid, melted, and/or vaporized projectile and target materials. Typical global responses include the denting, buckling, or tearing of an internal missile component such as a fuel or oxidizer tank.

This report presents the results of a 12-week investigation into the composition of the material in a debris cloud created by the normal hypervelocity impact of a right circular cylinder on a flat thin target plate. The research described is the first step in a long-term research program whose overall objective is to develop a general model of the response of a target structure to a KEW impact over the anticipated impact velocity regime of 4-16 km/sec. The objectives of the work performed thus far were to 1) characterize the shock loading and release of the projectile and target materials due to a hypervelocity impact in the 4-16 km/sec impact velocity regime; 2) estimate the percentages of solid, liquid, and gaseous materials in the debris cloud created in a hypervelocity impact; 3) estimate the amount of mass in each of the three states of matter for the debris cloud material; and 4) estimate the velocities of various portions of the debris cloud.

2.0 LETHALITY ASSESSMENT MODEL REQUIREMENTS

The key to conducting an accurate lethality assessment is the use of a robust assessment methodology. The methodology should incorporate all the significant response and damage mechanisms which result from all hypervelocity weapon-target interactions. To accurately determine the total damage level sustained by an impacted target, a lethality assessment methodology must include the effects of discrete and simultaneous debris cloud fragment impacts, as well as impulsive target debris cloud loadings. Discrete or simultaneous impacts by individual fragments can pose a lethal threat to the inner wall or to an interior component of a target, depending on the fragments' speed, density, and trajectory, and on the density and strength of the target inner wall or interior component material. Individually, the molten and/or vaporous fragments in a debris cloud may not do significant damage; however, as a whole, they can produce a significant impulsive loading over a relatively large area inside the target. This in turn can result in further damage to the target at later times. Clearly then, to accurately assess the total damage to a target impacted by a KEW, the amounts and types of debris in a debris cloud produced by a hypervelocity impact must be known.

A number of empirical and semi-analytical procedures have been developed over the past decade to determine the lethal effectiveness of KEW systems. While these procedures are capable of assisting engineers and system architects in optimizing weapon designs and in performing cost trade-off studies, they are significantly limited in their characterization of the material in the debris clouds created by hypervelocity impacts. Unfortunately, very little impact test data for relatively massive projectiles (on

the order of 10 gms or more) is available at speeds above 8 km/sec. This makes it difficult to properly characterize the nature of the material in the debris clouds over the entire impact velocity regime of interest. Electrostatic devices which can launch small particles to speeds as high as 100 km/sec exist, but these systems can only launch micron-size particles [3,4]. Other electric gun systems have launched Kapton flyer plates to speeds of 11 km/sec, but cannot reach that velocity with chunky projectiles [5]. Thus, existing lethality assessment models must be used with a fair amount of caution, especially in scenarios involving impact velocities greater than those attainable in experiments.

Current semi-analytical lethality assessment models usually fall into one of two broad groups: discrete particle models [6-17] and expanding shell models [18-22]. Discrete particle models typically account for only solid fragments [6-9,14-17], or track only a small number of discrete fragments [10-13] in the debris cloud created by a high speed impact. These models are best suited for applications in which the debris clouds generated by the initial impact contain only a relatively small number of fragments and in which melting or vaporization of the projectile and target materials do not occur.

The expanding shell models typically assume that all of the debris cloud material is homogeneously distributed over a uniformly expanding spherical shell. These models are applicable only in those impact situations where complete projectile and target material vaporization occurs. Flash X-ray photographs of the debris clouds created in lead-on-lead impacts at speeds high enough to cause melting and vaporization do show that the assumptions of the spherical shell model are valid at least for the leading

portion of the debris clouds [23]. However, when a debris cloud is comprised primarily of solid fragments, then similarly obtained photographs show the debris clouds to be elliptical with an eccentricity of approximately 1.6 [23].

It is evident, therefore, that the need exists to bridge the gap between the discrete particle models, which consider only a finite number of solid fragments, and the expanding shell models, which are valid only when complete vaporization occurs. Specifically, a lethality assessment model that considers the creation and subsequent effects of debris clouds containing all three matter states is needed. FATEPEN [6-9], KAPP-II [11-13], and PEN-4 [16,17] are discrete particle lethality assessment models which can be modified to include the effects of non-solid debris cloud constituents.

KAPP-II was developed for the Defense Nuclear Agency to predict damage to complex three-dimensional aerospace targets impacted by multiple hypervelocity projectiles, including chunky fragments, rods, and hollow cylinders [11]. It is the fusion of the previously developed KAPP and KNAPP computer codes [12,13]. KAPP-II has been calibrated with an extensive experimental database covering an impact velocity range of approx. 1-9 km/sec. The empirical relationships within KAPP-II allow the user to characterize the state of the projectile as it passes through the target as well as the response of the target system to the impact loadings of the initial projectile and the debris created by the initial impact.

The FATE family of codes was developed for the Naval Surface Weapons Center (NSWC) for analyzing the impacts of warhead fragments against aircraft structures over a range of impact velocities from 2.5 to 5.0 km/sec. Initially called FATE [6], later FATE-2 [7], and now FATEPEN [8.9], the code

has been modified over the years to include projectile tip erosion even at impact velocities below shatter velocity. The equations within the FATEPEN code predict the number of plates perforated in a multi-plate target configuration as well as the holes in the perforated plates. In addition, FATEPEN also predicts the number, size, trajectories, and velocities of the fragments in the debris clouds created as the projectile first impacts the outermost plate and then as its remains move through the multi-plate target.

The PEN-4 lethality assessment model was developed for the NSWG in an attempt to model fragment impact against thin plates over a wider range of impact velocities [16]. This model is similar to the FATEPEN model in that the equations used in the model require a number of simplifying assumptions and experimentally derived factors. By restricting the lower limit of the impact velocity to 3.6 km/sec, PEN-4 is able to neglect shear failures in the projectile material: by restricting its upper limit to 7.6 km/sec, PEN-4 neglects material melting and vaporization. In more recent versions [17], PEN-4 has been updated to incorporate advanced fragmentation models [24-28]. These fragmentation models are considerable improvements over the models used in earlier versions of the code.

3.0 DEBRIS CLOUD CHARACTERIZATION

3.1 Introductory Comments

The research efforts discussed in this report were directed at the development of a procedure that would extend the applicability of existing discrete particle lethality assessment methodologies to impact scenarios in which the projectile and target materials were expected to melt and/or vaporize. Specifically, the work performed consisted of a series of tasks directed at determining to first-order accuracy the amount of projectile and target material in a debris cloud that is solid, molten, and/or vaporized. Projectiles considered were metallic monolithic right circular cylinders with a length-to-diameter ratio of 2 and which normally impacted thin flat metallic target plates with a zero angle of yaw. The mechanical and thermal properties of the target and projectile materials considered are shown in Tables 1 and 2, respectively.

3.2 Shock Loading and Release Analysis

3.2.1 Introductory Comments

Consider the impact of a cylindrical projectile on a flat target plate. Upon impact, strong shock waves are set up in the projectile and target materials. The pressures associated with these shocks typically exceed the strengths of the projectile and target materials by several orders of magnitude. For example, in an 8 km/sec aluminum-on-aluminum impact, the ratio of the impact pressure (116.5 GPa=1.15 MBar) to the strength of the material (310 MPa for aluminum 6061-T6) is approximately 375, or roughly 2.5 orders of magnitude. As the shock waves propagate, the projectile and target materials are heated adiabatically and non-isentropically. The release of the shock pressures occurs isentropically through the action of rarefaction

waves that are generated as the shock waves interact with the free surfaces of the projectile and target. This process leaves the projectile and target materials in high energy states and can cause either or both to fragment, melt or vaporize, depending on the material properties, geometric parameters, and the velocity of impact. At very early times during the impact event, only the area in the immediate vicinity of the impact site is affected by the impact. For the projectile and target geometries considered in this study, the shock waves can be considered to be initially planar. This allows one-dimensional relationships to be used for analyzing the creation and release of shock pressures.

The shock pressures, energies, etc., in the projectile and target materials were calculated using the three 1-D shock-jump conditions, a linear relationship between the shock wave velocity and particle velocity in each material, and continuity of pressure and velocity at the projectile/target interface. If we consider the 1-D impact of a projectile with velocity v_0 on a stationary target, conservation of mass, momentum, and energy across the shock front in the projectile and in the target yields

Projectile

Target

$$u_{sp}/V_{op} = (u_{sp} - u_{pp})/V_p \qquad u_{st}/V_{ot} = (u_{st} - u_{pt})/V_t \qquad (1a,b)$$

$$P_{Hp} = u_{sp} u_{pp}/V_{op} \qquad P_{Ht} = u_{st} u_{pt}/V_{ot} \qquad (2a,b)$$

$$E_{Hp} = P_{Hp} (V_{op} - V_{Hp})/2 \qquad E_{Ht} = P_{Ht} (V_{ot} - V_{Ht})/2 \qquad (3a,b)$$

where $V=1/\rho$ is specific volume, u_s and u_p are shock and particle velocity, respectively, and P_H and E_H are the pressure and energy state associated with the initial impact. In equations (1-3), the subscripts 'p', and 't'

refer to projectile and target quantities, respectively. Furthermore, in the development of equations (1-3), the initial conditions ahead of the projectile and target shock waves were taken to be zero (with the exception of density which is $\rho_0 = 1/V_0$) and the shock velocity in the projectile is taken relative to a 'stationary' projectile.

The linear shock velocity-particle velocity relationships for the projectile and target materials are in the form

$$u_s = c_0 + ku_p \quad (4)$$

where $c_0 = \sqrt{KV_0}$ is the material bulk speed of sound, $K = E/3(1-2\nu)$ is the adiabatic bulk modulus, E and ν are Young's modulus and Poisson's ratio, respectively, and k is an empirically-derived constant. At the projectile/target interface, pressure equilibrium implies that

$$P_{Hp} = P_{Ht} \quad (5)$$

while continuity at the interface implies that

$$v_0 = u_{pp} + u_{pt} \quad (6)$$

Solving equations (1-6) simultaneously yields expressions for projectile and target particle velocities which can then be used to calculate shock velocities, pressures, internal energies, and material densities after the passage of a shock wave.

The shock loading of a material is an irreversible process that results in an increase of the internal energy of the shocked material. However, the release of a shocked material occurs isentropically along an 'isentropes' or

'release adiabat'. The difference between the area under the isentrope and the energy of the shocked state is the amount of residual energy that remains in the material and can cause the material to melt or even vaporize. A sketch of a generic Hugoniot and a generic release isentrope with initial, shocked, and final material states highlighted is shown in Figure 1. In order to calculate the release of the projectile and target materials from their respective shocked states (each characterized by P_H , E_H , and V_H), an appropriate equation-of-state is needed for each material. To keep the analysis relatively simple, the Mie-Gruneisen [24] and Tillotson [25] equations-of-state were examined for suitability for use in this study.

3.2.2 Mie-Gruneisen Equation-of-State

The Mie-Gruneisen equation-of-state (EOS) is an accurate thermodynamic description of most metals in the solid regime and is relatively easy to use. It has the form

$$P = P_H + \rho\Gamma(E - E_H) \quad (7)$$

where the time-dependent Gruneisen coefficient Γ is given for most metals as

$$\Gamma = \Gamma_0 \rho_0 / \rho \quad (8)$$

where $\Gamma_0 = K\beta / \rho_0 C_p$ is the ambient Gruneisen coefficient, K is the adiabatic bulk modulus, $\beta = 3\alpha$ is the volumetric coefficient of thermal expansion, and C_p is specific heat at constant pressure. Invoking the Second Law of Thermodynamics

$$dE = TdS - PdV \quad (9)$$

along with the isentropic constraint $dS=0$ for the release process allows us

to construct the release isentrope in P-V space for a material referenced to the material Hugoniot in P-V space and a given initial shocked state defined by P_H , V_H , E_H . Using the procedure outlined by McQueen, et.al. [24], the pressure P_i and internal energy E_i at a specific position 'i' along the isentrope can be shown to be given by

$$P_i = [P_{Hi} + (\Gamma/V)_i (E_{i-1} - P_{i-1} \Delta V/2 - E_{Hi})] / [1 + (\Gamma/V)_i \Delta V/2] \quad (10)$$

where ΔV is the incremental change in volume used to create the release isentrope, and P_{Hi} and E_{Hi} are the pressure and energy along the Hugoniot corresponding to the i-th position in the release process. The release process is continued using equation (10) until the release isentrope so determined crosses the V-axis (i.e. until P_i becomes zero).

Based on its thermodynamic origins, the Mie-Gruneisen EOS cannot be expected to give accurate results in the expanded liquid regime or in the vapor regime. This is because as impact energy increases, the assumption that the Gruneisen coefficient is a function of density alone is no longer valid. At high impact energies, the Gruneisen coefficient is a function of internal energy as well as density. Experience has shown, however, that it does yield fairly accurate end-state results even when there is a small percentage of molten material present [1].

3.2.3 Tillotson Equation-of-State

The Tillotson EOS has a slightly more complicated form. In its original form [25], it has two parts. The choice of which part to use depends on the location of the release isentrope within P-V-E space. The first part applies when the material is in compression regardless of the internal energy (i.e. for $V < V_0$ and for all $E > 0$) and in the small region of expan-

sion in which $V_0 < V < V_s$ provided that $E < E_s' = E_s + H_v$ where E_s is the total heat needed to produce incipient vaporization and H_v is the latent heat of vaporization. The quantity $V_s = 1/\rho_s$ corresponds to the volume (or density) of a material that completes its release process with an internal energy $E = E_s$. In these two regions, the Tillotson EOS has the form

$$P_1 = [a + b/f(E, \rho)]E\rho + A\mu + B\mu^2 \quad (11)$$

where $\mu = V/V_0 - 1$ and

$$f(E, \rho) = (E/E_0)(\rho_0/\rho)^2 + 1 \quad (12)$$

Equation (11) applies in particular to shock loadings in which the material remains a solid after it isentropically returns to ambient pressure. In equation (11), $A = \rho_0 c_0^2$ and $a + b = \Gamma_0$. For most metals, a value of $a = 0.5$ will yield satisfactory results. In his report, Tillotson states that the constants E_0 and B should be adjusted to give the best fit for the EOS surface [25]. However, recent efforts by Mullin, et al. [26] show that the constant B can be approximated reasonably well as

$$B = \rho_0 c_0^2 (2k - 1 - \Gamma_0/2) \quad (13)$$

but that E_0 still has to be treated as a curve-fitting parameter. One of the dangers of improperly guessing a value for E_0 is that the isentrope would actually curve up from its starting point (P_H, V_H, E_H) instead of curving down as would be expected. If this were to occur, the release process would have to be terminated, another value of E_0 would have to be specified (usually a lower one), and the release process would have to start over again. The following empirical relationship was obtained as part of

this investigation for E_0 as a function of other material parameters to serve as a guide in the selection of an appropriate starting value for E_0 .

$$E_0/E_s' = 0.819\Gamma_0^{-0.768} k^{6.594} (T_m/T_v)^{-0.021} (H_f/H_v)^{0.572} \quad (14)$$

where H_f is the latent heat of fusion. This equation is based on the materials considered in this study and has a correlation coefficient of 87.21%. When compared with the given values of E_0 used to derive it, equation (14) had an average error of 2.6% with a standard deviation of 30%.

In a highly expanded state (i.e. for $V > V_s$ regardless of internal energy) or if the internal energy is high enough to cause complete vaporization even in a moderately expanded state (i.e. for $V_0 < V < V_s$ and if $E > E_s'$), the second part of the EOS is invoked:

$$P_2 = aE\rho + \{ [bE\rho/f(E,\rho) + A\mu \exp[-\beta(V/V_0 - 1)]] \exp[-\alpha(V/V_0 - 1)^2] \} \quad (15)$$

where the constants α and β are adjusted to control the rate of convergence of the EOS to that of an ideal gas. The exponential factors force the second term in equation (15) to approach zero at large expansion volumes. The remaining first term is then equivalent to the ideal gas term $(\gamma-1)E\rho$ with $\gamma=1.5$, which is a reasonable value for real gases [25].

In this two-part form, the Tillotson EOS is asymptotically correct in the compression and expansion regimes and reproduces many of the isentropic release features observed with much more complicated equations-of-state [26]. It should be noted that the release process as described by the Tillotson EOS does not always terminate in a simple, clear cut manner as it does with the Mie-Gruneisen EOS. For impact conditions in which the material remains in a solid state upon release, the isentrope generated with the

Tillotson EOS will in fact cross the V-axis in a manner analogous to that which is observed when using the Mie-Gruneisen EOS. However, for impact conditions that lead to material melt and vaporization, instead of crossing the V-axis, the isentrope created with the Tillotson EOS approaches the V-axis asymptotically and never crosses it. Therefore, an additional user-supplied parameter must be a cut-off point for the release process in the event of extreme gaseous expansion.

Closed-form expressions for P_i along the isentrope described by equations (11) and (15) can also be obtained using the procedure described in [25] and used in deriving P_i for the Mie-Gruneisen EOS. Three different variations of the incremental form of equation (9) with $dS=0$ were considered in the development of the expressions for P_i . These variations are

$$(\#1) E_i - E_{i-1} = -(P_i + P_{i-1})\Delta V/2 \quad (16a)$$

$$(\#2) E_i - E_{i-1} = -P_{i-1}\Delta V \quad (16b)$$

$$(\#3) E_i - E_{i-1} = -P_i\Delta V \quad (16c)$$

These three forms were considered in an attempt to simplify the final expression for P_i . In the procedure described in [25], equation (11) needs to be manipulated so that the unknown pressure P_i at the current increment is written in terms of quantities at the previous increment, including the previous pressure P_{i-1} . This is relatively easy to do using variation (#1), the most sensible of the three, for the Mie-Gruneisen EOS because the pressure terms in the Mie-Gruneisen EOS are easily separable. In the Tillotson EOS, the complexity arises from the fact $dE=-PdV$ is used in the denominator of only one term on the right-hand-side in equations (11) and (15). This

makes the separation of the pressure terms somewhat more cumbersome.

After deriving the expressions for P_i using each of the three proposed variations, the predictions of the three variations for the impact velocity required to produce melt and vaporization in materials for which such quantities were known were compared against known velocity values. It was found that variations (#2) and (#3) did not reproduce the known values very well. Thus, variation (#1) was selected for further use in the development of the equations for P_i . The final expressions using equation (16a) are presented below.

$$(P_1)_i = [C_2 - \sqrt{(C_2^2 - 4C_1C_3)}] / 2C_1V_i \quad (17)$$

$$C_1 = V_i(\Delta V') [1 + a(\Delta V'/V_i)] \quad (18)$$

$$C_2 = C_1R_i/V_i(\Delta V') + (\Delta V'/V_i)R_i' + Q_iV_i^2(\Delta V') - P_{i-1}(\Delta V')V_i^2 [1 + a(\Delta V'/V_i)] \quad (19)$$

$$C_3 = (aE_{i-1} + Q_iV_i)R_i + bE_{i-1}E_oV_o^2 - P_{i-1}(\Delta V') [(1+a)E_{i-1}V_i^2 + (1+b)E_oV_o^2 + Q_iV_i^3] + [P_{i-1}(\Delta V')]^2V_i^2 \quad (20)$$

$$Q_i = A\mu_i + B\mu_i^2 \quad (21)$$

$$R_i = E_{i-1}V_i^2 + E_oV_o^2 \quad (22)$$

$$R_i' = aE_{i-1}V_i^2 + bE_oV_o^2 \quad (23)$$

and $\Delta V' = \Delta V/2$. Although a substantial amount of algebra is required to

derive equations (17-23), the manipulations involved in deriving a closed-form expression for $(P_2)_i$ can be reduced significantly if equation (15) is re-written in the following form:

$$P_2 = [a + b'/f(E,\rho)]E\rho + Q' \quad (24)$$

where $f(E,\rho)$ is still given by equation (12), $b'=bU$ and $Q'=US$ where

$$S = A\mu\exp[-\beta(V/V_0 - 1)] \quad (25)$$

$$U = \exp[-\alpha(V/V_0 - 1)^2] \quad (26)$$

Thus, the expression for P_2 can be written in exactly the same form as the expression for P_1 . As a result, we can use the expressions that were derived for $(P_1)_i$ can be used to give us $(P_2)_i$ as well provided that in every instance b is replaced with bU_i and Q_i is replaced with $U_i S_i$ where U_i and S_i are found using equations (25) and (26).

3.2.4 Modified Tillotson Equation-of-State

If we examine equations (11,15) in more detail, we note that they are continuous across $V=V_0$, which implies that the Tillotson EOS is continuous across $V=V_0$ for very high impact energies. However, at $V=V_s$, there is a discontinuous, abrupt jump in the release isentrope for moderate impact energies, that is, when $E_s < E < E'_s$ at $V=V_s$. This jump occurs because according to the original formulation proposed by Tillotson, whenever $E < E'_s$ equation (11) is used. even in the $V_0 < V < V_s$ region of the curve. However, once we move across $V=V_s$, equation (15) is invoked regardless of the impact energy. Since these two equations are not continuous at $V=V_s$, neither is the isentrope. Table 3 shows values of V_s calculated using the Tillotson EOS and the EOS parameters used to obtain them. Examination of the last

column in Table 3 reveals that the ratio V_s/V_o is relatively insensitive to the choice of material: the average value of V_s/V_o is 1.138 with a standard deviation of only 4.3% of the average value.

A modification in the form of a 'Mixed Phase Formulation' of the Tillotson EOS was proposed in an attempt to lessen the effects of the discontinuity at $V=V_s$ [27]. The Mixed Phase Formulation proposes that if $E_s < E < E_s'$ as the release isentrope crosses $V=V_o$, then for $V_o < V < V_s$ the pressure is to be calculated using the equation

$$P_3 = \{P_2(E - E_s) + P_1(E_s' - E)\} / (E_s' - E_s) \quad (27)$$

This ensures that the EOS and the release isentrope are continuous if $E=E_s$ or if $E=E_s'$ at $V=V_o$. This modification was motivated by the fact that if $E > E_s$ as the isentrope crossed $V=V_o$, then enough energy would be present to cause partial vaporization. Hence, the regime $V_o < V < V_s$ is referred to as a 'mixed-phase region' in which some gas is present in addition to the original solid material. Thus, rather than continue to use equation (11) when $E_s < E < E_s'$ in the regime $V_o < V < V_s$, equation (27) is to be implemented to account for some additional expansion of the material. This in turn implies that equation (11) is valid in $V_o < V < V_s$ only if $E < E_s$ instead of $E < E_s'$ as originally proposed by Tillotson.

The effect of implementing the Mixed Phase Formulation is illustrated with generic isentropes in Figures 2a-c. In Figure 2a, the energy as the isentrope crosses $V=V_o$ is less than E_s . No vaporization is expected to occur and calculation of the isentrope continues using equation (11) as originally proposed by Tillotson. The isentrope in this case terminates at

a specific volume $V_f < V_s$. In Figure 2b, the energy as the isentrope crosses V_0 is greater than E_s but less than E_s' . Thus, some vaporization is expected to occur and the Mixed Phase Formulation given by equation (27) is invoked. Since E is already larger than E_s , the isentrope in this case must terminate at a value of specific volume greater than V_s . Thus, in this case, the isentrope crosses $V=V_s$ and in doing so, equation (15) is invoked and the jump in the isentrope at $V=V_s$ is created. In Figure 2c, the energy as the isentrope crosses V_0 is already greater than E_s' . In this case, a significant amount of vaporization is expected to occur. Equation (15) is invoked automatically, the isentrope is continuous across $V=V_0$, and there is no jump at $V=V_s$.

While the Mixed Phase Formulation does allow for some gaseous expansion in moderately high energy impacts not possible with the original Tillotson EOS, it still does not address the discontinuity at $V=V_s$ shown in Figure 2b. In this case, the isentrope continues along a path that becomes asymptotic to the V -axis. In fact, for $V > V_s$ the path of the isentrope is similar to the one it would follow during a release process in which the material would be completely vaporized, that is, one in which E had been greater than E_s' as the isentrope crossed $V=V_s$. While this may be acceptable for values of E near E_s' , this is certainly not the case for release isentropes in which E is greater than E_s by only a small amount as the isentrope crosses $V=V_s$. Thus, the original Tillotson EOS and the Mixed Phase Formulation both tend to overpredict the amount of expansion that occurs in the release of a material from a moderately energetic state (i.e. one which is not sufficiently energetic to cause an appreciable amount of vaporization to occur).

To overcome this difficulty, it is proposed that when $V > V_s$ and $E_s < E < E_s'$

(i.e. in moderately high energy impacts), the jump in Tillotson EOS can be eliminated by uniformly subtracting the magnitude of the jump at $V=V_s$ from the pressure values calculated when $V>V_s$ using equation (15), that is, the original Tillotson EOS equation applicable when $V>V_s$. Thus, if $E_s < E < E_s'$ as the isentrope crosses $V=V_s$, then for $V>V_s$ the pressure is to be calculated using the equation

$$P_4 = P_2 - [P_2(V=V_s) - P_3(V=V_s)] \quad (28)$$

in which P_2 is calculated using equation (15) and P_3 is calculated using equation (27). As can be seen from equation (28), this correction is not intended to replace the Mixed Phase Formulation of the Tillotson EOS, but rather to complement its use.

The quantity within the square brackets of equation (28) is the amount of the jump in the release isentrope; it is largest if $E=(E_s)^+$ at $V=V_s$ and decreases as $E \rightarrow E_s'$. In the event that $E \geq E_s'$ at $V=V_s$, the proposed modification in the Tillotson EOS disappears, the EOS reverts back to its original form (i.e. $P_4 = P_2$), and continuity at $V=V_s$ is maintained. If $E < E_s$ as the isentrope crosses $V=V_0$, then the isentrope never reaches $V=V_s$ so that in such cases, the correction is never invoked. Thus, the proposed correction is only invoked when needed, that is, if $E_s < E < E_s'$ as the isentrope crosses $V=V_s$.

The difference in the isentrope for $V>V_s$ generated with the Mixed Phase Formulation and with the proposed jump correction is also illustrated in Figure 2b where the dashed line indicated the path of the isentrope if the proposed jump correction were implemented. As can be seen in Figure 2b, if

the proposed jump correction were implemented, the isentrope would cross the V-axis at a value much less than that which would be obtained with the Mixed Phase Formulation (or with the original Tillotson EOS for that matter).

A more detailed analysis of the effect of implementing the proposed modification to the Tillotson EOS on the nature of the release isentrope is shown in Figures 3a,b, and c for impact scenarios in which $E=(E_s)^+$, E is between E_s and E_s' , and $E=(E_s)'$, respectively, as the isentrope crosses $V=V_s$. As can be seen in Figures 3a-c, the proposed modification gives an appropriate amount of expansion when E is near E_s' and does not overpredict the amount of expansion when E is only slightly greater than E_s .

The following short table presents a summary of which equation to use in which regime of P-V-E space to generate a release with the Tillotson EOS.

V-Region	E-Region	Equation
$V < V_o$	all $E > 0$	(11)
$V_o < V < V_s$	$E < E_s$	(11)
$V_o < V < V_s$	$E_s < E < E_s'$	(27)
$V_o < V < V_s$	$E_s' < E$	(15)
$V_s < V$	$E_s < E < E_s'$	(28)
$V_s < V$	$E_s' < E$	(15)

3.2.5 Discussion

A one-dimensional shock loading and release process was used to determine the end state of the projectile and target material portions experiencing shock loading and release. However, because of its inherent limita-

tions, the Mie-Gruneisen EOS was eventually abandoned in favor of the Tillotson EOS. The internal energies in the shocked and released portions of the projectile and target materials were calculated using the Tillotson EOS and were translated into temperature increases using classical thermodynamics. Figures 4-7 compare the results of the release process for aluminum-on-aluminum impacts at three different energy levels using the Mie-Gruneisen and Tillotson equations-of-state.

In Figure 4, the release process as described by the Mie-Gruneisen EOS and the Tillotson EOS are nearly identical. This is to be expected for relatively low energy impact (i.e. those impacts in which the materials return to a solid matter state after release). Figure 5 shows the dramatic difference between using the Mie-Gruneisen EOS and the Tillotson EOS for very high energy impacts (i.e. those impacts in which the materials vaporize). The Mie-Gruneisen EOS cannot account for the expansion of the gaseous state and terminates the release process at a much lower specific volume than the Tillotson EOS.

Figure 6 highlights one of the difficulties in using the Tillotson EOS. This difficulty occurs under impact conditions that are not violent enough to vaporize the material, yet are strong enough to cause the material to melt and be in an energy state that is near incipient vaporization. Under these conditions, the jump in the release isentrope at $V=V_g$ generated by the original Tillotson EOS and the implementation of the Mixed Phase Formulation both result in a final volume that is artificially high. As stated previously, the final volume was considered to be artificially high because the jump at $V=V_g$ forced the release isentrope to follow a path as if complete vaporization of the material had occurred. Some vaporization will indeed

occur if the internal energy at $V=V_g$ is greater than that required to initiate vaporization of the material. However, there is no need for the release isentrope to follow the path of complete vaporization unless the internal energy is greater than that required for complete vaporization.

Implementation of the jump correction given by equation (28) in this impact energy regime caused the release processes to terminate at specific volume values that were much more reasonable. It is noted that this correction had no effect when the impact energy was relatively low or very high. Figure 7 shows the result of implementing the jump correction given by equation (28) for a 10 km/sec aluminum-on-aluminum impact. In a such a scenario, a fair amount of melting and expansion would be expected to occur. The Tillotson EOS release isentrope shown in Figure 7 after implementing the correction is more reasonable because it terminates at a specific volume that is greater than that predicted by the Mie-Gruneisen EOS which cannot account for greatly expanded states, yet is substantially less than that which would be obtained following the path of complete vaporization. The Tillotson EOS in which the jump correction is performed using equation (28) in conjunction with the Mixed Phase Formulation is hereafter referred to as the Modified Tillotson EOS.

The differences in the final specific volumes obtained in aluminum-on-aluminum impacts using the Mie-Gruneisen, Tillotson, and Modified Tillotson equations-of-state are shown in Figure 8. For low energy impacts (below approx. 9 km/sec), the results are, as expected, nearly identical. For very high energy impacts (above approx. 18 km/sec), the final values predicted by the Tillotson EOS and the Modified Tillotson EOS (upper curve) overlap and

exceed those predicted by the Mie-Gruneisen EOS (lower curve) due to the gaseous expansion of the released material at those impact velocities. The odd behavior in the final values of specific volume due to the jump in the Tillotson EOS begins for aluminum at approximately 9 km/sec (upper curve in Figure 8). However, the Modified Tillotson EOS (middle curve) produces a smooth transition as the material changes from a solid state (below approx. 6 km/sec) to a liquid state (between approx. 6 and 11 km/sec) to a gaseous state (above approx. 11 km/sec). It is the Modified Tillotson EOS that was used throughout the remainder of this study.

3.3 Computing the Percentages of Solid, Liquid, and Gaseous Debris Cloud Material

Once the residual internal energies in the shocked and released portions of the projectile and target materials had been obtained, the percentages of the various states of matter in the resulting debris cloud were estimated using the following procedure. This procedure requires the knowledge of the materials' solid and liquid specific heats (C_{ps}, C_{pl}), their melting and boiling points (T_m, T_v), and their heats of fusion and vaporization (H_f, H_v) in addition to the residual internal energy (E_r).

If $E_r < C_{ps} T_m$, then all of the shocked and released materials was considered to remain in a solid matter state, that is,

$$\begin{aligned}
 P_s &= 1.0 \\
 P_l &= 0.0 \\
 P_v &= 0.0
 \end{aligned}
 \tag{29a,b,c}$$

If $C_{ps} T_m < E_r < C_{ps} T_m + H_f$, then the quantity $(E_r - C_{ps} T_m) / H_f$ represented the fraction of the shocked and released material that was melted, while the remaining

shocked and released material was assumed to be in solid form, that is,

$$\begin{aligned}
 P_s &= 1.0 - (E_r - C_{ps} T_m) / H_f \\
 P_l &= (E_r - C_{ps} T_m) / H_f \\
 P_v &= 0.0
 \end{aligned}
 \tag{30a,b,c}$$

If $C_{ps} T_m + H_f < E_r < C_{ps} T_m + H_f + C_{pl} (T_v - T_m)$, then all of the shocked and released material was considered to be in a liquid state, that is,

$$\begin{aligned}
 P_s &= 0.0 \\
 P_l &= 1.0 \\
 P_v &= 0.0
 \end{aligned}
 \tag{31a,b,c}$$

If $C_{ps} T_m + H_f + C_{pl} (T_v - T_m) < E_r < C_{ps} T_m + H_f + C_{pl} (T_v - T_m) + H_v$, then the quantity $(E_r - [C_{ps} T_m + H_f + C_{pl} (T_v - T_m)]) / H_v$ represented the fraction of the shocked and released material that was vaporized, while the remaining shocked and released material was considered to be in liquid form, that is,

$$\begin{aligned}
 P_s &= 0.0 \\
 P_l &= 1.0 - (E_r - [C_{ps} T_m + H_f + C_{pl} (T_v - T_m)]) / H_v \\
 P_v &= (E_r - [C_{ps} T_m + H_f + C_{pl} (T_v - T_m)]) / H_v
 \end{aligned}
 \tag{32a,b,c}$$

If $C_{ps} T_m + H_f + C_{pl} (T_v - T_m) + H_v < E_r$, then all of the shocked and released material was vaporized, that is,

$$\begin{aligned}
 P_s &= 0.0 \\
 P_l &= 0.0 \\
 P_v &= 1.0
 \end{aligned}
 \tag{33a,b,c}$$

3.4 Computing the Masses of the Solid, Liquid, and Gaseous Debris Cloud Material

The material in the debris cloud created by the initial impact consists of the target material removed by the impact and the impacting projectile mass. While the mass of the projectile material in the debris cloud was known a priori, the mass of the target material in the debris cloud had to be determined by multiplying the target hole-out area by the target thickness and the target material density. The diameter of the hole created in the target plate by the initial impact (D) was calculated using an empirical equation for target hole diameter [11]. This equation is of the form

$$D/d_p = 1 + (D_{inf}/d_p - 1)(1 - \exp[-h(t_s/d_p)^{2/3}]) \quad (34)$$

where

$$D_{inf}/d_p = a(\rho_p/\rho_t)^b (3L_p/2d_p)^c [(\rho_p v_o^2)/(2eB_t)]^{1/3} \quad (35)$$

$$h = f(B_t/\rho_p)^g \quad (36)$$

and a, b, c, e, f, g are empirical constants defined in [11]. While the empirical nature of the equation mandates its use only within the impact velocity regime for which it was designed, the results obtained for velocities outside the prescribed regime were not unreasonable.

To calculate the masses of the various states of the projectile and target materials in the debris cloud, the amounts of shocked and released target and projectile material had to be determined. These quantities were obtained by determining the locations in the target plate and in the projectile where the rarefaction waves had overtaken the corresponding shock wave [28]. It was the material through which both the shock wave and the release

wave had travelled that was shocked and released and which was therefore either melted or vaporized, depending on the particulars of the impact event. Any material beyond the point at which the rarefaction wave had overtaken the shock wave was assumed, for the purposes of this study, not to have been shocked and to have remained in a solid matter state. If the point at which the release wave had overtaken the shock wave was beyond the thickness of the target plate or the length of the projectile, then all of the target and/or projectile material had been shocked and released.

Referring to Figure 9a,b [28] and utilizing the results in Reference 28, for the projectile, rarefaction wave R_1 overtakes the shock wave S_1 on the axis of symmetry at a point in the projectile given by

$$L_1 = 0.72d_p \quad (37)$$

where L_1 is measured from the front face of the initially uncompressed projectile. Furthermore, rarefaction wave R_4 will overtake the shock wave S_1 at a point in the projectile given by

$$L_4 = t_s [(c_{st} + u_{st} - u_{pt}) / (c_{sp} - u_{sp} + u_{pp})] (c_{sp} / c_{st}) (u_{sp} / u_{st}) \quad (38)$$

where t_s is the target thickness, and c_{st}, c_{sp} are the speeds of sound in the shocked target, projectile materials and are given by [28]

$$c_{s(t,p)}^2 = u_{s(t,p)}^2 (0.49 + [(u_{s(t,p)} - u_{p(t,p)}) / u_{s(t,p)}]^2) \quad (39)$$

respectively. Thus, if $L_1 < L_4$, then L_1 overtakes S_1 first and the shocked and released projectile length is taken to be equal to L_1 ; if $L_1 > L_4$, then L_4 is the first to overtake S_1 and the shocked and released projectile length is taken to be equal to L_4 .

For the target, referring again to Figure 9 [28], rarefaction wave R_2 overtakes the shock wave S_2 on the axis of symmetry at a point in the target given by

$$L_2 = 0.72d_p \quad (40)$$

where L_2 is measured from the upper surface of the undisturbed target. If $t_s < L_2$, then the side rarefaction waves will never meet the target shock waves before it reflects back from the shield. In this case, the entire thickness of the target is shocked and released. If $t_s > L_2$, then the depth through which the target material is shocked and released is given by L_2 .

Once the projectile and target mass contributions to the debris cloud and the fractions of these masses that were shocked and released were obtained, the masses of the target and projectile materials in each of the three states of matter were computed by multiplying each matter state percentage by the appropriate total shocked and released mass. The mass of the solid shocked and released material (if any) was then added to the mass of the unshocked material (if any) to obtain the total mass of the solid component of the material in the debris cloud.

Thus, if we let L_o and t_o denote the length and depth of the shocked and released portions of the projectile (original length L_p) and target, respectively, then the total masses in each of the three states of matter are given by

<u>Target</u>	<u>Projectile</u>	
$M_{st} = M_t - T_{sr} + M_{st}'$	$M_{sp} = M_p - P_{sr} + M_{sp}'$	(41a,b)
$M_{st}' = P_{st} T_{sr}$	$M_{sp}' = P_{sp} P_{sr}$	(42a,b)
$M_{lt} = P_{lt} T_{sr}$	$M_{lp} = P_{lp} P_{sr}$	(43a,b)
$M_{vt} = P_{vt} T_{sr}$	$M_{vp} = P_{vp} P_{sr}$	(44a,b)
$T_{sr} = (t_o/t_s) M_t$	$P_{sr} = (L_o/L_p) M_p$	(45a,b)
$M_t = \pi D_s^2 \rho_t / 4$	$M_p = \pi d_p^2 L_p \rho_p / 4$	(46a,b)

where: $M_{st}, M_{sp}, M_{lt}, M_{lp},$ and M_{vt}, M_{vp} are the total masses of the solid, liquid, and vapor components of the target and projectile contributions to the debris cloud, respectively; $P_{st}, P_{sp}, P_{lt}, P_{lp},$ and P_{vt}, P_{vp} are the percentages of the solid, liquid, and vapor constituents of the shocked and released portions of the target, and projectile, respectively; $T_{sr},$ and P_{sr} are the portions of the target and projectile that are shocked and released; ρ_t, ρ_p and M_t, M_p are the mass densities and total original masses of the target and projectile, respectively; and, M_{st}' and M_{sp}' are the masses of the shocked and released portions of the target and projectile that remain in a solid matter state upon release. This procedure has two major limitations which are discussed below.

The first limitation is the assumption that the impact pressure acts uniformly on an area equal to the target plate hole area. In fact, if shear and viscous forces are neglected, there are no net forces acting on the projectile and target masses immediately after impact. This implies that the force exerted by the projectile on the target equals the force exerted by the target on the projectile. Combining this result with equation (5) and noting that force is the product of pressure and area, the effective area of the target on which the impact pressure acts must, to an first-order

approximation, equal the presented area of the projectile. This in turn implies that the shocked target material comes from an area of the target approximately equal to the presented area of the projectile (see also [1] and [29]).

The second limitation of this procedure is the assumption that no further projectile and/or target loading and unloading had occurred beyond the point where the release waves had overtaken the corresponding shock wave. This is not completely correct since the shock wave does not simply cease to exist once it is overtaken by a rarefaction wave. Rather, its magnitude decreases over a finite amount of time and a finite extent of material. Some additional projectile and target material will be heated and possibly melted until the strength of the shock wave diminishes to a point below which melt due to plastic deformation no longer occurs. However, the procedure set forth does allow the calculation of first-order accurate mass quantities for projectile and target materials in the three states of matter.

3.5 Debris Cloud Velocities

Many of the expanding shell models discussed previously contain equations that can be used to calculate the velocities of various portions of a debris cloud created in high speed impact. Alternatively, many of the discrete particle models contain equations to calculate velocities of individual particles within a debris cloud. This section presents the results of some preliminary work that was performed in attempt to determine the velocities of the front and rear of debris cloud along the axis of propagation, as well as the velocity of the debris cloud center-of-mass also along the axis of propagation.

Consider the impact of a projectile on a thin target and the debris cloud created by it as shown in Figure 10. As indicated in the Figure, the velocities of interest are v_F , v_I , and v_R . As the initial shock wave created by the impact strikes the rear surface of the target it creates a rarefaction wave that travels back into the target and eventually in some form into the projectile. This action and interaction of the shock wave and the free surface impacts a velocity u_{fst} to the target rear surface equal to the sum of the particle velocity in the target material due to the shock wave u_{pt} and the particle velocity due to the rarefaction wave u_{rt} , that is,

$$u_{fst} = u_{pt} + u_{rt} = u_{pt} + \int_0^{P_H} \sqrt{(-dV/dP)} \Big|_{isen} dP \quad (47)$$

where the P-V curve used in the integration is the isentrope for the target material. Since $u_{rt} = u_{pt}$ [24], an alternative form for equation (47) is

$$u_{fst} = 2u_{pt} \quad (48)$$

As in a previous study of debris cloud velocities [30], the velocity of the leading edge of the debris cloud v_F can be approximated with u_{fst} :

$$v_F = u_{fst} = u_{pt} + \int_0^{P_H} \sqrt{(-dV/dP)} \Big|_{isen} dP \quad (49)$$

The velocity of the debris cloud center-of-mass can be found using simple momentum conservation before and after the impact on the target:

$$v_I = M_p V_p / (M_t + M_p) \quad (50)$$

Finally, using an argument similar to that in the development of an equation

for v_R , the velocity of the trailing edge of the debris cloud is argueably given by

$$v_R = v_o - u_{fsp} = v_o - [u_{pp} + \int_0^{P_H} \sqrt{(-dV/dP)} \Big|_{\text{isen}} dP} \quad (51)$$

where in this case the isentrope used in the integration is that for the projectile material.

4.0 RESULTS AND DISCUSSION

4.1 Introductory Comments

A FORTRAN program called DEBCLD was written to implement the various procedures described in the preceding section. The source code is given in Appendix A, with sample input and output files in Appendix B and C, respectively. A word of caution: while the Tillotson EOS is relatively straightforward to implement, its use requires a fair amount of familiarity with its peculiarities.

DEBCLD is an interactive program that prompts the user for the following information:

- 1) projectile material;
- 2) target material;
- 3) impact velocity; and,
- 4) E_0 multiplier.

DEBCLD requires two input files: INDATA, which is a material library; and GPARAM, which contains projectile and target geometry information. INDATA also contains the choice of the $dE-PdV$ approximation, the Tillotson EOS parameters α and β , and the Tillotson EOS parameter ϵ which tells the program when to stop a release process in which the isentrope is asymptotic to the V-axis. The units for the data in the files INDATA and GPARAM are presented at the end of the sample files in Appendix B and C, respectively.

DEBCLD generates two output files: PLOT, which contains plottable information for the target and projectile materials' P-V curves and release isentropes; and IMPOUT, which contains a detailed summary of the following information:

- 1) projectile and target geometric and material properties;

- 2) impact conditions;
- 3) projectile and target material EOS parameters;
- 4) projectile and target material end-state calculation results, including the waste heat generated, the resulting temperature increase, the percent of solid, liquid, and vaporous material, and the masses of the solid, liquid, and vaporous components; and,
- 5) debris cloud velocities v_F , v_I , and v_R .

Two samples of the output file IMPOUT generated by DEBCLD are given in Appendix C.

4.2 Material Characterization

Figures 11-15 present the results obtained using the code for aluminum-on-aluminum impacts at velocities between 4 and 25 km/sec. Figures 11-13 can be used to compare the effects of using the Mie-Gruneisen, Tillotson, and Modified Tillotson equations-of-state to determine the percentages of the various matter states in aluminum-on-aluminum impacts. Figures 14 and 15 show the distribution of the projectile and target material among the three matter states for some of the impact velocities considered. Figures 16-19 show a comparison of the predictions of various empirical hole diameter equations for different L/D ratios.

As can be seen in Figure 11, the Mie-Gruneisen EOS predicted only a small amount of vaporized material at an impact velocity as high as 25 km/sec. However, both the Tillotson and the Modified Tillotson equations-of-state predicted that the aluminum was completely vaporized at an impact velocity between 20 and 25 km/sec. This difference is due to the fact that the Mie-Gruneisen EOS did not account for the expansion of the material as

it nears vaporization and completed the release process with the material in a much lower energy state than the Tillotson EOS.

Comparing Figures 12 and 14 reveals that the Tillotson and the Modified Tillotson equations-of-state agreed in the percentages of the various states of matter at speeds below approx. 9 km/sec and above approx. 18 km/sec. However, within the moderate impact energy regime, the Modified Tillotson EOS predicted vaporization to begin at an impact velocity that was lower than that predicted by the Tillotson EOS. Had this characterization scheme been used in an actual lethality assessment for an impact velocity between approx. 9 and 18 km/sec, the result would have been conservative since there would have been fewer potentially lethal solid fragments remaining in the debris cloud.

In Figure 14, the total projectile mass remained constant because the projectile length and diameter were fixed in all of the impact scenarios considered. The solid dark region represents the mass of the projectile that was unshocked and therefore was not subjected to melting and/or vaporization. This quantity increased with impact velocity because the speed of the rarefaction wave in the projectile increased at a faster rate than did the speed of the shock wave in the projectile. As the impact velocity increased, the rarefaction wave caught up with the shock wave within a shorter period of time. This in turn increased the amount of the projectile material that was not subject to melting and/or vaporization. The remaining shaded areas in Figure 14 show the amounts of the shocked and released projectile material in each of the three matter states as the impact velocity increased from 4 to 25 km/sec.

Figure 15 shows that the amount of target material in the debris cloud increased as impact velocity increases due to the growth in target hole size that accompanied an increase in impact velocity. For the projectile and target geometries considered, all of the target material was shocked and released. Hence, there is no solid dark area in Figure 15, only the three lighter-shaded areas which show the amounts of shocked and released target material in each of the three states of matter.

One of the interesting features of Figure 15 (and of equation (34) which was used in its development) is that the amount of target mass in the debris cloud continues (and will continue) to grow as the impact velocity is increased. This is because the velocity term in the hole diameter predictor equation has a $2/3$ power -- hole diameter is proportional to $V^{2/3}$. However, this is not necessarily the case, especially in the case of very thin target. For thin targets, one would expect the hole to increase until a certain critical impact velocity (which depends on relative target and projectile material and geometric properties) and then level off.

Up until the critical impact velocity, there would be substantial interaction between the projectile and the target as the projectile moves through the target; above the critical impact speed, the projectile would move through the target so fast (because of the relative thinness of the target) that there is only a minimal amount of projectile/target interaction. Hence, one would expect impact velocity to have a minimal effect on hole diameter in a thin target beyond a certain critical value. Unfortunately, equation (34) does not have this characteristic.

A brief study was made using equation (34), two other hole diameter

predictor equations in KAPP-II, and the hole diameter predictor equation in PEN4.v10 for aluminum projectiles impacting thin aluminum targets at speeds between 2 and 25 km/sec. The results are presented in Figures 16-19; each Figure corresponds to a different relative geometric configuration that was considered. In each of the Figures, the curve corresponding to equation (33) is that which corresponds to 'KII/HSA01'. In Figure 16, the projectile length-to-diameter ratio (L_p/d_p) was 2 while the ratio of the target thickness to the projectile diameter (t_s/d_p) was 0.1; in Figure 17, $L_p/d_p=2$ while $t_s/d_p=0.5$; in Figure 18, $L_p/d_p=0.1$ and $t_s/d_p=0.1$; and in Figure 19, $L_p/d_p=0.1$ and $t_s/d_p=0.5$.

Thus, in Figures 16 and 17, a relatively long rod impacted a relatively thin and thick plate, respectively, while in Figures 18 and 19, a relatively thin disk impacted and relatively thin and thick plate, respectively. A common feature of all four figures is that only the PEN4.v10 equation possessed the ability to level off in hole diameter beyond a certain impact velocity. However, the PEN4.v10 equation is for spheres only; the diameter used in the equation was taken to be equal to d_p , and not some 'equivalent diameter' that would be larger than d_p and confuse the issue. Thus, the predictions of the PEN4.v10 equation are affected only by target thickness and not projectile length.

Another common feature of all four figures is that the predictions of all three KAPP-II equations continue to grow as impact velocity increases. Of these three equations, the one denoted by 'KII/HSS02' appears to have some tendency to flatten out as the impact velocity increases. Thus, it would appear that KII/HSS02 offers some promise in being able to be modified to reflect what would be expected of hole diameter as a function of impact

velocity. It is clear that this particular area needs additional work.

4.3 Debris Cloud Velocities

Debris cloud velocities were calculated using the equations presented herein and compared against experimental results and 1-D hydrocode predictions for copper disks impacting aluminum plates [30]. The results are presented in Table 4. As can be seen in Table 4, the predictions of DEBCLD for v_F and v_R are in excellent agreement with those of the 1-D hydrocode and the experimental results. However, the predictions of DEBCLD for v_I are significantly different from the numerical and experimental results. This discrepancy can be explained by the following consideration.

In Reference 30, v_I was calculated using equation (50) with $d_h = d_p$. That is, in calculating M_t , in Reference 29, the target hole diameter was taken to be equal to the projectile diameter. This was justified in Reference 29 by the fact that thin copper disks were used to impact thin aluminum plates and that in such impacts, the hole diameter was always nearly equal to the diameter of the copper disk. However, DEBCLD computed v_I using equation (34) in which target hole diameter varied with the thickness of the target plate, the impact velocity, etc. Apparently, equation (34) over-predicted the hole diameter in the target which resulted in an overly-massive debris cloud. This naturally served to decrease the velocity of the center-of-mass of the debris cloud. Thus, it would appear that equation (34) needs to be re-examined and possibly revised for thin-disk projectiles.

Finally, it is important to note that equation (51) can occasionally yield rear surface velocities that may be questionable. For example, for like-into-like impacts, $u_{fsp} = 2u_{pp} = 2(v_o/2) = v_o$ so that equation (51) yields

$v_R=0$. However, this may in fact be an acceptable result of one recalls the debris clouds in the x-ray photographs of lead-on-lead impacts, for example [23]. In these photographs, the debris cloud appears to remain attached to the target plate, thereby giving the impression that the rear end of the cloud does not move, i.e. that $v_R=0$. In the copper-on-aluminum impacts in Reference 29, the rear end of the copper projectile does in fact move through the aluminum target plate so that the rear end of the debris cloud does have a rather clear forward velocity component.

In addition, equation (51) was also found to yield negative values in some cases where a less dense projectile impacted a more dense target plate. But even in this case, perhaps the negative velocity is that of the back-splash that would undoubtedly occur and which may be significant in such as case. In any event, caution should be exercised when using equation (51) to calculate the velocity of the rear surface of the debris cloud.

5.0 SUMMARY AND RECOMMENDATIONS

A robust lethality assessment methodology must include the effects of discrete particle impacts as well as the response of the target to impulsive debris cloud loadings. A first-order accurate scheme has been implemented to determine the amount of material in each of the three states of matter in a debris cloud created by a hypervelocity impact on a thin target. A modified version of the Tillotson EOS was used to calculate the residual energy in the projectile and target materials upon release from their respective shocked states. Elementary thermodynamic principles were used to determine the percentages of shocked and released projectile and target materials that were melted and/or vaporized during the release process. Using assumed projectile and target geometries, these percentages were then used to calculate the mass of the projectile and target materials in solid, liquid, and gaseous form. Based on the work completed thus far, the following recommendations are offered for continuing the development of a lethality assessment model that would be applicable in impact scenarios where material melt and/or vaporization can be expected to occur.

The next step in the first-order characterization of the debris clouds created in a hypervelocity impact would be to determine the nature of the debris cloud solid fragment population. This includes calculating the number of projectile and target material fragments, as well as their sizes, speeds, and trajectories. In addition to the fragmentation models in FATE-PEN, PEN-4, and KAPP-II, the fragmentation models developed by Grady, et.al. [31-33] can be used to predict the number of fragments that would result from a KEW impact. The predictions of the various fragmentation models can be compared against one another and against available experimental data to

determine which fragmentation model is best suited for use in a lethality assessment methodology. Hypervelocity impact test results for a variety of target systems are available from a number of sources, including NASA [34], NSWC [35], NRL [36], BRL [37], and others [38-44].

After a satisfactory first-order accurate procedure that characterizes debris cloud composition is completed, the accuracy of the procedure needs to be improved. This includes modifying the methods presented herein to include a more appropriate hole diameter predictor equation, the impact of non-monolithic projectiles that are more representative of actual KEW geometries, and the impact of yawed and/or obliquely incident projectiles. Additional modifications to improve the accuracy of the debris cloud calculations are as follows.

First, the method of calculating the percentages of projectile and target material in the three states of matter should also be replaced with a more rigorous thermodynamic procedure. One method (see, e.g. [23]) would require calculating the entropy of the shocked state, that is, the entropy imparted to the material by shocking it to a given pressure. The material will retain that entropy during isentropic release to the final release pressure and specific volume. The calculation is completed by identifying the material state with that entropy at the final release pressure by consulting classical thermodynamic tables (see, e.g. [45,46]).

Second, a shock wave attenuation procedure [47,48] should be implemented to obtain more accurate mass values for the material that is melted and/or vaporized in a high speed KEW impact. Such a procedure will result in a residual energy profile along the length of the projectile and through

the thickness of the target. Energy levels at various positions can then be compared to energy levels necessary to begin material melt or vaporization. In addition, the assumption that the impact pressure acts on an area equal to the area of the hole created in the target plate needs to be reconsidered.

Third, the debris cloud velocity calculation scheme should be expanded to include the radial expansion velocity of the debris cloud. In addition, the calculation of the debris cloud trailing edge velocity should be validated for a greater variety of materials and modified if necessary to more accurately reflect experimental results. A possible method for calculating the radial expansion velocity involves calculating the forward-motion kinetic energy of the debris cloud constituents, adding to it the energy lost during the impact event, and comparing the sum to the kinetic energy of the impacting projectile. Any energy remaining, to first-order, can be said to be responsible for debris cloud expansion.

Fourth, in its present formulation, it is entirely possible that the value of the parameter E_0 in the Tillotson EOS can be different for different impact velocities even when the projectile and target materials are held constant. Since E_0 is part of an EOS and an EOS is a material property, the value of E_0 should be constant and should not depend on impact conditions. If E_0 were to change with a change in impact conditions, this would imply the existence of an EOS surface that also changes with impact conditions, which is not possible [49]. Thus, it is imperative to address the manner in which the value of E_0 is chosen in the application of the Tillotson EOS.

Subsequent to the development of a satisfactory debris cloud character-

ization scheme, an impulsive loading algorithm for the target should be developed to account for the effects of the non-solid debris cloud constituents as well as the solid non-perforating debris cloud fragments. This effort requires as input the masses and velocities of the non-solid debris cloud materials, the area of the inner wall over which the impulsive loading is applied, and the geometric and material properties of the inner wall, including the spacing between the outer and inner walls and the orientation of the inner wall with respect to that of the outer wall. Issues to be addressed include whether the impacts of the target and projectile debris cloud materials need to be considered separately or can be considered simultaneously, whether the effects of the molten and vaporous debris cloud components need to be considered separately or can be combined, and how to account for the decreasing time of the load application and the increasing area over which it is applied as the initial impact velocity increases.

The impulsive loading algorithm can be validated at velocities attainable using existing hypervelocity launchers by comparing the predictions of the algorithm with available impact test data. The algorithm can be modified if necessary until a satisfactory level of accuracy is reached. It can then be combined with the debris cloud characterization scheme and a suitable fragmentation model to yield an improved, robust lethality assessment method for high speed KEW impacts.

6.0 REFERENCES

1. Anderson, C.E., Trucano, T.G., and Mullin, S.A., "Debris Cloud Dynamics", *Int. J. Impact Engng.*, Vol. 9, No. 1, pp. 89-113, 1990.
2. Hopkins, A.K., Swift, H.F., and Lee, T.W., "Material Phase Transformations Effects Upon Performance of Spaced Bumper Systems", *J. Spacecraft Rockets*, Vol. 9, No. 5, pp. 342-345, 1972.
3. Idzorek, G.C., Keaton, P.W., Stradling, G.L., Callopy, M.T., Curling, H.L., and McColl, D.B., "Data Acquisition System for a Hypervelocity-Microparticle-Impacts Laboratory", *Int. J. Impact Engng.*, Vol. 10, pp. 261-270, 1990.
4. Iglseider, H., and Idenbergs, E., "Crater Morphology at Impact Velocities Between 8 and 17 km/sec", *Int. J. Impact Engng.*, Vol. 10, pp. 271-280, 1990.
5. Osher, J., Gathers, R., Chau, H., Lee, R., Pomykal, G., and Weingart, R., "Hypervelocity Acceleration and Impact Experiments with the LLNL Electric Guns", *Int. J. Impact Engng.*, Vol. 10, pp. 439-452, 1990.
6. Yatteau, J.D., High Velocity Multiple Plate Penetration Model, NSWC-TR-82-123, Dahlgren, Virginia, 1982.
7. Yatteau, J.D., Modifications to Program FATE - Fragment Residual Mass Calculations, Final Report, Denver Research Institute, University of Denver, Denver, Colorado, 1983.
8. Yatteau, J.D., Zernow, R.H., and Recht, R.F., Compact Fragment Multiple Plate Penetration Model, Volume I: Model Description, NSWC-TR-91-399, Dahlgren, Virginia, 1991.
9. Yatteau, J.D., Zernow, R.H., and Recht, R.F., Compact Fragment Multiple Plate Penetration Model, Volume II: Computer Code User's Manual, NSWC-TR-91-399, Dahlgren, Virginia, 1991.
10. Penetration Mechanics Handbook for Kinetic Energy Penetrators, 61-JTCG/ME-77-16-Rev-1, 1977.
11. Greer, R., and Hatz, M., KAPP-II user's Manual, Version 1.1, Kaman Sciences Corporation, K92-17U(R), Colorado Springs, Colorado, 1992.
12. Snow, P., KAPP - Kaman Analytical Penetration Program, Kaman Sciences Corporation, K85-7U(R), Colorado Springs, Colorado, 1985.
13. Cohen, L., Kaman New Analytical Penetration Program (KNAPP) Space-Based Interceptor Modelling Effort, AFATL-TR-90-02, Eglin AFB, Florida, 1990.
14. Lundeberg, J.F., Stern, P.H., Bristow, J.R., Meteoroid Protection for Spacecraft Structures, NASA-CR-54201, Washington, D.C., 1965.
15. Burch, G.T., Multi-Plate Damage Study, AFATL-TR-67-116, Eglin AFB, Florida, 1967.

16. Henderson, B.J., and Zimmerschied, A.B., Very High Velocity Penetration Model, NSWC-TR-83-189, Dahlgren, Virginia, 1983.
17. Bjorkman, M.D., Geiger, J.D., and Wilhelm, E.E., Space Station Integrated Wall Design and Penetration Damage Control, Task 3: Theoretical Analysis of Penetration Mechanics, Boeing Aerospace Corporation, Final Report, Contract NAS8-36426, Seattle, Washington, 1987.
18. Swift, H.F., Bamford, R., and Chen, R., "Designing Space Vehicle Shields for Meteoroid Protection: A New Analysis", *Adv. Space Research*, Vol. 2, No. 12, 1983, pp 219-234.
19. Richardson, A.J., "Theoretical Penetration Mechanics of Multi-Sheet Structures Based on Discrete Debris Particle Modelling", *J. Spacecraft*, Vol. 7, No. 4, 1970, pp 486-489.
20. Swift, H.F., "On Predicting Projectile Breakup During Thin Plate Impact", *Int. J. Impact Engng.*, Vol. 10, 1990, pp. 579-585.
21. Grady, D.E., and Passman, S.L., "Stability and Fragmentation of Ejecta in Hypervelocity Impact", *Int. J. Impact Engng.*, Vol. 10, 1990, pp. 197-212.
22. Lawrence, R.J., "A Simple Model for the Optimization of Stand-Off Hypervelocity Particle Shields", *Int. J. Impact Engng.*, Vol. 5, 1987, pp. 451-461.
23. Bjork, R.L., Vaporization and SDI Lethality, DNA-TR-89-28, Alexandria, Virginia, 1990.
24. Rice, M.H., McQueen, R.G., and Walsh, J.M., "Compression of Solids by Strong Shock Waves", Solid State Physics, Vol. 6, Seitz, F. and Turnbull, D., eds., Academic Press, New York, 1958.
25. Tillotson, J.H., Metallic Equations of State for Hypervelocity Impact, General Dynamics, General Atomic Division, Report No. GA-3216, 1962.
26. Mullin, S.A., Littlefield, D.L., Anderson, C.A., Velocity Scaling for Lethality Applications, Southwest Research Institute, Final Report, Project No. 06-4438, 1992.
27. Holian, K., and Burkett, M.W., "Sensitivity of Hypervelocity Impact Simulations to Equations-of-State", *Int. J. Impact Engng.*, Vol. 5, pp. 331-341, 1987.
28. Maiden, C.J., Gehring, J.W., and McMillan, A.R., Investigation of Fundamental Mechanism of Damage to Thin Targets by Hypervelocity Projectiles, General Motors Defense Research Laboratory, TR-63-225, Santa Barbara, California, 1963.
29. Herrmann, W., and Wilbeck, J.S., "Review of Hypervelocity Impact Penetration Theories", *Int. J. Impact Engng.*, Vol. 5, pp. 307-322, 1987.
30. Piekutowski, A.J., "A Simple Dynamic Model for the Formation of Debris

- Clouds", Int. J. Impact Engng., Vol. 10, 1990, pp. 453-471.
31. Grady, D.E., "Local Inertial Effects in Dynamic Fragmentation", J. Appl. Phys., Vol. 53, No. 1, 1982, pp. 322-325.
32. Grady, D.E., "Fragmentation of Solids Under Impulsive Stress Loading", J. Geophys. Res., Vol. 86, No. B2, 1981, pp. 1047-1054.
33. Grady, D.E., and Kipp, M.E., "Geometric Statistics and Dynamic Fragmentation", J. Appl. Phys., Vol. 58, No. 3, 1985, pp. 1210-1222.
34. Schonberg, W.P., Bean, A.J., and Darzi, K., Hypervelocity Impact Physics, NASA-CR-4343, Washington, D.C. 1991.
35. Dickinson, D., Investigation of High Velocity Fragments Impacting Plate Arrays, NSWC-TR-79-66, 1979.
36. Williams, A.E., and Saravane, I., Debris Characterization Study, NRL Letter Report 4680-196, 1990.
37. Wenzel, A.E., and Dean, J.K., Behind Armor Spallation Tests, BRL-CR-262, 1975.
38. Watson, R.W., "The Perforation of Thin Plates by High Velocity Fragments", Proceedings of the Fifth Hypervelocity Impact Symposium, Vol. 1, Pt. 2, Colorado School of Mines, Denver, Colorado, 1961, pp. 581-592.
39. Spells, K.E., "Velocities of Steel Fragments After Perforation of a Steel Plate", Proc. Phys. Soc. (London), Vol. B64, 1951, pp. 212-218.
40. Swift, H.F., Praonias, D.D., and Turpin, W.C., "Debris Clouds Behind Plates Impacted by Hypervelocity Pellets", J. Spacecraft, Vol. 7, No. 3, 1970, pp. 313-318.
41. Piekutowski, A.J., "Properties of Largest Fragment Produced by Hypervelocity Impact of Aluminum Spheres with Thin Aluminum Sheets", AIAA Space Programs and Technology Conference, Huntsville, Alabama, Paper No. 92-1588, 1992.
42. Stilp, A.J., Hohler, V., Schneider, E., and Weber, K., "Debris Cloud Expansion Studies", Int. J. Impact Engng., Vol. 10, 1990, pp. 543-553.
43. Klopp, R.W., Shockey, D.A., Osher, J.E., and Chau, H.H., "Characteristics of Hypervelocity Impact Debris Clouds", Int. J. Impact Engng., Vol. 10, 1990, pp. 323-335.
44. Finnegan, S.A., Schulz, J.C., and Heimdahl, O.E.R., "Spatial Fragment Mass and Velocity Distributions", Int. J. Impact Engng., Vol. 10, 1990, pp. 159-170.
45. Stull, D.R., and Prophet, H., JANAF Thermochemical Tables, Second Edition, U.S. Department of Commerce, National Bureau of Standards, Washington, D.C., 1971.

46. Stull, D.R., and Sinke, G.C., "Thermodynamic Properties of the Elements", in Advances in Chemistry, No. 18, American Chemical Society, Washington, D.C., 1956.

47. Fowles, G.R., "Attenuation of the Shock Wave Produced in a Solid by a Flying Plate", J. Appl. Phys., Vol. 31, No. 4, 1960, pp. 655-661.

48. Cohen, L., "Integrated Technology Support for Debris Cloud Material State Modelling", Science Applications International Corporation, Tech. Inf. Memo. WU4/TIM92-2, Shalimar, Florida, 1992.

49. Hoffman, M., Hypervelocity Impact Debris Cloud Characterization, Science Applications International Corporation, Tech. Memo. WU4/TM92-1, Shalimar, Florida, 1992.

50. Mullin, S.A., Private Communication, 1992.

Table 1. Material Mechanical Properties

MATERIAL	C (km^9/s)	k	ρ (gm/cm^3)	BHN (kg/mm^2)	E (GPa)	ν
ALUMINUM	5.380	1.34	2.71	120	71.0	0.35
BERYLLIUM	7.975	1.12	1.82	120	290.0	0.08
CADMIUM	2.307	1.64	8.64	24	46.2	0.33
COPPER	3.940	1.49	8.93	37	131.0	0.34
GOLD	3.060	1.57	19.24	33	85.5	0.42
IRON	4.580	1.49	7.87	95	200.0	0.30
LEAD	2.030	1.47	11.34	7	13.8	0.45
MAGNESIUM	4.490	1.24	1.74	45	44.1	0.29
MOLYBDENUM	5.173	1.22	10.20	200	317.2	0.31
NICKEL	4.667	1.53	8.86	200	227.5	0.30
PLATINUM	3.680	1.50	21.37	70	191.0	0.39
SILVER	3.230	2.50	10.49	25	82.7	0.37
4340 STEEL	4.570	1.55	7.83	290	200.0	0.30
TANTALUM	3.374	1.20	16.65	200	179.3	0.35
TIN	2.560	1.52	7.28	4	41.4	0.33
TITANIUM	4.786	1.05	4.51	330	124.1	0.30
TUNGSTEN	4.150	1.24	19.17	400	406.8	0.30
ZINC	3.042	1.50	7.14	82	74.5	0.33

Table 2. Material Thermal Properties

MATERIAL	Γ_o	α ($\times 10^{-4}/^{\circ}\text{C}$)	C_P (cal/gm $^{\circ}\text{C}$)	T_m ($^{\circ}\text{C}$)	T_v ($^{\circ}\text{C}$)	H_f (cal/gm)	H_v (cal/gm)
ALUMINUM	2.13	0.240	0.235	660	2450	95	2450
BERYLLIUM	1.16	0.140	0.570	1281	2884	260	8195
CADMIUM	2.27	0.343	0.058	321	765	13	212
COPPER	2.00	0.170	0.097	1083	2590	49	1150
GOLD	3.10	0.161	0.034	1063	2960	16	413
IRON	1.57	0.120	0.120	1539	3035	65	1591
LEAD	2.77	0.293	0.031	327	1740	6	210
MAGNESIUM	1.50	0.300	0.295	650	1110	88	1326
MOLYBDENUM	1.52	0.061	0.079	2610	5555	70	1242
NICKEL	1.80	0.143	0.130	1454	2865	74	1523
PLATINUM	2.94	0.110	0.037	1769	4349	26	632
SILVER	2.50	0.211	0.062	961	2210	25	554
4340 STEEL	1.67	0.112	0.110	1510	3070	65	1590
TANTALUM	1.69	0.065	0.033	2996	5425	38	1007
TIN	1.85	0.269	0.058	235	2450	14	580
TITANIUM	1.10	0.100	0.150	1676	3260	99	2182
TUNGSTEN	1.48	0.040	0.035	3410	5900	53	1054
ZINC	2.15	0.274	0.100	420	907	25	420

Table 3. Values of V_s for Materials Considered

MATERIAL	Initial E_o Multiplier ¹	α	β	v (km ³ /s)	V (cm ³ /gm)	V (cm ³ /gm)	V_s/V_o
ALUMINUM	1.1	5.0	5.0	10.2	0.369	0.424	1.149
BERYLLIUM	1.0	5.0	5.0	17.3	0.549	0.620	1.129
CADMIUM	1.0	5.0	5.0	3.2	0.116	0.128	1.106
COPPER	1.0	10.0	10.0	7.1	0.112	0.130	1.161
GOLD	0.3	10.0	10.0	5.3	0.052	0.060	1.154
IRON	1.0	10.0	10.0	7.8	0.127	0.145	1.141
LEAD	0.3	10.0	10.0	3.5	0.088	0.101	1.148
MAGNESIUM	1.0	5.0	5.0	7.4	0.575	0.626	1.089
MOLYBDENUM	0.5	10.0	10.0	9.4	0.098	0.109	1.112
NICKEL	1.0	10.0	10.0	8.5	0.113	0.133	1.177
PLATINUM	0.2	10.0	10.0	6.1	0.047	0.053	1.128
SILVER	1.0	10.0	10.0	4.6	0.095	0.122	1.284
TANTALUM	0.2	10.0	10.0	6.0	0.060	0.067	1.116
TIN	1.0	10.0	10.0	4.9	0.137	0.163	1.187
TITANIUM	0.3	10.0	10.0	9.0	0.222	0.238	1.072
TUNGSTEN	0.3	10.0	10.0	6.6	0.052	0.057	1.096
ZINC	1.0	10.0	10.0	4.5	0.140	0.155	1.107

¹Initial E_o Guess Based on E_o (J/kg) = $2.56 \times 10^{-4} A^{0.94}$, $A = \rho_o c_o^2$ (N/m²) [50]

Table 4. Debris Cloud Velocities: Comparison with Experimental Results and 1-D Hydrocode Predictions

t_s (mm)	M_p (gms)	v_0 (km/s)	v_F/v_0			v_I/v_0			v_R/v_0		
			SWAP ¹	EXP ²	WPS ³	SWAP ¹	EXP ²	WPS ³	SWAP ¹	EXP ²	WPS ³
Effect of Bumper Thickness											
1.0	1.0	6.39	1.44	1.41	1.40	0.91	0.89	0.71	0.36	0.34	0.35
1.5	1.0	6.36	1.44	1.41	1.40	0.88	0.83	0.57	0.36	0.34	0.34
2.0	1.0	6.38	1.42	1.41	1.40	0.83	0.79	0.46	0.35	0.34	0.34
2.5	1.0	6.53	1.46	1.41	1.40	0.79	0.76	0.37	0.35	0.34	0.33
Effect of Impact Velocity											
1.5	1.0	3.45	1.37	1.39	1.39	0.86	0.84	0.68	0.43	0.36	0.36
1.5	1.0	4.85	1.43	1.40	1.39	0.87	0.84	0.63	0.39	0.35	0.35
1.5	1.0	6.36	1.44	1.41	1.40	0.88	0.83	0.57	0.36	0.34	0.34
Effect of Projectile Mass											
2.0	1.0	6.38	1.42	1.41	1.40	0.83	0.79	0.46	0.35	0.34	0.34
2.9	3.0	5.66	1.44	1.40	1.40	0.82	0.80	0.48	----	0.34	0.34
4.4	10.0	5.12	1.40	1.40	1.39	0.83	0.80	0.50	0.36	0.35	0.35

¹1-D Hydrocode Results from Reference 30.

²Experimental Results from Reference 30.

³Numerical Results Obtained Using DEBCLD.

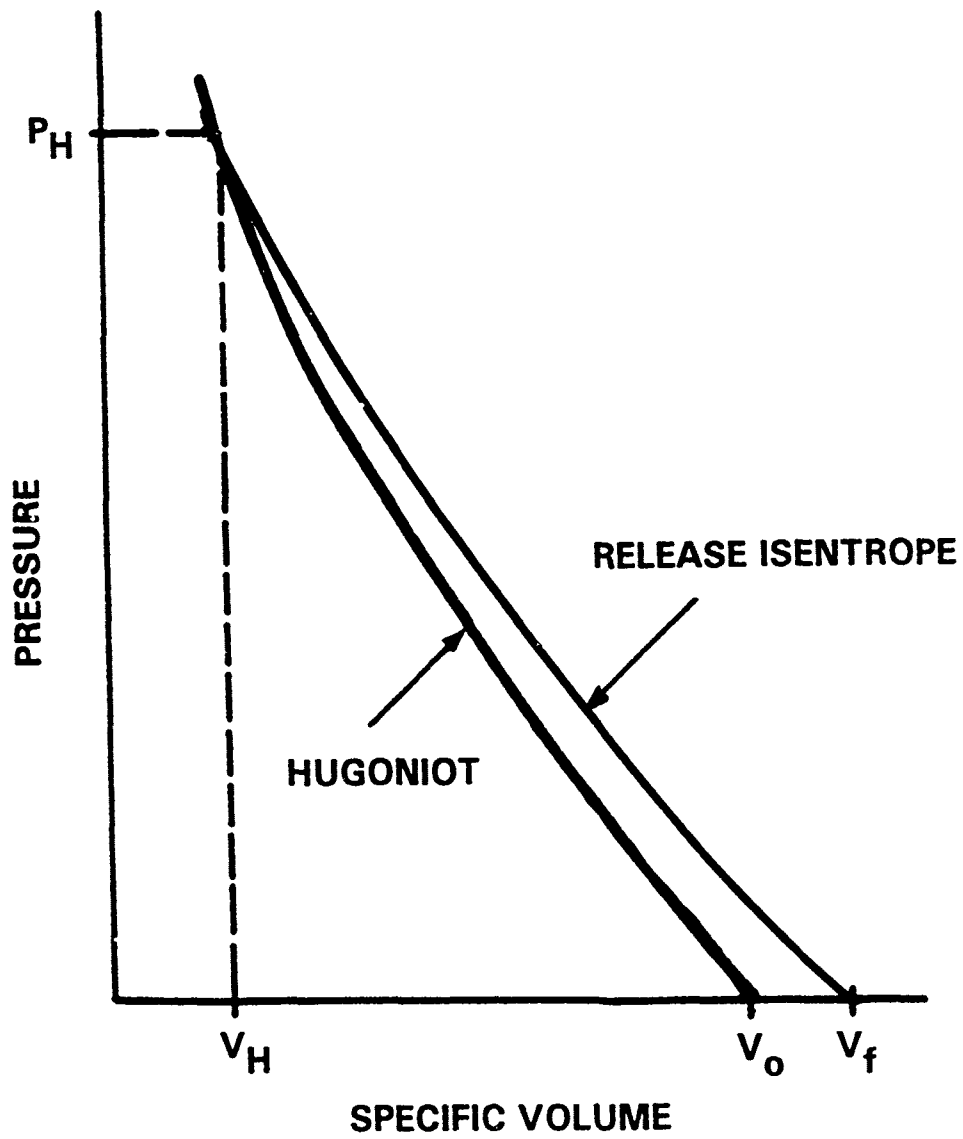


Figure 1. Generic Hugoniot and Release Isentrope

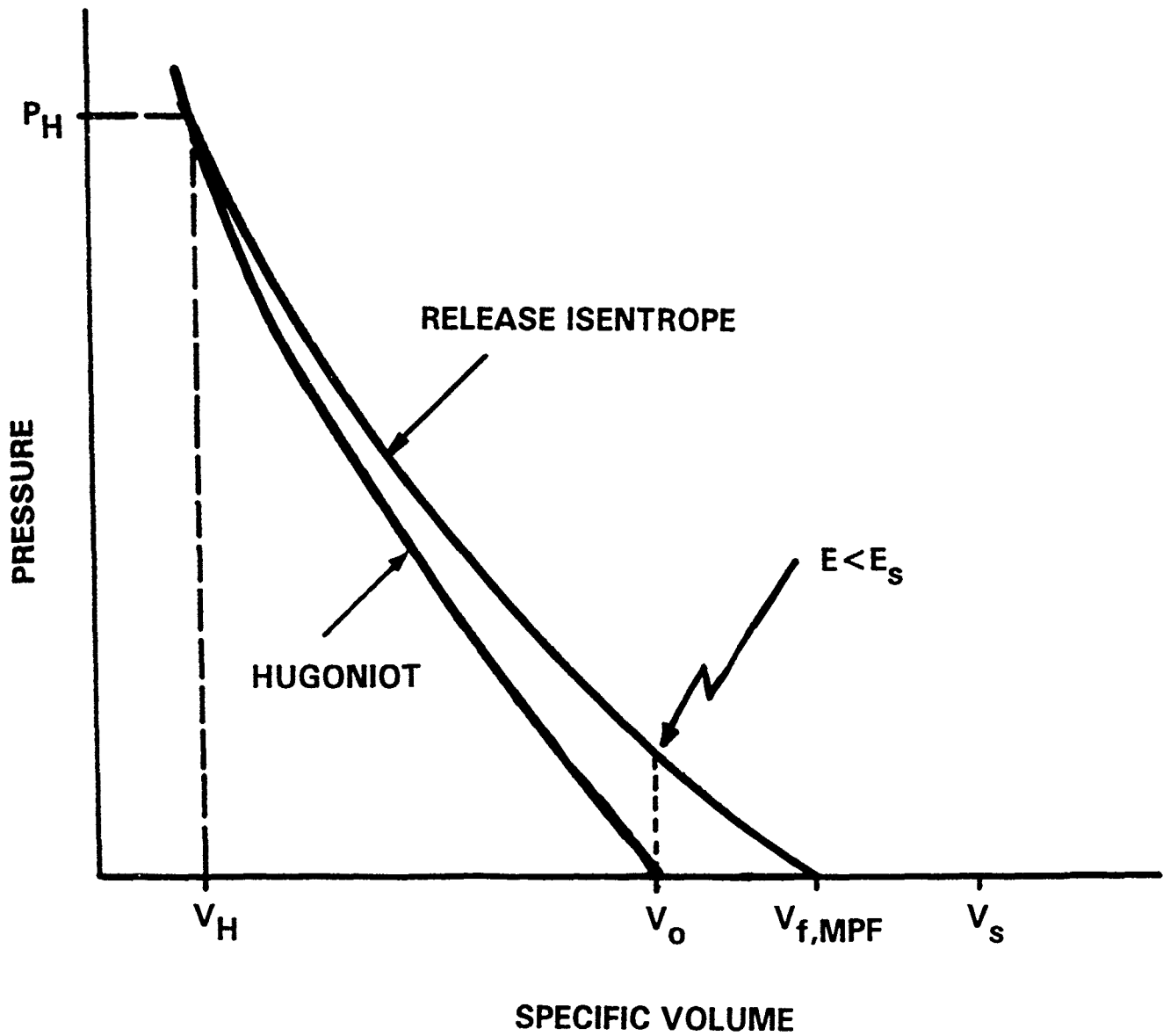


Figure 2a. Tillotson Equation-of-State with Mixed Phase Formulation and $E < E_S$

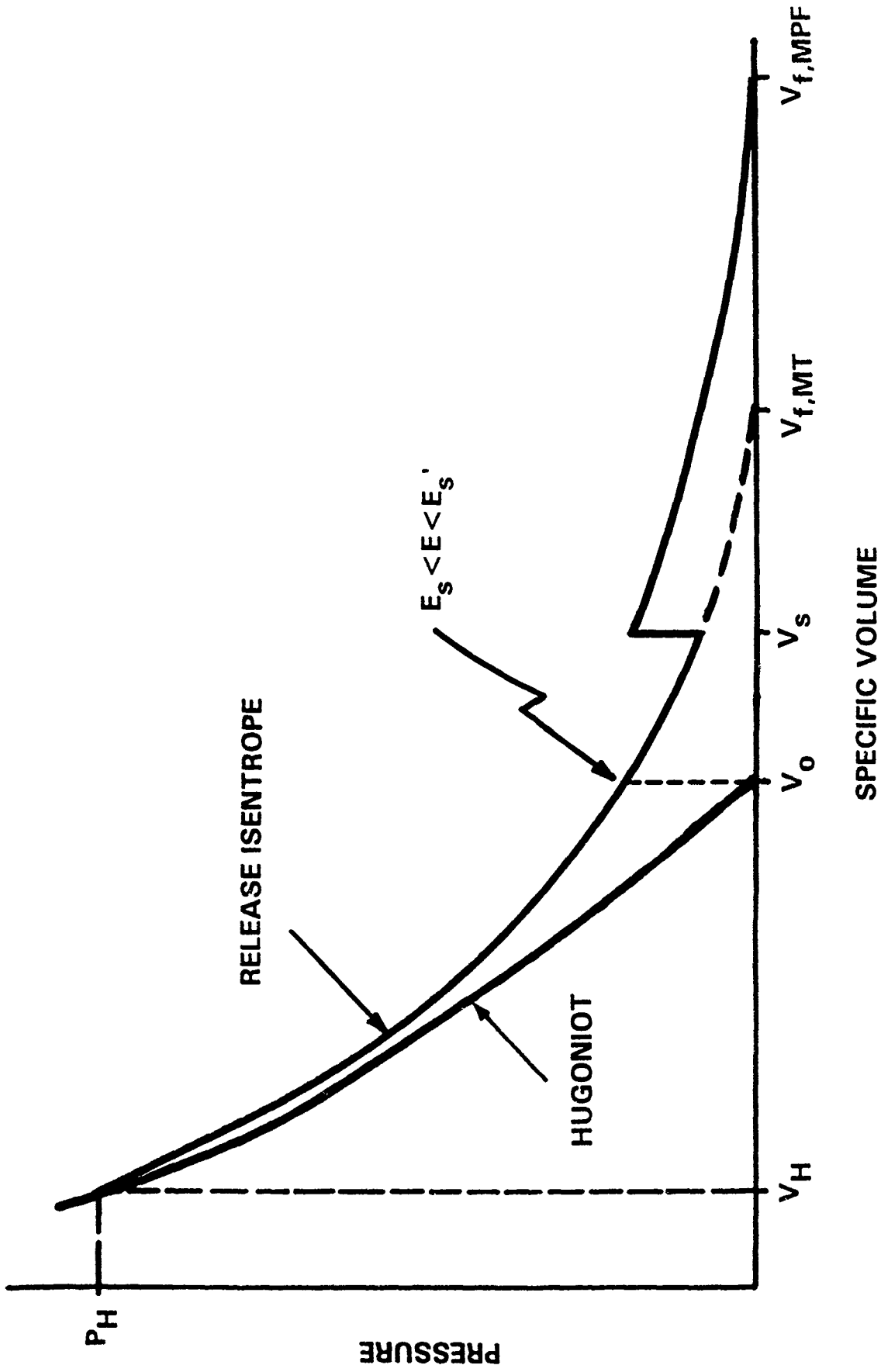


Figure 2b. Tillotson Equation-of-State with Mixed Phase Formulation and $E_S < E < E'_S$

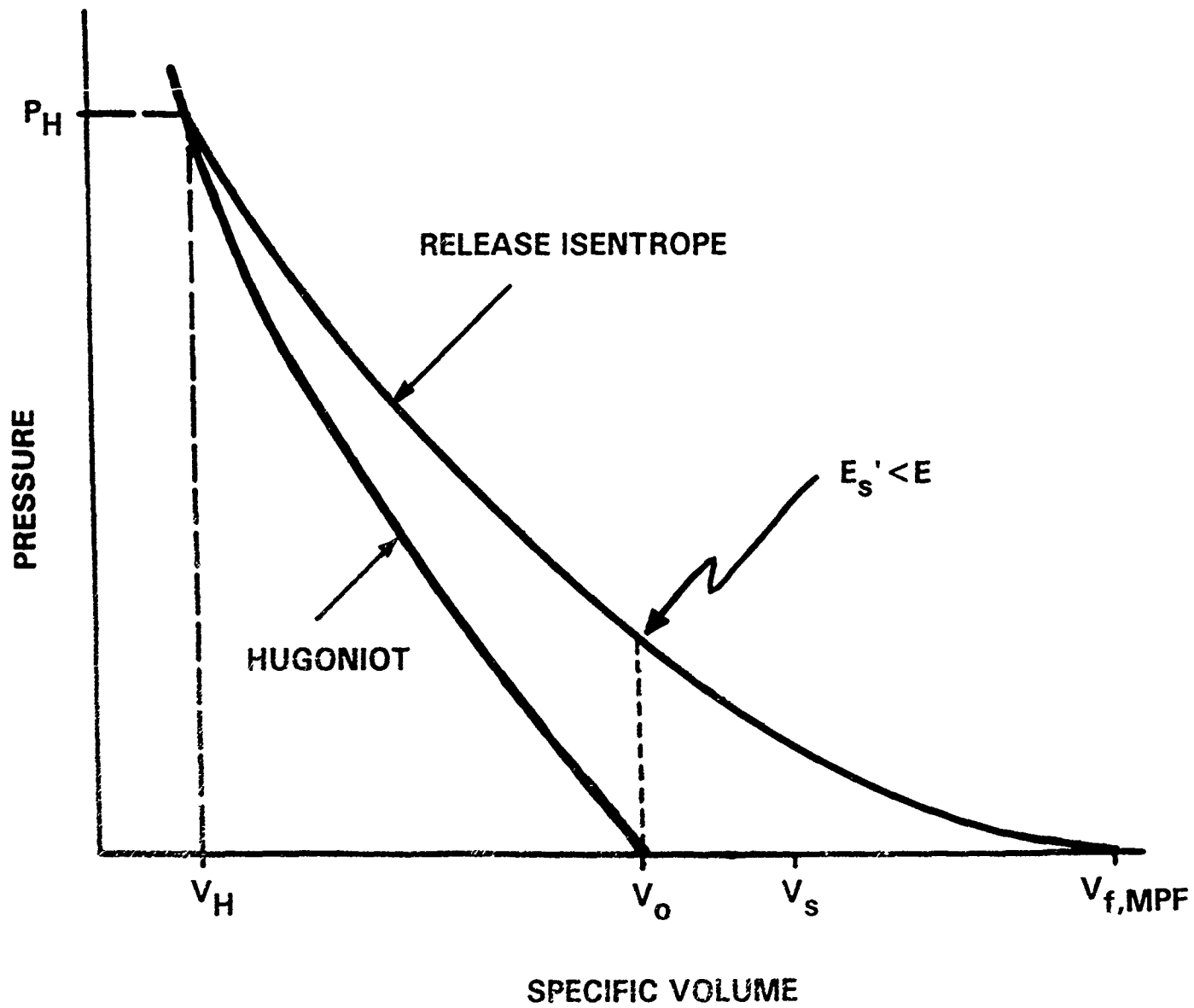


Figure 2c. Tillotson Equation-of-State with Mixed Phase Formulation and $E_S' < E$

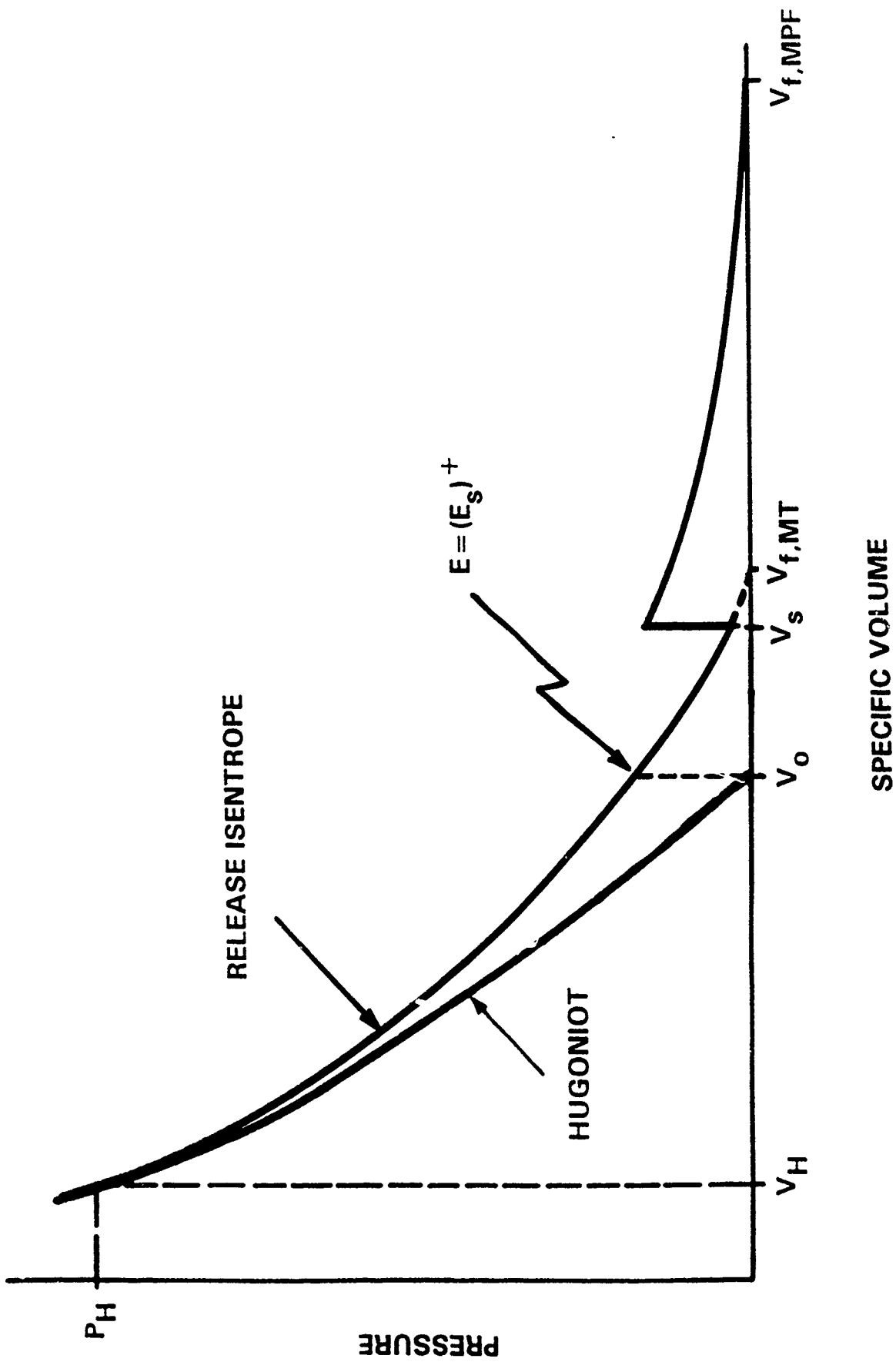


Figure 3a. Modified Tillotson Equation-of-State with $E = (E_s)^+$

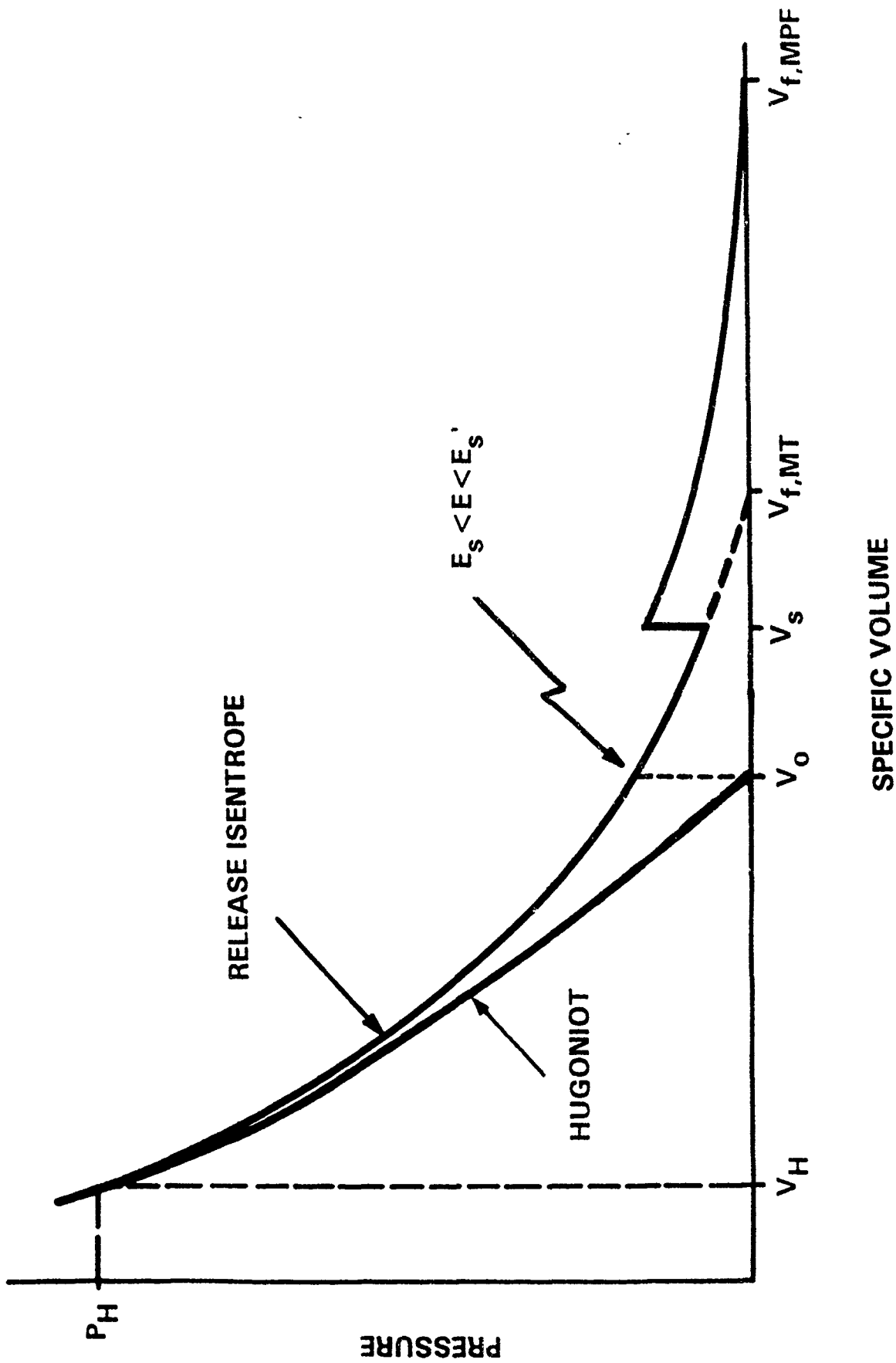


Figure 3b. Modified Tillotson Equation-of-State with and $E_S < E < E_S'$

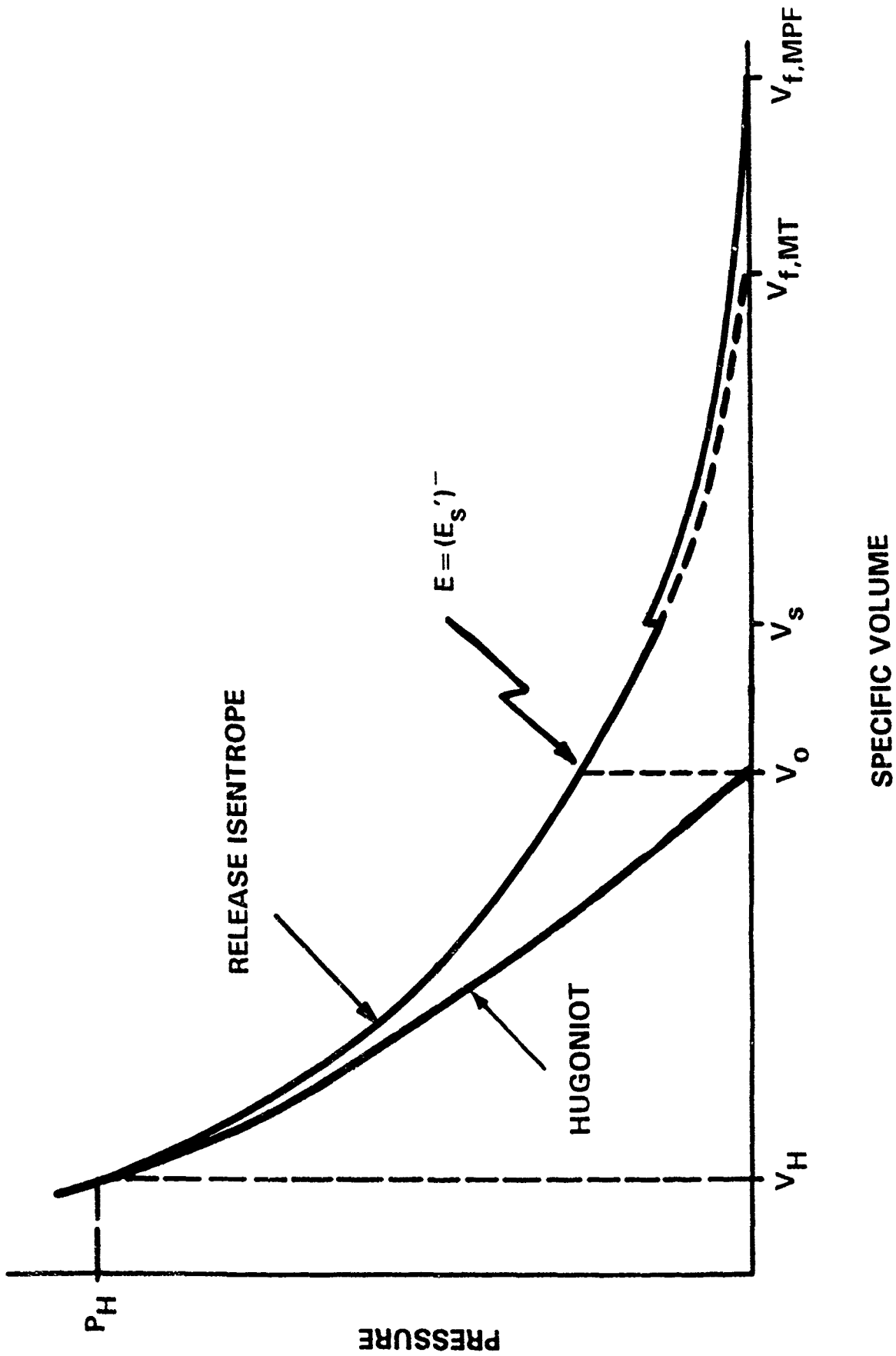


Figure 3c. Modified Tillotson Equation-of-State with $E = (E'_S)^-$

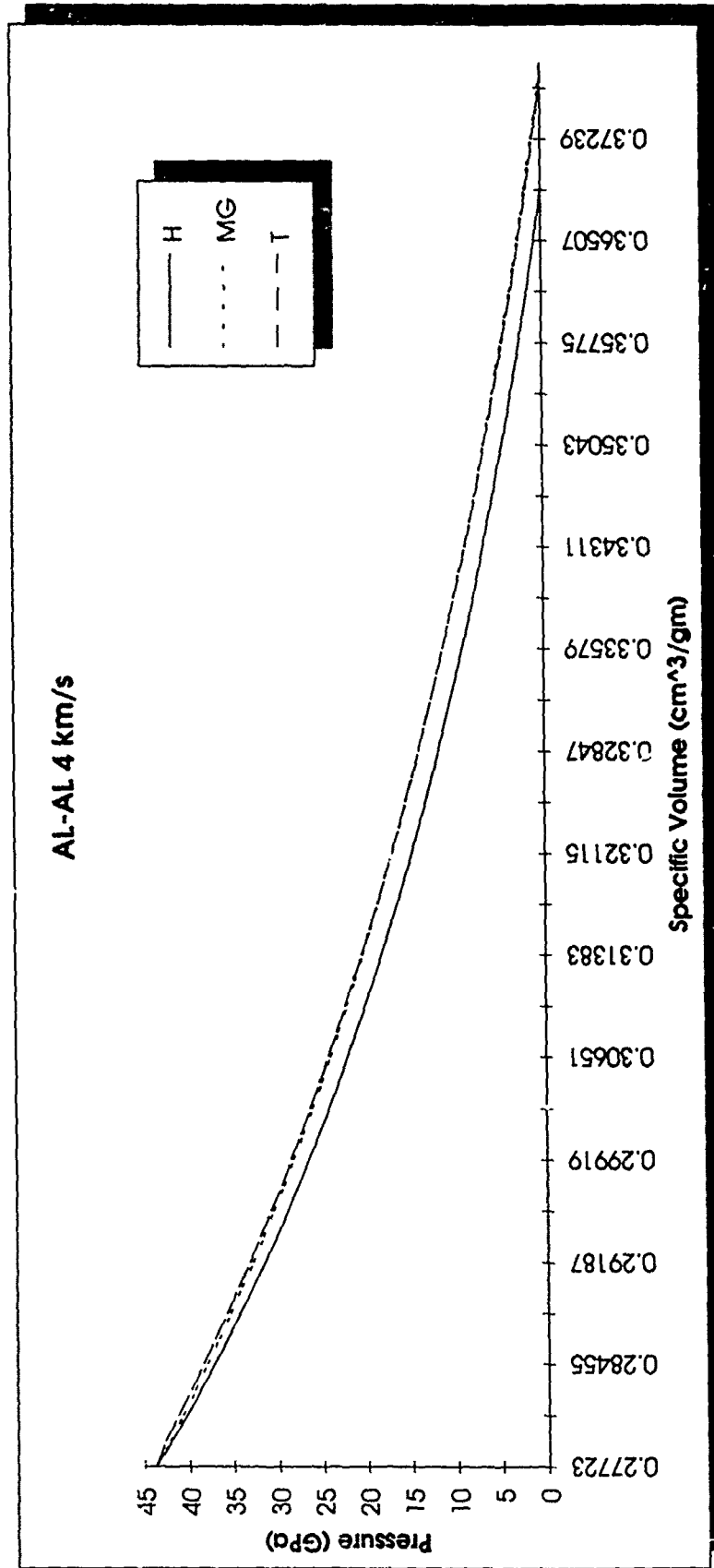


Figure 4. Low Energy Impact Shock Loading and Release Curves (H ... Hugoniot, MG ... Mie-Gruneisen EOS Release Isentrope, T ... Tillotson EOS Release Isentrope)

AL-AL 25 km/s

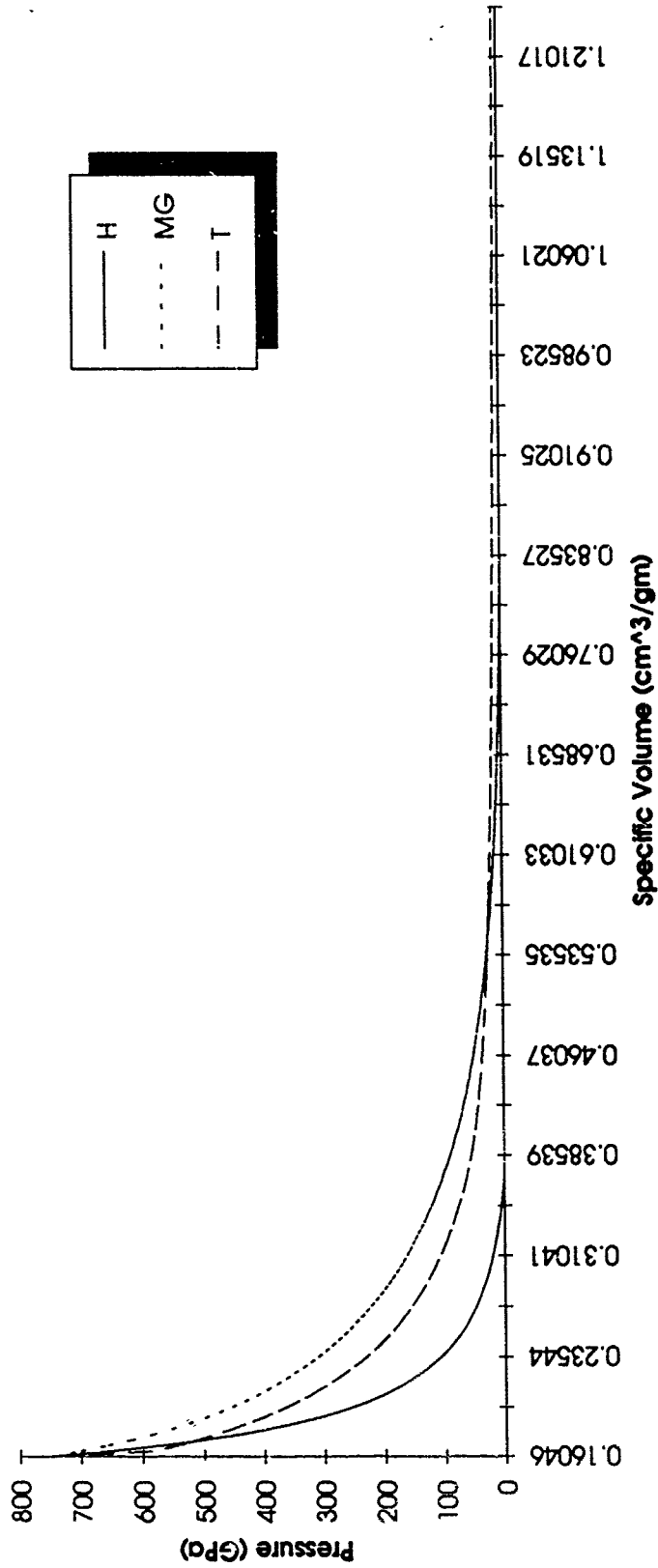


Figure 5. High Energy Impact Shock Loading and Release Curves (H ... Hugoniot, MG ... Mie-Grüneisen EOS Release Isentrope, T ... Tillotson EOS Release Isentrope)

AL-AL 10 km/s

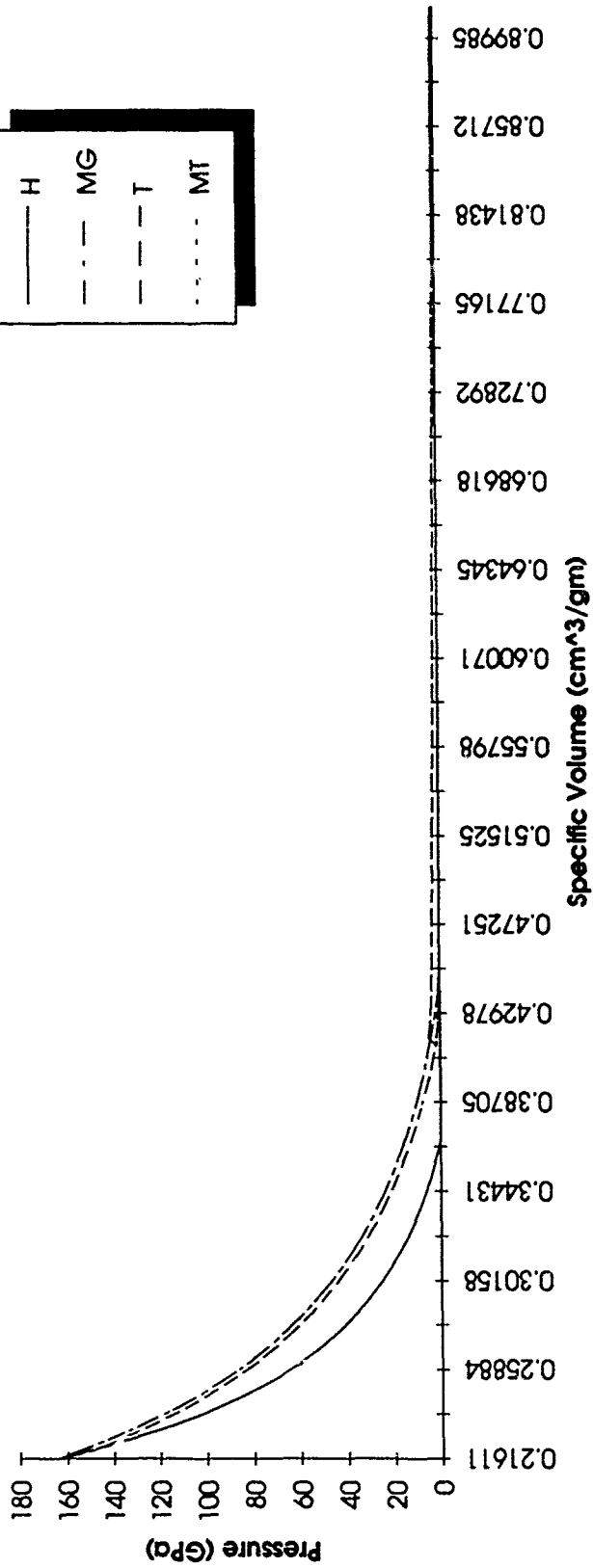


Figure 6. Moderate Energy Impact Shock Loading and Release Curves (H ... Hugoniot, MG ... Mie-Gruneisen EOS Release Isentrope, T ... Tillotson EOS Release Isentrope, MT ... Modified Tillotson EOS Release Isentrope)

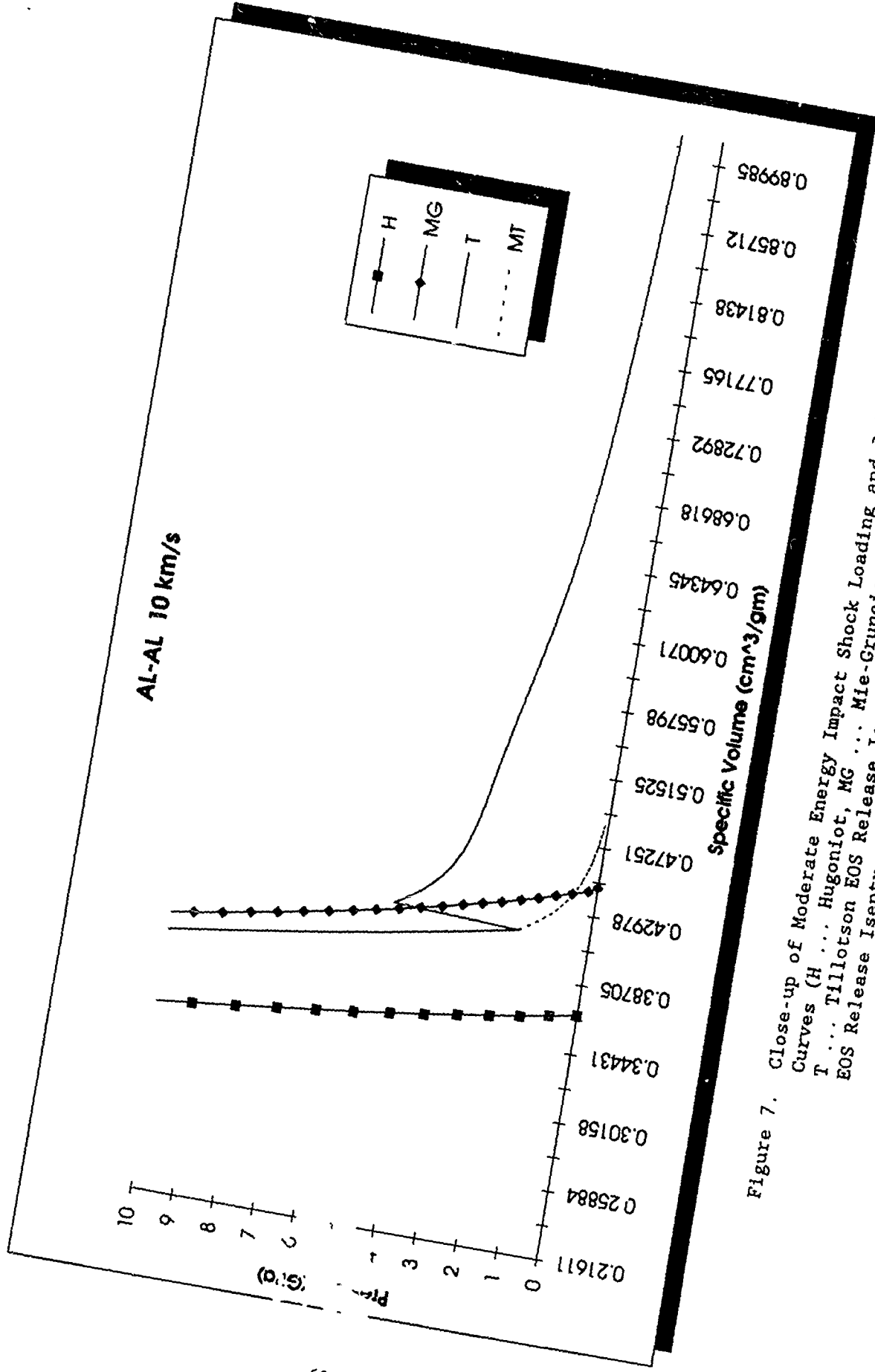


Figure 7. Close-up of Moderate Energy Impact Shock Loading and Release Curves (H ... Hugoniot, MG ... Tillotson EOS Release Isentrope, T ... Tillotson EOS Release Isentrope, MT ... Modified Tillotson EOS Release Isentrope)

AL-AL VI Data

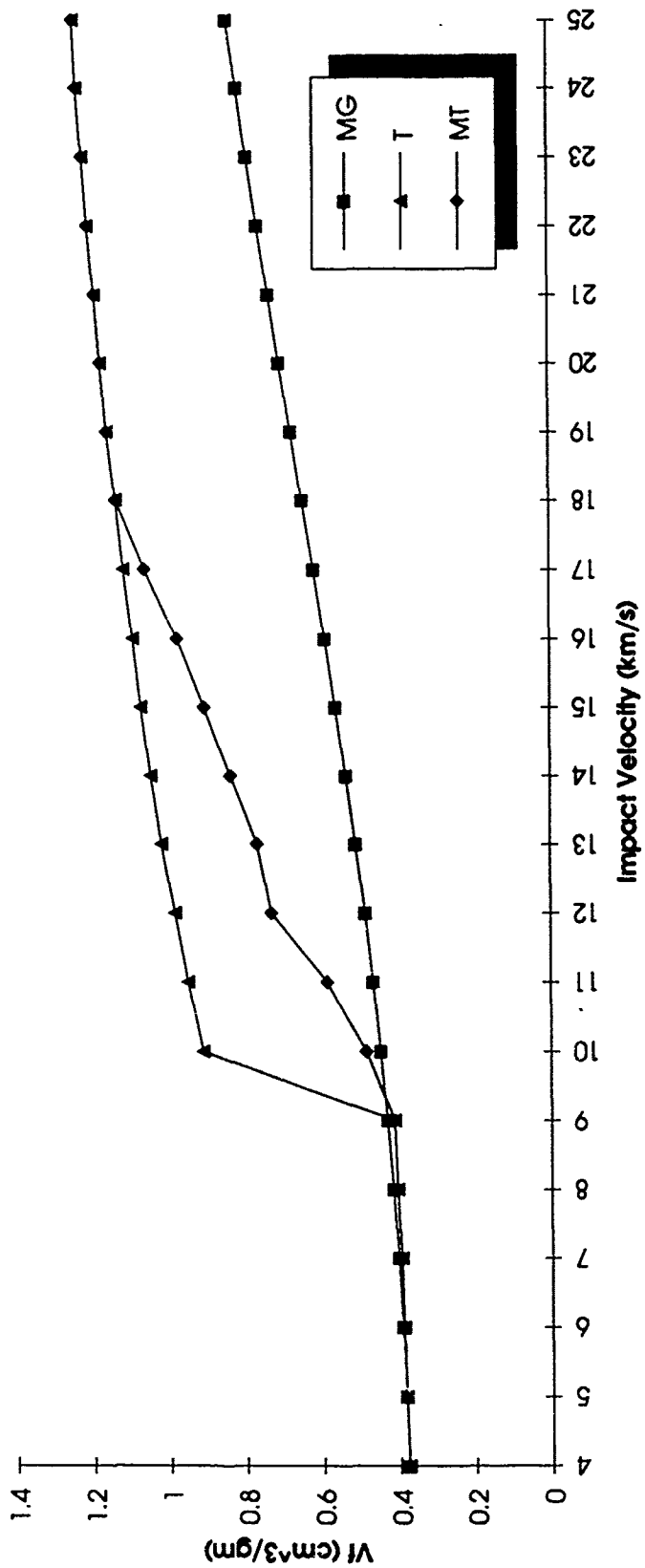
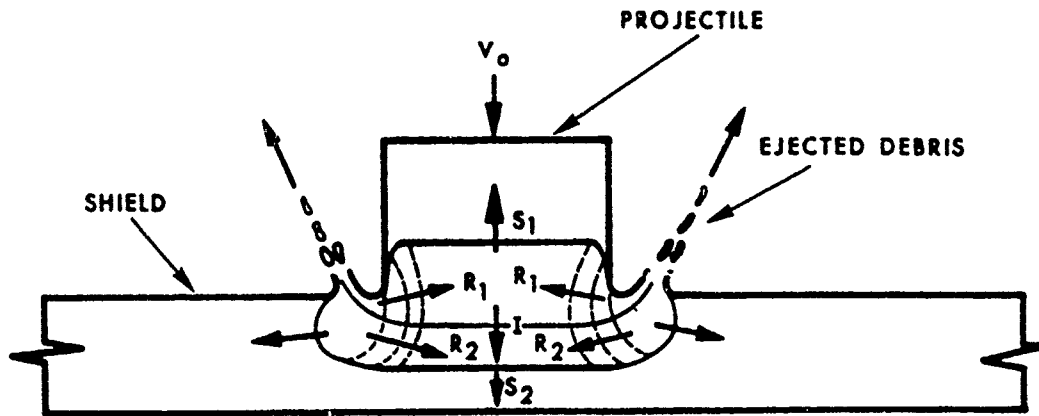
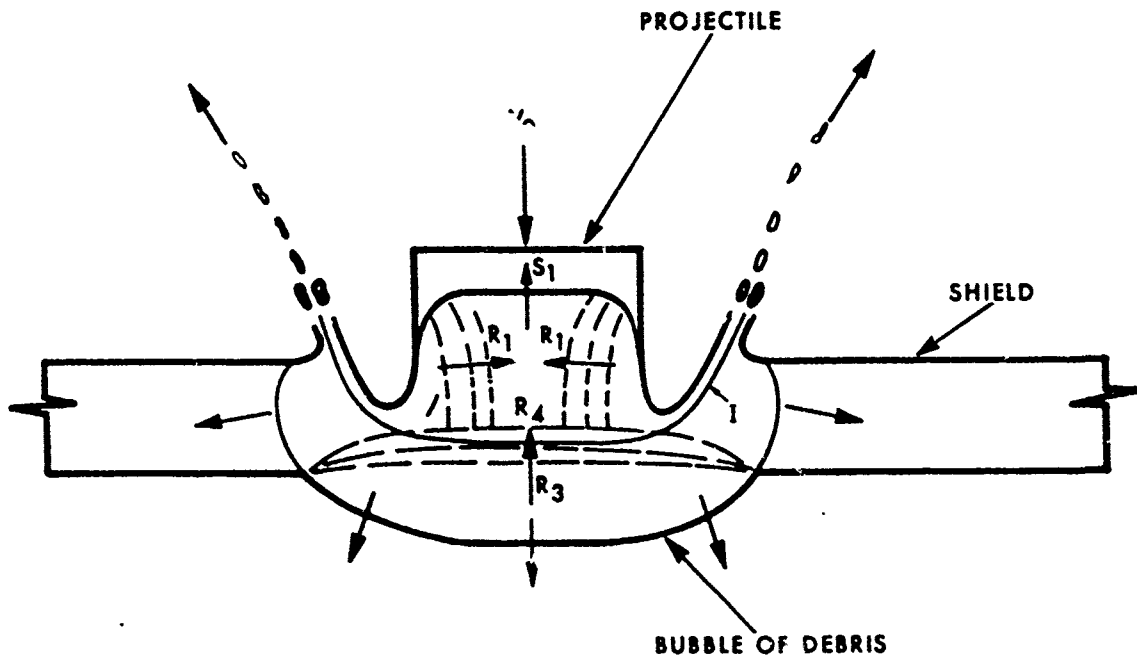


Figure 8. Final Specific Volume vs. Impact Velocity (MG ... Mie-Gruneisen EOS Values, T ... Tillotson EOS Values, MT ... Modified Tillotson EOS Values)



(a) In a Projectile and Shield Soon After Impact



(b) After the Shock in the Shield Has Reflected From the Bottom Face of the Shield

Figure 9. Wave Patterns in a Projectile and an Impacted Target [28]

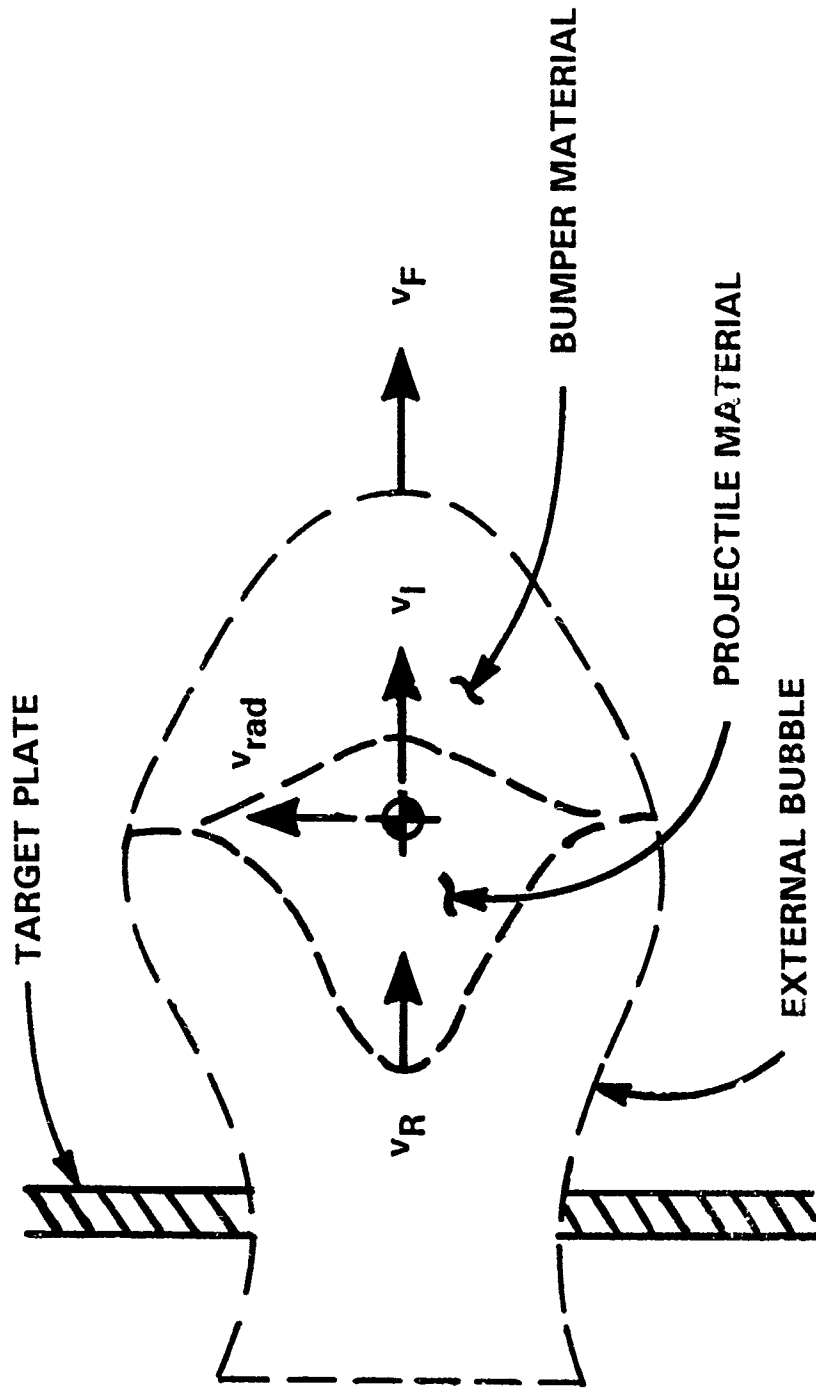


Figure 10 Debris Cloud Velocities [30]

Debris Cloud Composition, Mie-Grüneisen Release

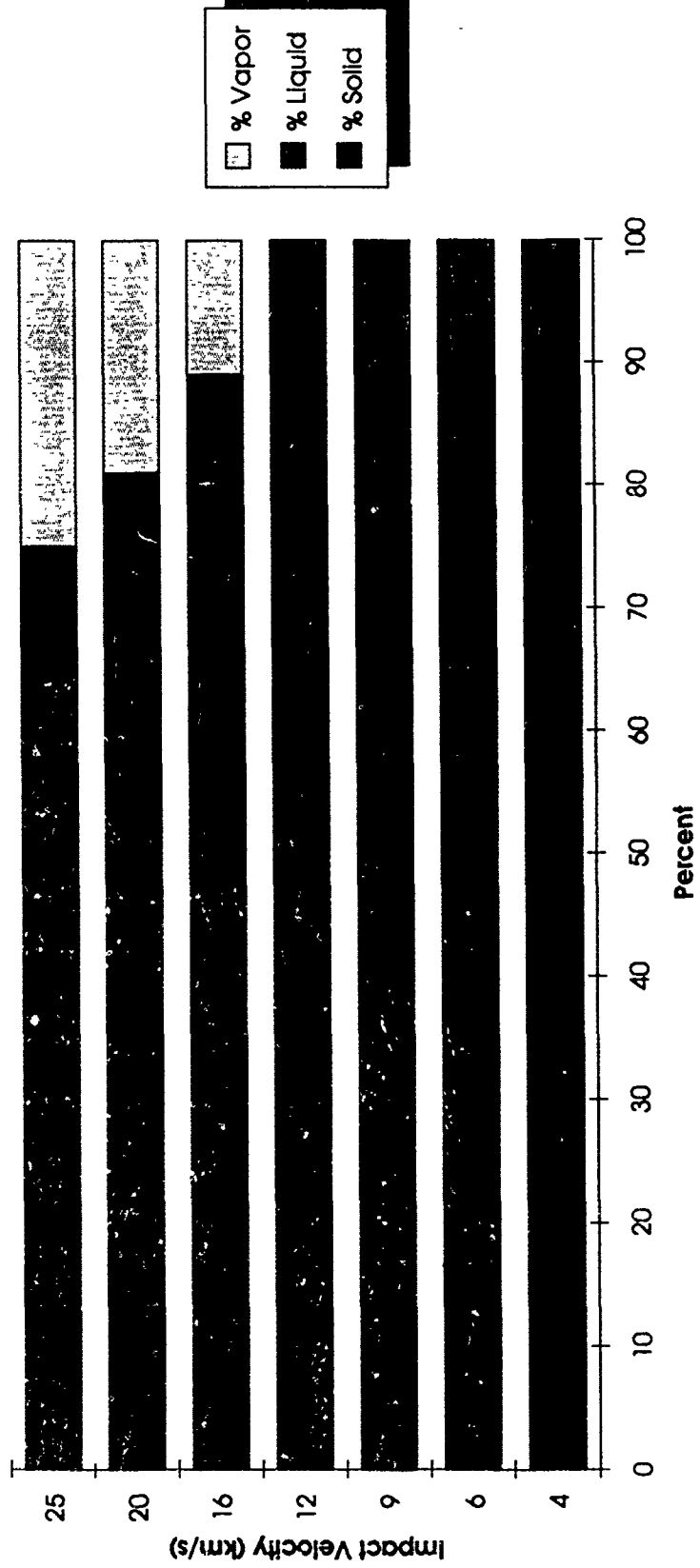


Figure 11. Debris Cloud Material Composition Using the Mie-Grüneisen EOS, Aluminum-on-Aluminum Impact

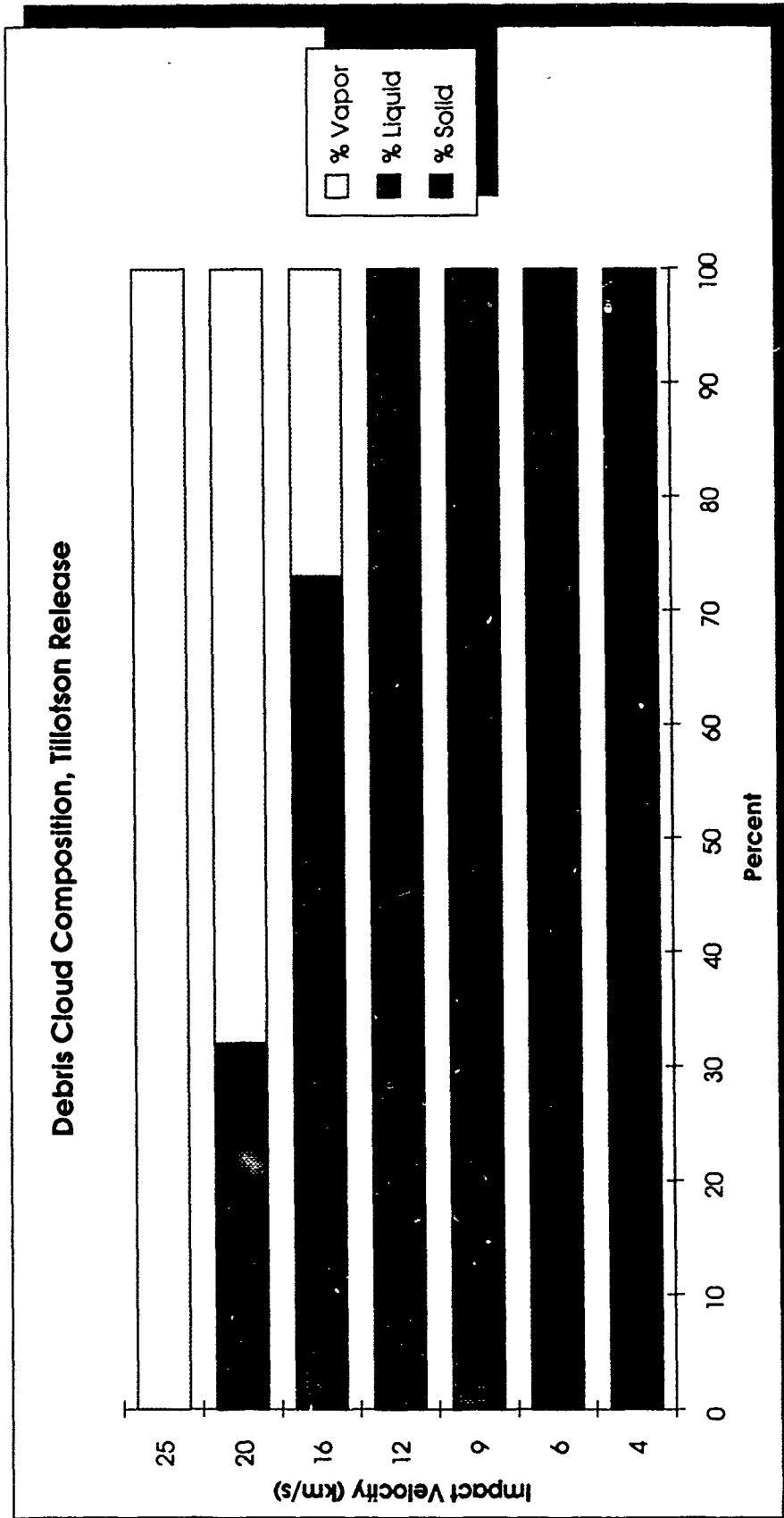


Figure 12. Debris Cloud Material Composition Using the Tillotson EOS, Aluminum-on-Aluminum Impact

Debris Cloud Composition, Modified Tillotson Release

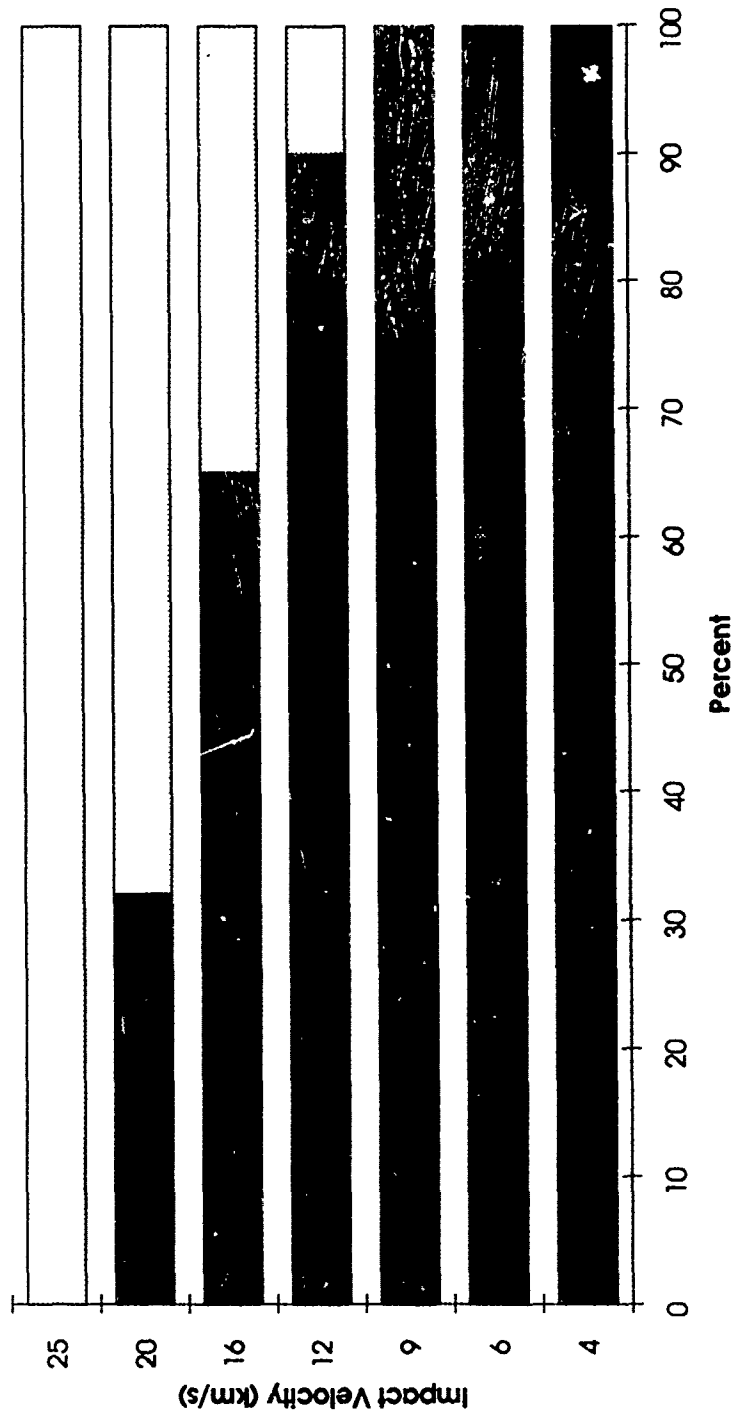


Figure 13. Debris Cloud Material Composition Using the Modified Tillotson EOS, Aluminum-on-Aluminum Impact

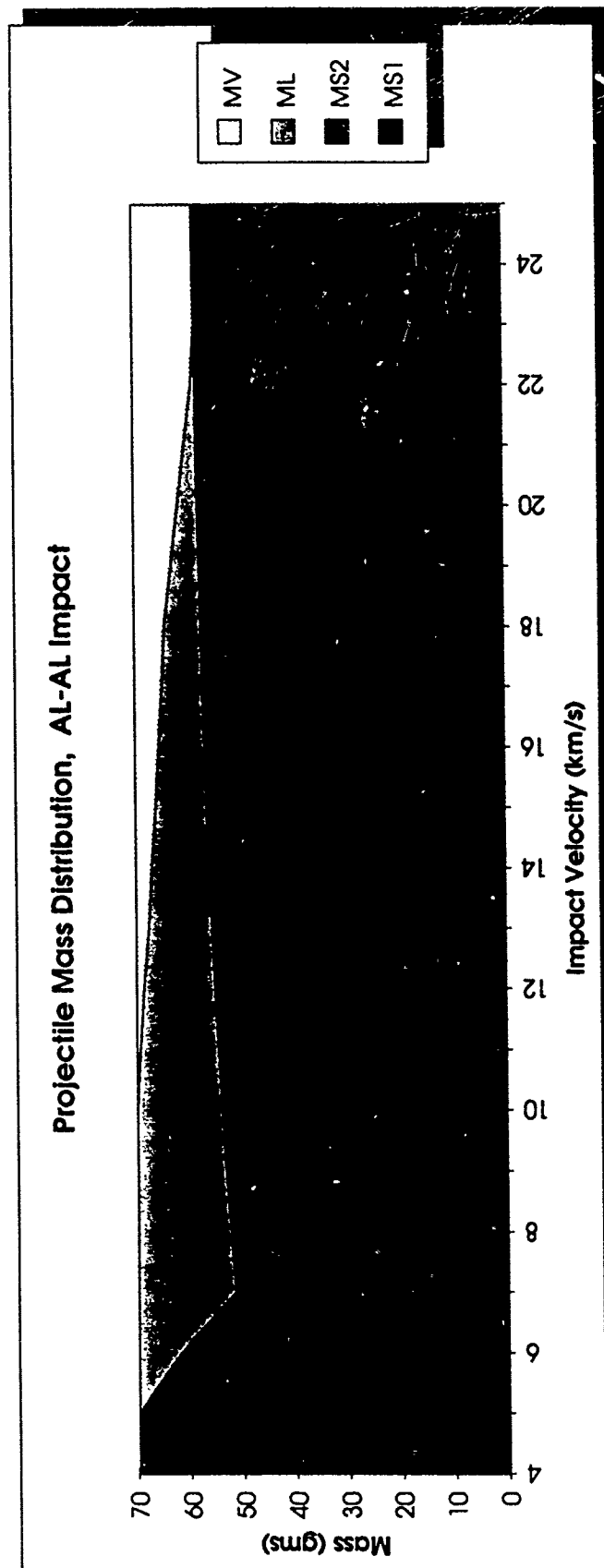


Figure 14. Projectile Material Mass Distribution, Aluminum-on-Aluminum Impact

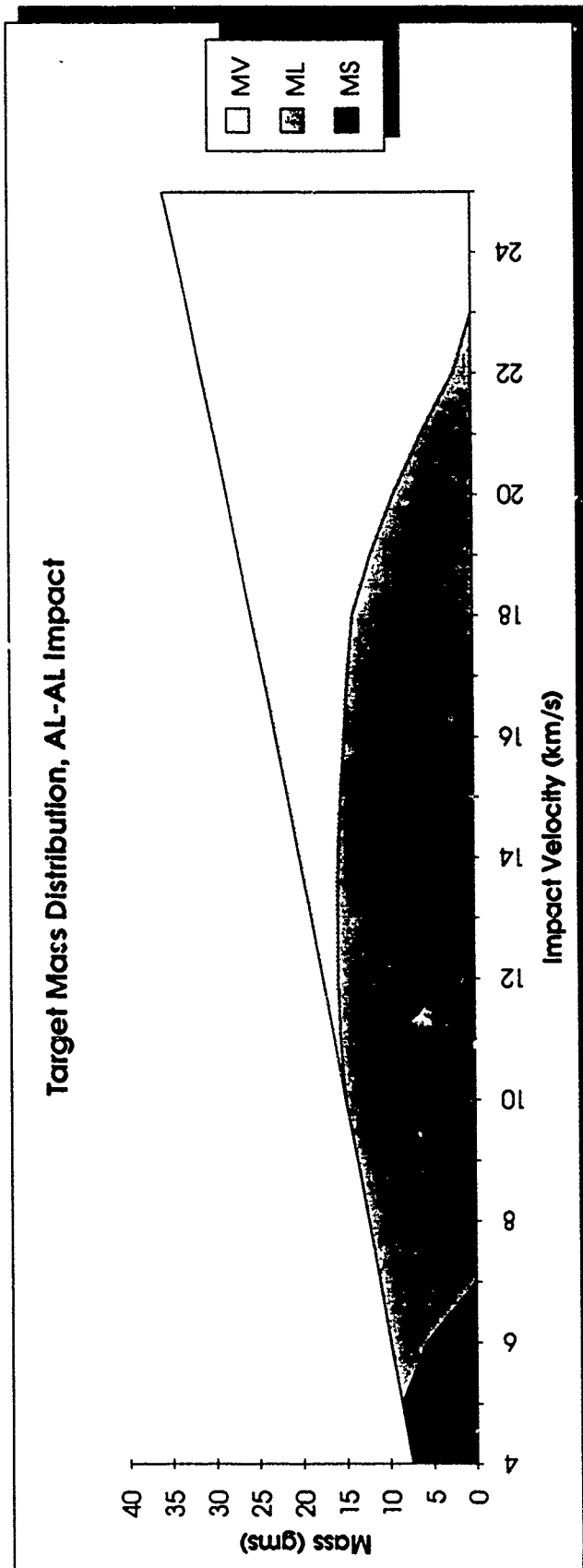


Figure 15. Target Material Mass Distribution, Aluminum-on-Aluminum Impact

HOLE DIAMETER COMPARISON, NORMAL IMPACT, AL-ON-AL, L=5.08 CM, D=2.54 CM,
 T=0.254 CM

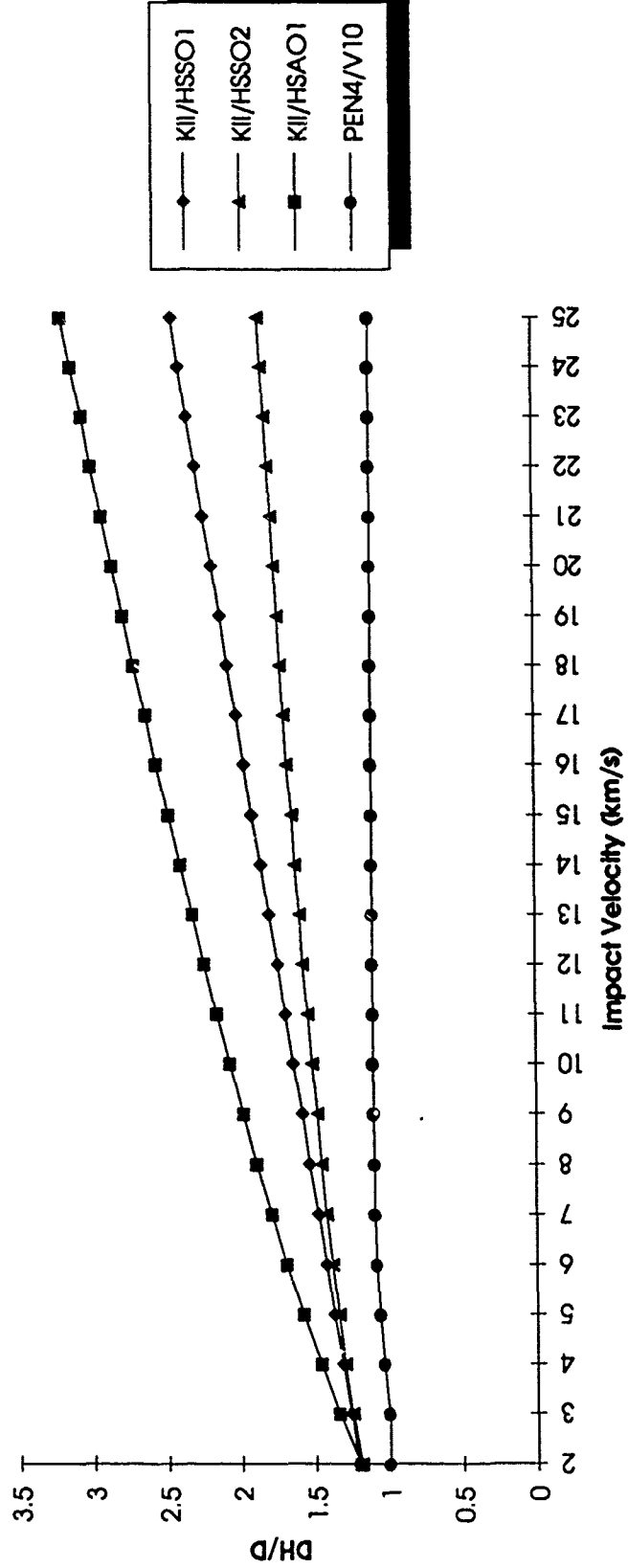


Figure 16. Target Hole Diameter Prediction Comparison, Aluminum-on-Aluminum Impact, L/D=2.0, T/D=0.1

HOLE DIAMETER COMPARISON, NORMAL IMPACT, AL-ON-AL, L=5.08 CM, D=2.54 CM,
 T=1.27 CM

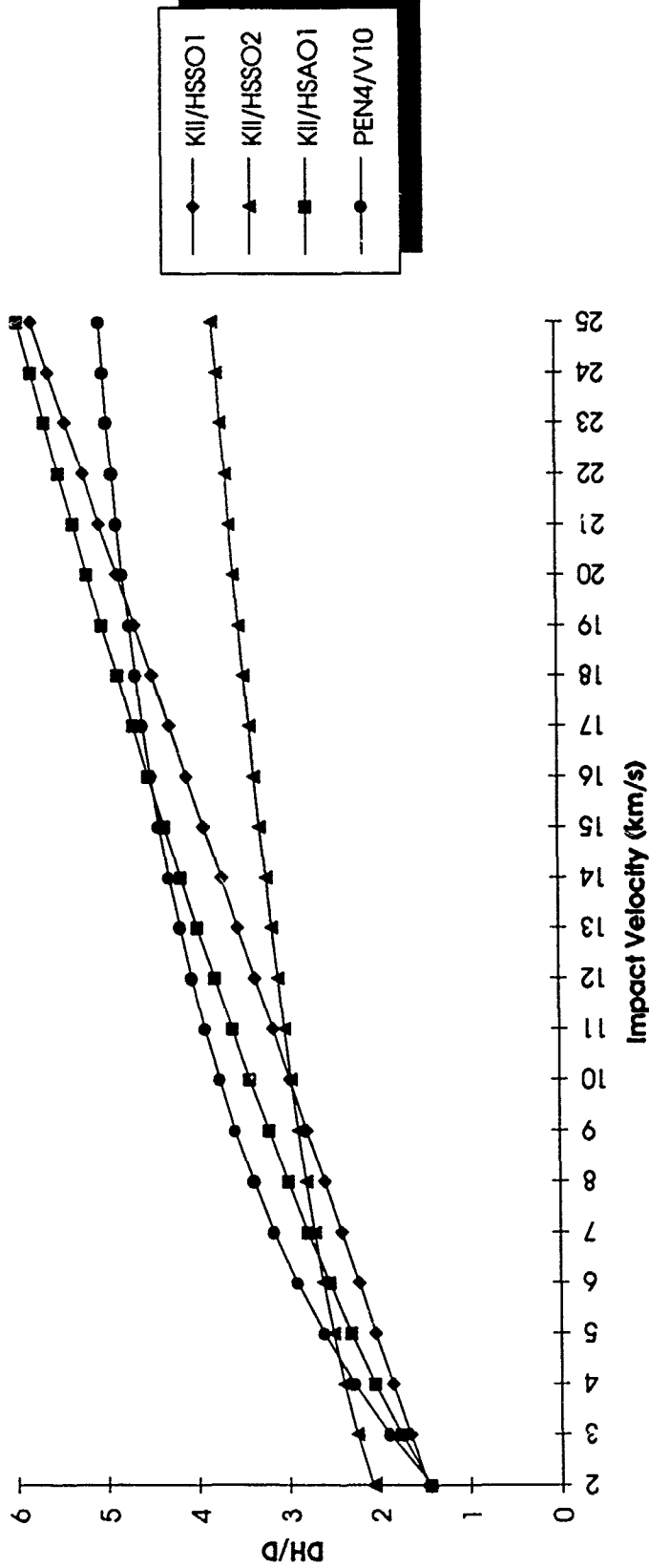


Figure 17. Target Hole Diameter Prediction Comparison, Aluminum-on-Aluminum
 Impact, L/D=2.0, T/D=0.5

HOLE DIAMETER COMPARISON, NORMAL IMPACT, AL-ON-AL, L=0.254 CM, D=2.54 CM,
T=0.254 CM

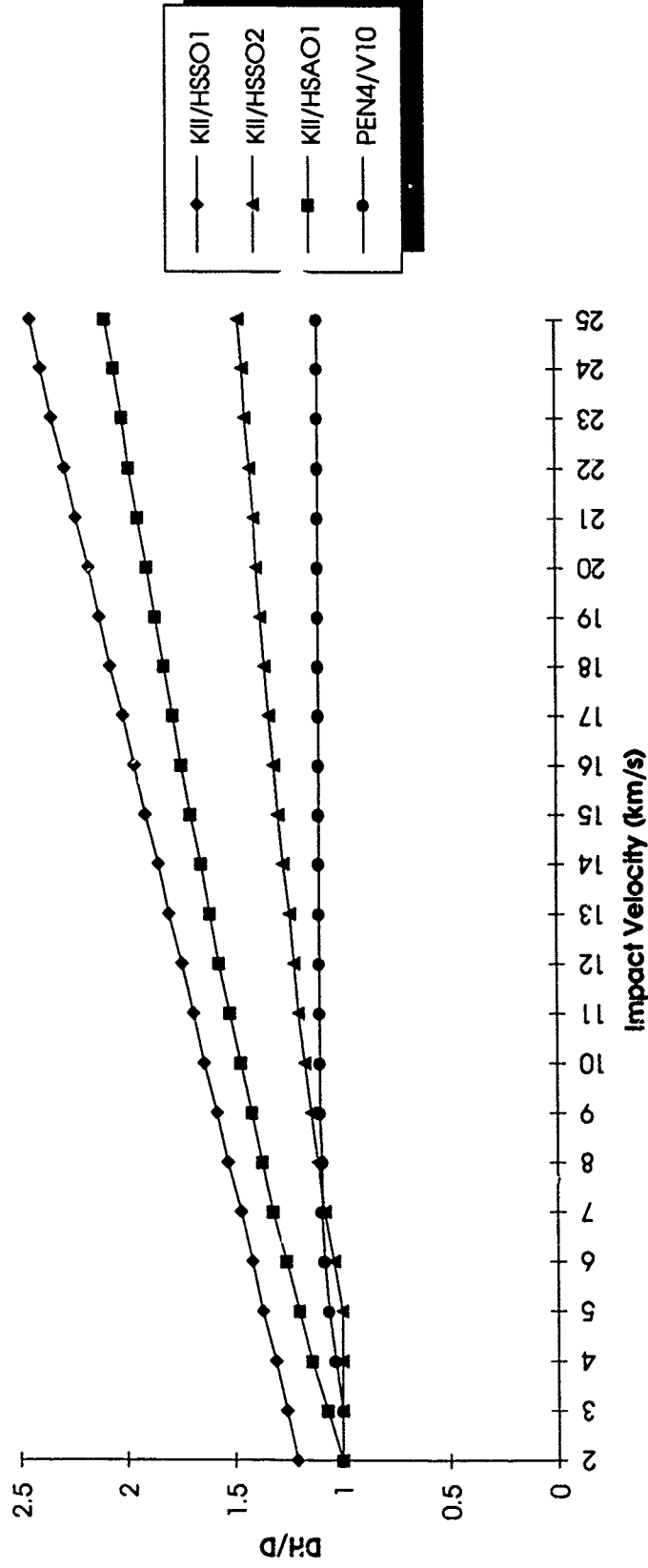


Figure 18. Target Hole Diameter Prediction Comparison, Aluminum-on-Aluminum Impact, L/D=0.1, T/D=0.1

HOLE DIAMETER COMPARISON, NORMAL IMPACT, AL-ON-AL, L=0.254 CM, D=2.54 CM,
 $T=1.27$ CM

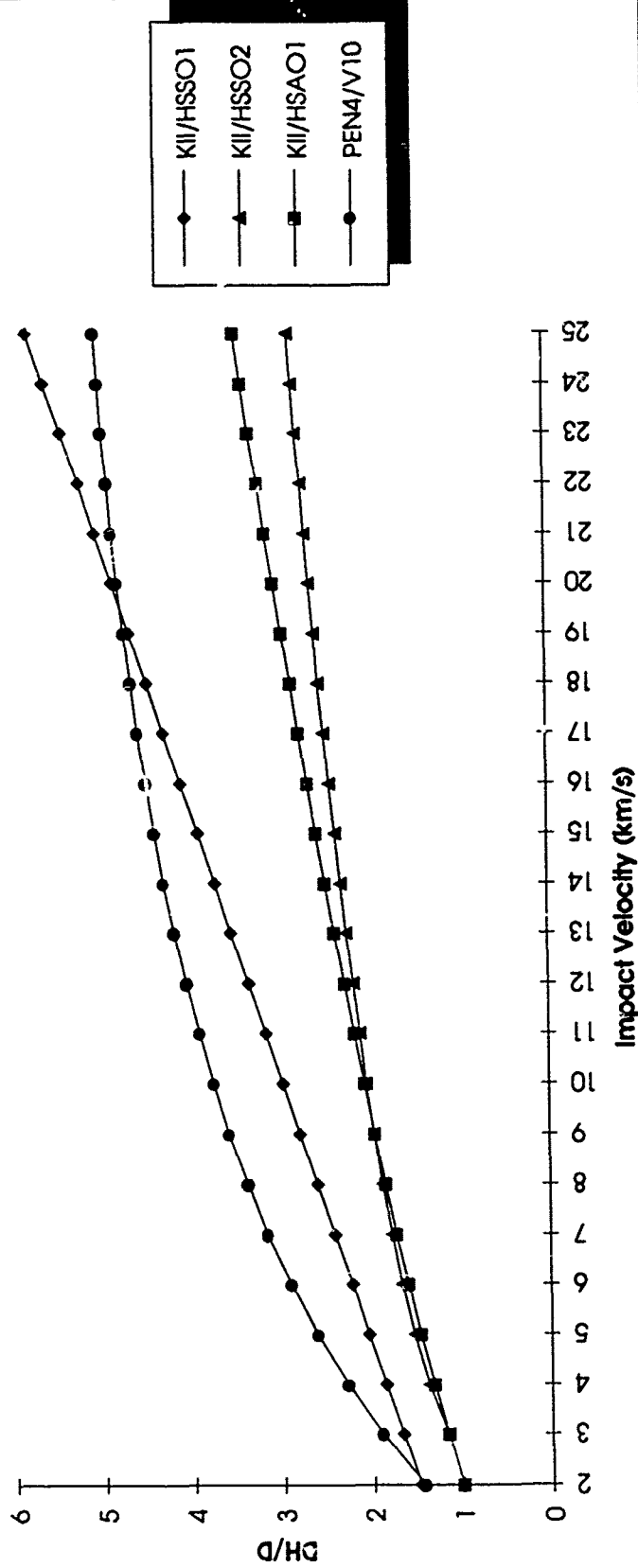


Figure 19. Target Hole Diameter Prediction Comparison, Aluminum-on-Aluminum Impact. $L/D=0.1$, $T/D=0.5$

APPENDIX A -- DEBCLD Source Code

```

PROGRAM DEBRIS
IMPLICIT DOUBLE PRECISION (A-H,O-Z)
DOUBLE PRECISION IMEP, IVEP, IMET, IVET, KSP, KST, KP, KT, LP, NUP, NUT,
$           MPROJ, MTARG

```

```

C
C..... THIS PROGRAM PERFORMS THE FOLLOWING TASKS:
C.....
C.....     1. IT CALCULATES THE RELEASE OF TARGET AND PROJECTILE
C.....     MATERIALS FROM SHOCKED CONDITIONS DUE TO A HYPERVELOCITY IMPACT
C.....     USING THE TILLOTSON EQUATION OF STATE TO CALCULATE THE RELEASE
C.....     ISENTROPE.
C.....
C.....     2. AFTER RELEASE, IT CALCULATES THE RESIDUAL MATERIAL
C.....     TEMPERATURES FOR THE TARGET AND PROJECTILE MATERIALS.
C.....
C.....     3. IT ESTIMATES THE PERCENTAGES OF THE TARGET AND PRO-
C.....     JECTILE MATERIALS IN EACH OF THE THREE MATTER STATES BASED ON
C.....     THE WASTE HEAT GENERATED BY THE RELEASE PROCESS.
C.....
C.....     4. IT CALCULATES THE AMOUNT OF SOLID, LIQUID, AND GAS-
C.....     EOUS MASS IN THE PROJECTILE AND TARGET MATERIAL CONTRIBUTIONS
C.....     TO THE DEBRIS CLOUD CREATED IN A HYPERVELOCITY IMPACT.
C.....
C..... THE VERSION OF THE TILLOTSON EQUATION OF STATE USED BY THIS
C..... PROGRAM INCLUDES THE MIXED PHASE EQUATIONS, THE CHECK AT V=VS,
C..... AND A CORRECTION TO THE EQUATION OF STATE WHEN V>VS TO ELIMINATE
C..... THE JUMP AT V=VS.

```

```

C
INTEGER ROPT,ROPTP,ROPTT
CHARACTER*1 PTOPT, IOPT
CHARACTER*2 PID, TID, PIDCHK, TIDCHK
CHARACTER*10 PMAT, TMAT
COMMON/TDATA/A, B, AA, BB, ALF, BET, EO, EOM, EOI, ROPT
OPEN(1, FILE='INDATA')
OPEN(2, FILE='IMPOUT')
OPEN(3, FILE='PLOT')
OPEN(4, FILE='GPARAM')
OPEN(5, FILE='FINOUT')

```

```

C
C..... READ PROJECTILE AND TARGET MATERIAL PROPERTIES. THE PARAMETERS
C..... MUST BE IN THE FOLLOWING UNITS:
C.....
C.....     PID, TID ..... PROJECTILE AND TARGET MATERIAL ID CODES
C.....     PMAT, TMAT ..... PROJECTILE AND TARGET MATERIALS
C.....     COP, COT ..... ADIABATIC BULK SOUND SPEED, KM/S
C.....     RP, RT ..... AMBIENT MATERIAL DENSITY, GM/CU.CM.
C.....     KP, KT ..... SLOPE OF US-UP LINE, DIMENSIONLESS
C.....     EP, ET ..... ELASTIC MODULUS, LBS/SQ.IN.
C.....     ALFAP, ALFAT ... LINEAR COEFF OF TERMAL EXP, 1/DEG-C
C.....     CPSP, CPST ..... SPECIFIC HEAT (SOLID), CAL/GM-DEG-C
C.....     CPLP, CPLT ..... SPECIFIC HEAT (LIQUID), CAL/GM/DEG-C
C.....     TMP, TMT ..... MELT TEMPERATURE, DEG-C
C.....     TVP, TVT ..... VAPORIZATION TEMPERATURE, DEG-C

```

```

C.....      HFP,HFT ..... LATENT HEAT OF FUSION, CAL/GM
C.....      HVP,HVT ..... LATENT HEAT OF VAPORIZATION, CAL/GM
C.....      BHNP,BHNT ..... BRINELL HARDNESS NUMBER, KG/SQ.MM
C.....      ALFP,ALFT ..... TILLOTSON EOS CONSTANTS
C.....      BETP,BETT ..... TILLOTSON EOS CONSTANTS
C.....      EPSP,EPST ..... TILLOTSON EOS CONSTANTS
C.....      ROPTP,ROPTT ... TILLOTSON EOS RELEASE OPTION
C.....      ROPT=1 ... BACKWARD PRESSURE APPROXIMATION
C.....      ROPT=2 ... AVERAGE PRESSURE APPROXIMATION
C.....      ROPT=3 ... CURRENT PRESSURE APPROXIMATION
C
      WRITE(*,3)
3 FORMAT(' ENTER PROJECTILE MATERIAL ID CODE (A2) AND HIT ENTER')
      READ(*,5) FID
5 FORMAT(A2)
      WRITE(*,7)
7 FORMAT(' ENTER TARGET MATERIAL ID CODE (A2) AND HIT ENTER')
      READ(*,9) TID
9 FORMAT(A2)
C
      REWIND 1
      READ(1,4)
4 FORMAT(//////)
C
99 READ(1,1) PIDCHK
1 FORMAT(A2)
      IF (PID.EQ.PIDCHK) THEN
      READ(1,10) PMAT,COP,KP,RP,GPI,BHNP
10 FORMAT(A10,5F10.5)
      READ(1,100) EP,NUP,ALPHA,P,CPSP,CPLP,EPSP
100 FORMAT(2(E10.3,F10.5),2(F10.5))
      READ(1,102) TMP,TVP,HFP,HVP,ALFP,BETP
102 FORMAT(6F10.5)
      READ(1,104) ROPTP
104 FORMAT(I1)
      ENDIF
      IF (PID.NE.PIDCHK) THEN
      IF (PIDCHK.EQ.'XX') THEN
      WRITE (*,17)
17 FORMAT(' PROJECTILE MATERIAL NOT FOUND IN MATERIAL LIBRARY.',/,
$ ' PLEASE CHECK PROJECTILE MATERIAL ID CODE AND BEGIN AGAIN.')
      STOP
      ENDIF
      IF (PIDCHK.NE.'XX') THEN
      READ (1,2)
2 FORMAT(////////)
      GOTO 99
      ENDIF
      ENDIF
C
      REWIND 1
      READ(1,4)
999 READ(1,1) TILORR

```

```

IF (TID.EQ.TIDCHK) THEN
READ(1,10) TMAT,COT,KT,RT,GTI,BHNT
READ(1,100) ET,NUT,ALPHAT,CPST,CPLT,EPST
READ(1,102) TMT,TVT,HFT,HVT,ALFT,BETT
READ(1,104) ROPTT
ENDIF
IF (TID.NE.TIDCHK) THEN
IF (TIDCHK.EQ.'XX') THEN
WRITE (*,117)
117 FORMAT(' TARGET MATERIAL NOT FOUND IN MATERIAL LIBRARY.',/,
$' PLEASE CHECK TARGET MATERIAL ID CODE AND BEGIN AGAIN.')
STOP
ENDIF
IF (TIDCHK.NE.'XX') THEN
READ (1,2)
GOTO 999
ENDIF
ENDIF
C
C..... READ IMPACT VELOCITY IN KM/S
C
WRITE(*,29)
29 FORMAT(' INPUT IMPACT VELOCITY IN KM/SEC (F5.2) AND HIT ENTER')
READ(*,30) V
30 FORMAT(F5.2)
C
C..... CALCULATE PROJECTILE AND TARGET MATERIAL PARTICLE AND SHOCK WAVE
C..... VELOCITIES AND INTERFACE HUGONIOT PRESSURE
C
IF (TMAT.EQ.PMAT) GOTO 35
A=KP-KT*(RT/RP)
B=2.0*KP*V+COP+COT*(RT/RP)
C=COP*V+KP*V*V
D=B*B-4.0*A*C
UTP=(B-SQRT(D))/(2.0*A)
GOTO 38
35 UTP=V/2.0
38 UPP=V-UTP
UTS=COT+KT*UTP
UPS=COP+KP*UPP
PP=RP*UPS*UPP
PT=RT*UTS*UTP
C
ET=ET*68947.0
BETAT=3.0*ALPHAT
IF (NUT.LT.0.5) THEN
KST=ET/3.0/(1.0-2.0*NUT)
COTC=DSQRT((KST/10.0)/(RT*1000.0))/1000.0
ENDIF
IF (NUT.EQ.0.5) THEN
KST=-1 0
COTC=-1.0
ENDIF

```

```

C
EP=EP*68947.0
BETAP=3.0*ALPHAP
IF (NUP.LT.0.5) THEN
KSP=EP/3.0/(1.0-2.0*NUP)
COPC=DSQRT((KSP/10.0)/(RP*1000.0))/1000.0
ENDIF
IF (NUP.EQ.0.5) THEN
KSP=-1.0
COPC=-1.0
ENDIF

C
WRITE(2,40) PMAT, TMAT
40 FORMAT('HYPERVELOCITY IMPACT OF A ',A10,' PROJECTILE ON A ',A10,
$' TARGET.')
WRITE(2,45) V
45 FORMAT(/,'IMPACT VELOCITY ... V = ',F5.2,' KM/S')
WRITE(2,50) PMAT,COP,COPC,KP,RP, TMAT,COT,COTC,KT,RT
50 FORMAT(/,'PROJECTILE PROPERTIES ... ',/,5X,'MAT = ',A10,/,3X,
$'CO = ',F6.3,' KM/S (INPT)',/,3X,'CO = ',F6.3,' KM/S (CALC)',/,
$3X,'K = ',F6.3,/,3X,'RHO = ',F6.3,' GM/CU.CM.',/, 'TARGET PROPERT
$IES ... ',/,3X,'MAT = ',A10,/,3X,'CO = ',F6.3,' KM/S (INPT)',/,
$3X,'CO = ',F6.3,' KM/S (CALC)',/,3X,'K = ',F6.3,/,3X,'RHO = ',
$F6.3,' GM/CU.CM.')

C
C..... TARGET MATERIAL RELEASE CALCULATION PHASE
C
WRITE(2,59)
59 FORMAT(/,'***** TARGET MATERIAL RELEASE CALCULATION *****')
WRITE(2,60) UTP,UTS,PT
60 FORMAT(/,'TARGET PARTICLE VELOCITY ... UP = ',F8.3,' KM/S',/,
$'TARGET SHOCK WAVE SPEED .... US = ',F8.3,' KM/S',/, 'HUGONIOT IMPA
$CT PRESSURE ... PH = ',F8.3,' GPA')

C
VTO=1.0/RT
VT1=RT*UTS/(UTS-UTP)
VT1=1.0/VT1

C
C..... CALCULATE AMBIENT GRUNEISEN COEFFICIENT AND GAMMA/SP.VOL. RATIO
C..... FOR TARGET MATERIAL
C
PH=PT*1.0E09
IF (NUT.LT.0.5) GT=2.3885E-08*KST*BETAT/CPST/RT
IF (NUT.EQ.0.5) GT=GTI

C
WRITE(2,75) ET/10.0,NUT,KST/10.0,ALPHAT,CPST,CPLT
75 FORMAT(/,'PARAMETERS REQUIRED FOR CALCULATING TARGET MATERIAL RELE
$ASE FROM SHOCKED',/, 'STATE USING THE TILLOTSCN EQUATION OF STATE:'
$,/,3X,'TARG MATL ELASTIC MODULUS ..... E =',E10.4,
$' N/SQ.M.',/,3X,'TARG MATL POISSON RATIO ..... NU =',
$F10.3,/,3X,'TARG MATL BULK MODULUS ..... K =',E10.4,
$' N/SQ.M.',/,3X,'TARG MATL LI.I. COEF. OF THERM. EXP. ... ALFA =',
$E10.4,' /DEG-C',/,3X,'TARG MATL SP HEAT (SOLID) ..... CPS

```

```

$ =',F10.3,' CAL/GM/DEG-C',/,3X,'TARG MATL SP HEAT (LIQUID) .....
$. . . . CPL =',F10.3,' CAL/GM/DEG-C')
  EHT=0.5*PH*(VTO-VT1)/1000.0
  PHMB=PH/101.3E+09
  WRITE(2,80) PH,PHMB,EHT,VTO,VT1,GT,GTI
80 FORMAT(3X,'TARG MATL HUGON IMP PRESS (PA,MBAR) ... PH =',E10.4,
$,',F6.3,/,3X,'TARG MATL HUGON IMPACT ENERGY ..... EH =',
$E10.4,' JOULES/KG',/,3X,'TARG MATL SP VOL AT REST ..... V
$0 =',F10.3,' CU.CM./GM',/,3X,'TARG MATL SP VOL AT IMPACT .....
$. . . . V1 =',F10.3,' CU.CM./GM',/,3X,'TARG MATL AMB M-GRUN COEF (
$CAL,INP) ... GAMO =',F10.3,',',F6.3)
  WRITE(2,85) TMT,TVT,HFT,HVT
85 FORMAT(3X,'TARG MATL MELT TEMPERATURE ..... TM =',F10.2,
$, ' DEG-C',/,3X,'TARG MATL VAPOR TEMPERATURE ..... TV =',
$F10.2,' DEG-C',/,3X,'TARG MATL HEAT OF FUSION ..... HF
$= ',F10.2,' CAL/GM',/,3X,'TARG MATL HEAT OF VAPORIZATION ..... H
$V =',F10.2,' CAL/GM')
C
  SHST=CPST*4186
  SHLT=CPLT*4186
  HFT=HFT*4186
  HVT=HVT*4186
  IMET=TMT*SHST
  IVET=IMET+HFT+(TVT-TMT)*SHLT
C
  WRITE (2,76) IMET,IVET
76 FORMAT(3X,'TARG MATL INICIPIENT MELT ENERGY ..... IME =',
$E10.4,' JOULES/KG',/,3X,'TARG MATL INICIPIENT VAPOR ENERGY .....
$IVE =',E10.4,' JOULES/KG')
C
  WRITE (*,230)
230 FORMAT(/,1X,'ENTER EO MULTIPLIER VALUE (F4.2) FOR TARGET MATERIAL
SAND HIT RETURN ...')
  READ (*,240) EOM
240 FORMAT(F4.2)
C
  ALF=ALFT
  BET=BETT
  ROPT=ROPI T
  CALL TCONST(VTO,COT,KT,GT,TMT,TVT,HFT,HVT,IVET)
  CALL TRELS1(VTO,VT1,PH,EXT,UTP,URT,UFST1,UFST2,IVET,HVT,COT,KT,
$,
  EPST)
  CALL TINC(SHST,SHLT,TMT,TVT,HFT,HVT,EXT,IMET,IVET,PS,PL,PV,TRT)
C
  WRITE(2,87) UFST1,UFST2
87 FORMAT(/,'FREE SURF VEL (UP+UR) .....',F7.3,' KM/SEC',/, 'FREE S
SURF VEL (2.0*UP) .....',F7.3,' KM/SEC')
  WRITE (5,187) UFST1
187 FORMAT(F10.5)
  VL=UFST1
C
  CALL TMCALC(V,PS,PL,PV,RP,RT,TRT,TMT,TVT,TS.LP,DP,BHNT,TMS,TML,
$,
  TMV,MTARG)

```

```

C
C..... PROJECTILE MATERIAL RELEASE CALCULATION PHASE
C
      WRITE (*,101)
101 FORMAT(/,1X,'DO YOU WISH TO RELEASE THE PROJECTILE MATERIAL AS WEL
      $L?'/,1X,'ENTER Y FOR YES OR N FOR NO AND HIT RETURN ...')
      READ (*,103) PTOPT
103 FORMAT(A1)
      IF (PTOPT.EQ.'N') STOP
      IF (PTOPT.EQ.'Y') CONTINUE
C
      WRITE(2,89)
89 FORMAT(/,'***** PROJECTILE MATERIAL RELEASE CALCULATION *****')
      WRITE(2,93) UPP,UPS,PP
93 FORMAT(/,'PROJECTILE PARTICLE VELOCITY ... UP = ',F8.3,' KM/S',/
      $,'PROJECTILE SHOCK WAVE SPEED .... US = ',F8.3,' KM/S',/,'HUGONIOT
      $ IMPACT PRESSURE ..... PH = ',F8.3,' GPA')
C
      VPO=1.0/RP
      VP1=RP*UPS/(UPS-UPP)
      VP1=1.0/VP1
C
C..... CALCULATE AMBIENT GRUNEISEN COEFFICIENT AND GAMMA/SP.VOL. RATIO
C..... FOR PROJECTILE MATERIAL.
C
      PH=PP*1.0E09
      IF (NUP.LT.0.5) GP=2.3885E-08*KSP*BETAP/CPSP/RP
      IF (NUP.EQ.0.5) GP=GPI
C
      WRITE(2,105) EP/10.0,NUP,KSP/10.0,ALPHAP,CPSP,CPLP
105 FORMAT(/,'PARAMETERS REQUIRED FOR CALCULATING PROJECTILE MATERIAL
      $RELEASE FROM',/,'SHOCKED STATE USING THE TILLOTSON EQUATION OF STA
      $TE:',/,3X,'PROJ MATL ELASTIC MODULUS ..... E =',E10.4,
      $' N/SQ.M.',/,3X,'PROJ MATL POISSON RATIO ..... NU =',
      $F10.3,/,3X,'PROJ MATL BULK MODULUS ..... K =',E10.4,
      $' N/SQ.M.',/,3X,'PROJ MATL LIN. COEF. OF THERM. EXP. ... ALFA =',
      $E10.4,' /DEG-C',/,3X,'PROJ MATL SP HEAT (SOLID) ..... CPS
      $ =',F10.3,' CAL/GM/DEG-C',/,3X,'PROJ MATL SP HEAT (LIQUID) .....
      $..... CPL =',F10.3,' CAL/GM/DEG-C')
      EHP=0.5*PH*(VPO-VP1)/1000.0
      PHMB=PH/101.3E+09
      WRITE(2,110) PH,PHMB,EHP,VPO,VP1,GP,GPI
110 FORMAT(3X,'PROJ MATL HUGON IMP PRESS (PA,MBAR) ... PH =',E10.4,
      $',',F6.3,/,3X,'PROJ MATL HUGON IMPACT ENERGY ..... EH =',
      $E10.4,' JOULES/KG',/,3X,'PROJ MATL SP VOL AT REST ..... V
      $0 =',F10.3,' CU.CM./GM',/,3X,'PROJ MATL SP VOL AT IMPACT .....
      $..... V1 =',F10.3,' CU.CM./GM',/,3X,'PROJ MATL AMB M-GRUN COEF (
      $CAL,IN?) ... GAMO =',F10.3,',',F6.3)
      WRITE(2,115) TMP,TVP,HFP,HVP
115 FORMAT(3X,'PROJ MATL MELT TEMPERATURE ..... TM =',F10.2,
      $' DEG-C',/,3X,'PROJ MATL VAPOR TEMPERATURE ..... TV =',
      $F10.2,' DEG-C',/,3X,'PROJ MATL HEAT OF FUSION ..... HF
      $ =',F10.2,' CAL/GM',/,3X,'PROJ MATL HEAT OF VAPORIZATION ..... H

```

```

$V  -,F10.2,' CAL/GM')
C
SHSP=CPL*4186
SHLP=CPLP*4186
HFP=HFP*4186
HVP=HVP*4186
IMEP=TMP*SHSP
IVEP=IMEP+HFP+(TVP-TMP)*SHLP
C
WRITE (2,77) IMEP,IVEP
77 FORMAT(3X,'PROJ MATL INICIPIENT MELT ENERGY ..... IME =',
$E10.4, ' JOULES/KG',/,3X,'PROJ MATL INICIPIENT VAPOR ENERGY .....
$IVE =',E10.4,' JOULES/KG')
C
WRITE (*,231)
231 FORMAT(/,1X,'ENTER EO MULTIPLIER VALUE FOR PROJECTILE MATERIAL (F4
$.2) AND HIT RETURN ...')
READ (*,241) EOM
241 FORMAT(F4.2)
C
ALF=ALFP
BET=RETP
ROPT=ROPTP
CALL TCONST(VPO,COP,KP,GP,TMP,TVP,HFP,HVP,IVEP)
CALL TRELS1(VPO,VPL,PH,EXP,UPP,URP,UFSP1,UFSP2,IVEP,HVP,COP,KP,
$ EPSP)
CALL TINC(SHSP,SHLP,TMP,TVP,HFP,HVP,EXP,IMEP,IVEP,PS,PL,PV,TRP)
C
CALL PMCALC(UPS,UTS,UPP,UTP,RP,PS,PL,PV,TS,LP,DP,PMS,PML,PMV,
$ MPROJ)
C
WRITE(2,87) UFSP1,UFSP2
VR=V-UFSP1
WRITE (5,187) VR
VCOM=MPROJ*V/(MTARG+MPROJ)
C
WRITE (2,500) PMS,PML,PMV,TMS,TML,TMV
500 FORMAT(//,'MASS DISTRIBUTION SUMMARY ...',/,3X,'PROJECTILE ... SOL
$ID .... ',F6.2,' GMS',/,3X,15X,'LIQUID ... ',F6.2,' GMS',/,3X,15X,
$'VAPOR .... ',F6.2,' GMS',/,3X,'TARGET ..... SOLID .... ',F6.2,
$' GMS',/,3X,15X,'LIQUID ... ',F6.2,' GMS',/,3X,15X,'VAPOR .... ',
$F6.2,' GMS')
C
WRITE(2,499) VR,VCOM,VL
499 FORMAT(//,'DEBRIS CLOUD VELOCITY SUMMARY ...',/,3X,'REAR SURF VEL
$(VR) ..... ',F7.3,' KM/SEC',/,3X,'CENTER-OF-MASS VEL (VI) ...
$... ',F7.3,' KM/SEC',/,3X,'LEADING EDGE VEL (VL) ..... ',F7.3,
$' KM/SEC')
C
CLOSE(1)
CLOSE(2)
CLOSE(3)
STOP

```

```

END
C
SUBROUTINE TCONST(VO,CO,K,G,TM,TV,HF,HV,ES)
  IMPLICIT DOUBLE PRECISION (A-H,O-Z)
  DOUBLE PRECISION K
  INTEGER ROPT
  COMMON/TDATA/A,B,AA,BB,ALF,BET,EO,EOM,EOI,ROPT
C
C..... THIS SUBROUTINE CALCULATES THE VALUES OF THE CONSTANTS
C..... REQUIRED BY THE TILLOTSON EQUATION OF STATE (SWRI FINAL
C..... REPORT FOR PROJ. NO. 06-4438).
C
AA=(1000.0/VO)*(CO*1000.0)*(CO*1000.0)
BB=AA*(2.0*K-1.0-0.5*G)
A=0.5
B=G-0.5
R1=TM/TV
R2=HF/HV
EOI=EXP(-0.199)*(K**6.5939)*(R2**0.5720)/(G**0.7680)
$   /(R1**0.0210)
EOI=EOI*(ES+HV)
EO=EOM*EOI
C
WRITE (2,10) AA,BB,A,B,ALF,BET,EOI,EOM,EO
10 FORMAT(/,'ADDITIONAL PARAMETERS REQUIRED FOR CALCULATING MATERIAL
$RELEASE FROM',/, 'SHOCKED STATE USING THE TILLOTSON EQUATION OF STA
$TE:',/,3X,'AA = ',E11.4,' N/SQ.M.',/,3X,'BB = ',E11.4,' N/SQ.M.'
$,/,3X,'A = ',F7.4,/,3X,'B = ',F7.4,/,3X,'ALF = ',F7.4,/,3X,
$'BET = ',F7.4,/,3X,'EOI = ',E11.4,' JOULES/KG',/,3X,'EOM = ',F7.4,
$,/,3X,'EO = ',E11.4,' JOULES/KG')
RETURN
END
C
SUBROUTINE TRELS1(VO,V1,PHO,EX,UP,UR,UFS1,UFS2,IVE,HV,CO,K,EPS)
  IMPLICIT DOUBLE PRECISION (A-H,O-Z)
  DOUBLE PRECISION Q(401),MU(401),V(401),E(401),P(401),R(401)
  DOUBLE PRECISION RP(401),U(401),S(401),PH(401),IVE,K
  INTEGER ROPT
  COMMON/TDATA/A,B,AA,BB,ALF,BET,EO,EOM,EOI,ROPT
C
C..... THIS SUBROUTINE, TOGETHER WITH THE SUBROUTINE PCALC, CALCULATE
C..... THE RELEASE OF THE PROJECTILE AND TARGET MATERIALS USING THE
C..... TILLOTSON EQUATION OF STATE. THE VERSION USED BY THIS SUB-
C..... ROUTINE INCLUDES THE MIXED PHASE EQUATIONS, THE CHECK AT V=VS,
C..... AND A CORRECTION TO THE EQUATION OF STATE WHEN V>VS TO ELIMINATE
C..... THE JUMP AT V=VS. IT IS ASSUMED FOR MOST METALS THAT THE
C..... SPECIFIC VOLUME VS IS ROUGHLY 13% HIGHER THAN AMBIENT.
C
ESP=IVE+HV
VS=1.131*VO
C
WRITE (2,5) IVE,HV,ESP,VS,EPS

```

```

5 FORMAT(3X,'ES = ',E11.4,' JOULES/KG',/,3X,'HV = ',E11.4,
$' JOULES/KG',/,3X,'ESP = ',E11.4,' JOULES/KG',/,3X,'VS = ',
$F7.4,' CU CM./GM',/,3X,'EPS = ',F7.4)

```

C

```

PH(1)=P-0
V(1)=V1
P(1)=PHO
E(1)=0.5*P(1)*(VO-V1)/1000.0
DELV=(VO-V1)/50.0
MU(1)=VO/V(1)-1.0
Q(1)=AA*MU(1)+BB*MU(1)*MU(1)
R(1)=EO*(VO/1000.0)*(VO/1000.0)
RP(1)=B*R(1)

```

C

C NOTE: MU(1),Q(1),R(1),RP(1) ARE INITIALIZED BUT NOT USED

C

```

PEQ2=0.0
DELP=0.0
DE=0.0
UR=0.0
II=0
DO 10 I=2,401
V(I)=V(I-1)+DELV
PH(I)=CO**2*(1000.0/VO)*(1.0-V(I)/VO)/(1.0-K*(1.0-V(I)/VO))**2
PH(I)=PH(I)*1.0E06
MU(I)=VO/V(I)-1.0
R(I)=E(I-1)*(V(I)/1000.0)*(V(I)/1000.0)
$      +EO*(VO/1000.0)*(VO/1000.0)

```

C

```

IF (V(I).LT.VO) THEN
Q(I)=AA*MU(I)+BB*MU(I)*MU(I)
RP(I)=A*E(I-1)*(V(I)/1000.0)*(V(I)/1000.0)
$      +B*EO*(VO/1000.0)*(VO/1000.0)
CALL PCALC(E(I-1),P(I-1),V(I),Q(I),R(I),RP(I),VO,DELV,P(I))
ENDIF

```

C

```

IF (V(I).GE.VO.AND.V(I).LT.VS) THEN

```

C

```

IF (E(I-1).LT.IVE) THEN
Q(I)=AA*MU(I)+BB*MU(I)*MU(I)
RP(I)=A*E(I-1)*(V(I)/1000.0)*(V(I)/1000.0)
$      +B*EO*(VO/1000.0)*(VO/1000.0)
CALL PCALC(E(I-1),P(I-1),V(I),Q(I),R(I),RP(I),VO,DELV,P(I))
ENDIF

```

C

```

IF (E(I-1).GE.IVE.AND.E(I-1).LT.ESP) THEN
Q(I)=AA*MU(I)+BB*MU(I)*MU(I)
RP(I)=A*E(I-1)*(V(I)/1000.0)*(V(I)/1000.0)
$      +B*EO*(VO/1000.0)*(VO/1000.0)
CALL PCALC(E(I-1),P(I-1),V(I),Q(I),R(I),RP(I),VO,DELV,PC)
C=V(I)/VO-1.0
U(I)=DEXP(-ALF*C*C)
S(I)=AA*MU(I)*DEXP(-BET*C)

```

```

B=B*U(I)
Q(I)=U(I)*S(I)
RP(I)=A*E(I-1)*(V(I)/1000.0)*(V(I)/1000.0)
$      +B*EO*(VO/1000.0)*(VO/1000.0)
CALL PCALC(E(I-1),P(I-1),V(I),Q(I),R(I),RP(I),VO,DELV,PE)
B=B/U(I)
T1=PE*(E(I-1)-IVE)
T2=PC*(ESP-E(I-1))
DEN=ESP-IVE
P(I)=(T1+T2)/DEN
ENDIF

```

C

```

IF (E(I-1).GE.ESP) THEN
C=V(I)/VO-1.0
U(I)=DEXP(-ALF*C*C)
S(I)=AA*MU(I)*DEXP(-BET*C)
B=B*U(I)
Q(I)=U(I)*S(I)
RP(I)=A*E(I-1)*(V(I)/1000.0)*(V(I)/1000.0)
$      +B*EO*(VO/1000.0)*(VO/1000.0)
CALL PCALC(E(I-1),P(I-1),V(I),Q(I),R(I),RP(I),VO,DELV,P(I))
B=B/U(I)
ENDIF

```

C

```

DELVS=VS-V(I)
IF (DELVS.LT.DELV) THEN
C=V(I)/VO-1.0
U(I)=DEXP(-ALF*C*C)
S(I)=AA*MU(I)*DEXP(-BET*C)
B=B*U(I)
Q(I)=U(I)*S(I)
RP(I)=A*E(I-1)*(V(I)/1000.0)*(V(I)/1000.0)
$      +B*EO*(VO/1000.0)*(VO/1000.0)
CALL PCALC(E(I-1),P(I-1),V(I),Q(I),R(I),RP(I),VO,DELV,PEQ2VS)
B=B/U(I)
DELP=PEQ2VS-P(I)
ENDIF

```

C

ENDIF

C

```

IF (V(I).GE.VS) THEN
C=V(I)/VO-1.0
U(I)=DEXP(-ALF*C*C)
S(I)=AA*MU(I)*DEXP(-BET*C)
B=B*U(I)
Q(I)=U(I)*S(I)
RP(I)=A*E(I-1)*(V(I)/1000.0)*(V(I)/1000.0)
$      +B*EO*(VO/1000.0)*(VO/1000.0)
CALL PCALC(E(I-1),P(I-1),V(I),Q(I),R(I),RP(I),VO,DELV,PEQ2)
B=B/U(I)
P(I)=PEQ2-DELP
ENDIF

```

C

```

C..... CALCULATE ENERGIES BASED ON RELEASE APPROXIMATION OPTION
C
  IF (ROPT.EQ.1) THEN
  E(I)=E(I-1)-P(I-1)*DELV/1000.0
  ENDIF
  IF (ROPT.EQ.2) THEN
  E(I)=E(I-1)-0.5*(P(I-1)+P(I))*DELV/1000.0
  ENDIF
  IF (ROPT.EQ.3) THEN
  E(I)=E(I-1)-P(I)*DELV/1000.0
  ENDIF
C
  DP=P(I)-P(I-1)
  IF (DP.GE.0.0) THEN
  WRITE (2,11) I
11 FORMAT('*** AN ERROR HAS OCCURRED IN RELEASE PROCESS AT THE ',I3,
  $'-TH ITERATION ***')
  STOP
  ENDIF
  DUR=DSQRT(-DP*(DELV/1000.0))
  UR=UR+DUR/1000.0
  II=II+1
  IF (P(I).GE.0.0) THEN
  IF (ROPT.EQ.1) DE=DE+P(I-1)*DELV/1000.0
  IF (ROPT.EQ.2) DE=DE+0.5*(P(I)+P(I-1))*DELV/1000.0
  IF (ROPT.EQ.3) DE=DE+P(I)*DELV/1000.0
  ADP=DABS(DP)
  DPR=ADP/(P(I-1)+DELP)
  IF (DPR.LT.EPS) GOTO 15
  ENDIF
  IF (P(I).LT.0.0) GOTO 15
10 CONTINUE
C
15 EX=E(1)-DE
  VF=V(II)
  UFS1=UP+UR
  UFS2=2.0*UP
C
  WRITE(2,20) VF,E(1),DE,EX
20 FORMAT(/,'END-STATE CALCULATION RESULTS USING THE TILLOTSON EOS ..
  $./,'MATERIAL FIN SP VOL (VF) ..... ',F10.3,' CU.CM./GM'./,
  $'MATERIAL ENERGY AT IMPACT .... ',E10.4,' JOULES/KG'./,'MATERIAL E
  $NERGY RECOVERED .... ',E10.4,' JOULES/KG'./,'WASTE HEAT GENERATED
  $..... ',E10.4,' JOULES/KG')
C
C..... STORE OUTPUT FOR PLOTTING
C
  DO 40 J=1,II+1
  PH(J)=PH(J)/1.0E09
  P(J)=P(J)/1.0E09
  WRITE(3,30) V(J),PH(J),P(J),E(J)
30 FORMAT(3F11.5,E11.4)
40 CONTINUE

```

```

C      RETURN
      END

C      SUBROUTINE PCALC(E,P,V,Q,R,RP,VO,DELV,PI)
      IMPLICIT DOUBLE PRECISION (A-H,O-Z)
      INTEGER ROPT
      COMMON/TDATA/A,B,AA,BB,ALF,BET,EO,EOM,EOI,ROPT

C      C..... CALCULATE PRESSURES BASED ON RELEASE APPROXIMATION OPTION
C
      IF (ROPT.EQ.1) THEN
      T1=E-P*DELV/1000.0
      DT1=T1/EO
      DEN=DT1*(V/VO)*(V/VO)+1
      PI=(A+B/DEN)*(T1/(V/1000.0))+Q
      ENDIF

C
      C2P=0.0
      C3P=0.0
      IF (ROPT.EQ.2) THEN
      DELV=DELV/2.0
      C2P=P*(DELV/1000.0)*(V/1000.0)*(V/1000.0)*(1.0+A*(2.0*DELV/V))
      C3P1=(1.0+A)*E*(V/1000.0)*(V/1000.0)
      $      +(1.0+B)*EO*(VO/1000.0)*(VO/1000.0)
      $      +Q*(V/1000.0)*(V/1000.0)*(V/1000.0)
      C3P=P*(DELV/1000.0)*C3P1
      $      -(P*(DELV/1000.0))*(P*(DELV/1000.0))*(V/1000.0)*(V/1000.0)
      ENDIF

C
      IF (ROPT.EQ.2.OR.ROPT.EQ.3) THEN
      C1=(V/1000.0)*(DELV/1000.0)*(1.0+A*(DELV/V))
      C2=C1*R/((V/1000.0)*(DELV/1000.0)+(DELV/V)*RP
      $      +Q*(V/1000.0)*(V/1000.0)*(DELV/1000.0)-C2P
      C3=(A*E+Q*(V/1000.0))*R+B*E*EO*(VO/1000.0)*(VO/1000.0)-C3P
      DISC=C2*C2-4.0*C1*C3
      PI1=(C2+DSQRT(DISC))/(2.0*(V/1000.0)*C1)
      PI2=(C2-DSQRT(DISC))/(2.0*(V/1000.0)*C1)
      PI=PI2
      ENDIF

C
      IF (ROPT.EQ.2) DELV=2.0*DELV

C
      RETURN
      END

C      SUBROUTINE TINC(SHS,SHL,TM,TV,HF,HV,EXH,IME,IVE,PS,PL,PV,TR)
      IMPLICIT DOUBLE PRECISION (A-H,O-Z)
      DOUBLE PRECISION IME,IVE

C
C..... THIS SUBROUTINE CALCULATES THE RESIDUAL TEMPERATURE INCREASE
C..... IN A MATERIAL THAT HAS BEEN RELEASED FROM THE SHOCKED STATE
C..... AND ESTIMATES THE PERCENTAGES OF VAPORIZED, MELTED, AND SOLID

```

```

C..... MATERIAL DUE TO THE RELEASE PROCESS.
C
C..... IF WASTE HEAT IS LESS THAN THE ENERGY REQ'D TO START MELT,
C..... CALCULATE TEMPERATURE RISE USING  $W.H.=S.H.*(TEMP.INCR.)$ 
C
      IF (EXH.LT.IME) THEN
      DT=EXH/SHS
      TR=DT
      DEL=0.0
      WRITE(2,50) IME,DEL,EXH
50 FORMAT('ENERGY REQ, INCIPIENT MELT ... ',E10.4,' JOULES/KG',/,
  '$ENERGY AVAILABLE FOR MELT .... ',E10.4,' JOULES/KG',/,
  '$EXCESS ENERGY AVAILABLE ..... ',E10.4,' JOULES/KG')
      PV=0.0
      PL=0.0
      PS=100.0
      GOTO 100
      ENDIF
C
C..... IF WASTE HEAT EXCEEDS THE ENERGY REQ'D TO START MELT, BUT IS
C..... LESS THAN THAT REQ'D TO COMPLETE MELT, RESET THE VALUE OF THE
C..... ENERGY AVAILA&LE FROM THE WASTE HEAT VALUE TO THE VALUE REQ'D
C..... TO START MELT. THIS IMPLIES THAT SOME ENERGY IS AVAILABLE FOR
C..... MELTING A PORTION OF THE MATERIAL. NOTE: THE TEMPERATURE RISE
C..... EQUALS THE MELT TEMPERATURE OF THE MATERIAL.
C
      IF (EXH.GE.IME.AND.EXH.LT.IME+HF) THEN
      TR=TM
      DEL=EXH-IME
      REQM=IME+HF
      WRITE(2,60) IME,REQM,DEL
60 FORMAT('ENERGY REQ, INCIPIENT MELT ... ',E10.4,' JOULES/KG',/,
  '$ENERGY REQ, COMPLETE MELT .... ',E10.4,' JOULES/KG',/,
  '$ENERGY AVAILABLE FOR MELT .... ',E10.4,' JOULES/KG')
      PV=0.0
      PL=100.0*DEL/HF
      PS=100.0-PL
      GOTO 100
      ENDIF
C
C..... IF THE WASTE HEAT EXCEEDS THE ENERGY REQ'D TO COMPLETELY MELT
C..... THE MATERIAL, BUT IS LESS THAN THAT REQ'D TO START VAPORIZA-
C..... TION, COMPUTE THE TEMPERATURE INCREASE CAUSED BY THE EXCESS
C..... ENERGY AND ADD IT TO THE MELT TEMPERATURE OF THE MATERIAL.
C
      IF (EXH.GE.IME+HF.AND.EXH.LT.IVE) THEN
      DEL=EXH-IME-HF
      DT=DEL/SHL
      TR=TM+DT
      REQM=IME+HF
      WRITE(2,70) IME,REQM,DEL
70 FORMAT('ENERGY REQ, INCIPIENT MELT ... ',E10.4,' JOULES/KG',/,
  '$ENERGY REQ, COMPLETE MELT .... ',E10.4,' JOULES/KG',/,

```

```

      $'EXCESS ENERGY AVAILABLE ..... ',E10.4,' JOULES/KG')
      PV=0.0
      PL=100.0
      PS=0.0
      GOTO 100
      ENDIF

C
C..... IF WASTE HEAT EXCEEDS THE ENERGY REQ'D TO START VAPORIZATION,
C..... BUT IS LESS THAN THAT REQ'D TO COMPLETE VAPORIZATION, RESET THE
C..... VALUE OF THE ENERGY AVAILABLE FROM THE WASTE HEAT VALUE TO THE
C..... VALUE REQ'D TO START VAPORIZATION. THIS IMPLIES THAT SOME
C..... ENERGY IS AVAILABLE FOR VAPORIZING A PORTION OF THE MATERIAL.
C..... NOTE: THE TEMPERATURE RISE EQUALS THE VAPORIZATION TEMPERATURE
C..... OF THE MATERIAL.
C
      IF (EXH.GE.IVE.AND.EXH.LT.IVE+HV) THEN
      DEL=EXH-IVE
      REQV=IVE+HV
      TR=TV
      WRITE(2,80) IVE,REQV,DEL
80  FORMAT('ENERGY REQ, INCIPIENT VAP .... ',E10.4,' JOULES/KG',/,
      $'ENERGY REQ, COMPLETE VAP ..... ',E10.4,' JOULES/KG',/,
      $'ENERGY AVAILABLE FOR VAP ..... ',E10.4,' JOULES/KG')
      PV=100.0*DEL/HV
      PL=100.0-PV
      PS=0.0
      GOTO 100
      ENDIF

C
      IF (EXH.GE.IVE+HV) THEN
      ECVAP=IVE+HV
      PV=100.0
      PL=0.0
      PS=0.0
      WRITE (2,90) ECVAP
90  FORMAT('ENERGY REQ, COMPLETE VAP ..... ',E10.4,' JOULES/KG',/,
      $'*** THE MATERIAL IS COMPLETELY VAPORIZED ***')
      GOTO 120
      ENDIF

C
100 WRITE(2,110) TR,PS,PL,PV
110 FORMAT('RESIDUAL MATERIAL TEMP ..... ',F10.3,' DEG-C',//,'PERCENT
      $T OF SHOCKED AND RELEASED MATERIAL ... ',/3X,' IN SOLID STATE ... '
      $,F6.2,'% ',/3X,' IN MOLTEN FORM ... ',F6.2,'% ',/3X,' IN VAPOR FORM
      $..... ',F6.2,'%')

C
120 RETURN
      END

C
      SUBROUTINE TMCALC(V, PS, PL, PV, RP, RT, TR, TM, TV, TS, LP, DP, BHN, TSOL,
      $ ML, MV, MTARG)
      IMPLICIT DOUBLE PRECISION (A-H,O-Z)
      DOUBLE PRECISION LP, L22, MTARG, MS, ML, MV, MUSM, MSR

```

```

C
C..... THIS SUBROUTINE CALCULATES THE MASSES OF SOLID, LIQUID, AND
C..... GASEOUS TARGET MATERIAL IN THE DEBRIS CLOUD..
C
C..... READ CONFIGURATION-SPECIFIC GEOMETRIC PARAMTERS.
C.....
C.....          LP ... PROJECTILE LENGTH, IN
C.....          DP ... PROJECTILE DIAMETER, IN
C.....          TS ... TARGET PLATE THICKNESS, IN
C
      READ (4,10) LP,DP,TS
10 FORMAT(3F10.5)
C
      LP=LP*2.54
      DP=DP*2.54
      TS=TS*2.54
      L22=0.72*DP
      PI=4.0*ATAN(1.0)
      CALL DHOLE(TS,DP,RP,RT,LP,V,BHN,DH)
      MTARG=PI*(DH/2.0)*(DH/2.0)*TS*RT
      R=L22/TS
      IF (R.GE.1.0) FSR=1.0
      IF (R.LT.1.0) FSR=R
      MSR=FSR*MTARG
      MUSM=MTARG-MSR
      MS=(PS/100.0)*MSR
      ML=(PL/100.0)*MSR
      MV=(PV/100.0)*MSR
      TSOL=MUSM+MS
      TNS=MTARG-TSOL
C
      WRITE (2,20) DP,TS,DH,MTARG,MUSM,MSR,MS,ML,MV,TSOL,TNS
20 FORMAT(/,'PROJECTILE DIAMETER .... ',F8.4,' CM',/, 'TARG PLATE THIC
      $KNNESS ... ',F8.4,' CM',/, 'TARG PLATE HOLE DIA .... ',F8.4,' CM',//
      $,'MASS OF REMOVED TARG MATL ..... ',F8.4,' GMS',/, 'MASS OF UNSH T
      $TARGET MATL ..... ',F8.4,' GMS',/, 'MASS OF SH AND REL TARG MATL .
      $.. ',F8.4,' GMS',/, 3X,'MASS OF S&R SOLID MATL ..... ',F8.4,' GMS'
      $,/, 3X,'MASS OF S&R LIQUID MATL ..... ',F8.4,' GMS',/, 3X,'MASS OF S
      $&R VAPOR MATL ..... ',F8.4,' GMS',/, 'TOTAL SOLID MASS COMPONENT .
      $.... ',F8.4,' GMS',/, 'TOTAL NON-SOLID COMPONENT ..... ',F8.4,
      $' GMS')
C
C..... WRITE TARGET MASS CALCULATION RESULTS TO A FILE THAT WILL BE
C..... READ BY A FRAGMENTATION PROGRAM.
C
      WRITE (5,30) MUSM,MS,ML,MV
30 FORMAT(4F10.5)
C
      RETURN
      END
C
      SUBROUTINE DHOLE(TS,DP,RP,RT,LP,V,BHN,DH)
      IMPLICIT DOUBLE PRECISION (A-H,O-Z)

```

DOUBLE PRECISION K,LP

C
C..... THIS SUBROUTINE CALCULATES THE HOLE IN A THIN PLATE DUE TO
C..... THE NORMAL IMPACT OF A SOLID RIGHT CIRCULAR CYLINDER USING
C..... KAPPII EQUATIONS (AFATL-TR-90-02).

C
A=
B=
C= see AFATL-TR-90-02
E=
F=
G=
K=F*((BHN/RT)**G)

C
R1=RP/RT
R2=(3.0*LP)/(2.0*DP)
R3=(RP*V*V)/(2.0*E*BHN)
DR=A*(R1**B)*(R2**C)*(R3**0.3333333333)
R4=(TS/DP)**0.6666666666
DHDP=1.0+(DR-1.0)*(1.0-DEXP(-K*R4))
DH=DP*DHDP

C
RETURN
END

C
SUBROUTINE PMCALC(UPS,UTS,UPP,UTP,RP,PS,PL,PV,TS,LP,DP,TSOL,
ML,MV,MPROJ)
\$ IMPLICIT DOUBLE PRECISION (A-H,O-Z)
DOUBLE PRECISION LP,L41,L11,LO,MPROJ,MS,ML,MV,MSR,MUSM

C
C..... THIS SUBROUTINE CALCULATES THE MASSES OF SOLID, LIQUID, AND
C..... GASEOUS PROJECTILE MATERIAL IN THE DEBRIS CLOUD.

C
PI=4.0*ATAN(1.0)
MPROJ=PI*(DP/2.0)*(DP/2.0)*LP*RP

C
L11=0.72*DP
T11=L11/UTS

C
CST=CS(UTS,UTP)
CSP=CS(UPS,UPP)
T1N=CST+UTS-UTP
T1D=CSP-UPS+UPP
T1=T1N/T1D
T2=CSP/CST
T3=UPS/UTS
L41=TS*T1*T2*T3
T41=L41/UPS

C
IF (T11.LT.T41) LO=L11
IF (T11.EQ.T41) THEN
IF (L11.LT.L41) LO=L11
IF (L11.GE.L41) LO=L41

```

ENDIF
IF (P11.GT.T41) LO=L41
IF (LO.LT.LP) FSR=LO/LP
IF (LO.GE.LP) FSR=1.0
MSR=FSR*MPROJ
MUSM=MPROJ-MSR
MS=(PS/100.0)*MSR
ML=(PL/100.0)*MSR
MV=(PV/100.0)*MSR
TSOL=MUSM+MS
TNS=MPROJ-TSOL
C
WRITE (2,100) CST,CSP,LP,DP,MPROJ
100 FORMAT(/,'SHOCKED TARG MATL CO ... ',F8.4,' KM/S',/,',SHOCKED PROJ
$MATL CO ... ',F8.4,' KM/S',/,',PROJECTILE LENGTH ..... ',F8.4,
$' CM',/,',PROJECTILE DIAMETER .... ',F8.4,' CM',/,',PROJECTILE MASS
$. .... ',F8.4,' GMS')
C
WRITE (2,200) MUSM,MSR,MS,ML,MV,TSOL,TNS
200 FORMAT(/,'MASS OF UNSH PROJ MATERIAL ..... ',F8.4,' GMS',/,',MASS O
$F SH AND REL PROJ MATL ... ',F8.4,' GMS',/,3X,'MASS OF S&R SOLID M
$ATL ..... ',F8.4,' GMS',/,3X,'MASS OF S&R LIQUID MATL ..... ',
$F8.4,' GMS',/,3X,'MASS OF S&R VAPOR MATL ..... ',F8.4,' GMS',/,
$'TOTAL SOLID MASS COMPONENT ..... ',F8.4,' GMS',/,',TOTAL NON-SOLID
$ COMPONENT ..... ',F8.4,' GMS')
C
C..... WRITE PROJECTILE MASS CALCULATION RESULTS TO A FILE THAT WILL BE
C..... READ BY A FRAGMENTATION MODEL ASSESSMENT PROGRAM.
C
WRITE (5,30) MUSM,MS,ML,MV
30 FORMAT(4F10.5)
C
RETURN
END
C
DOUBLE PRECISION FUNCTION CS(US,UP)
IMPLICIT DOUBLE PRECISION (A-H,O-Z)
C
C..... THIS FUNCTION CALCULATES THE SPEED OF A RAREFACTION WAVE IN A
C..... SHOCKED MEDIUM
C
T1=(US-UP)/US
CSQ=US*US*(0.49+T1*T1)
CS=DSQRT(CSQ)
RETURN
END

```

APPENDIX B -- Sample Input Files

1) Input File INDATA:

```

-----
--MAT'L-- | ---CO--- | ---K--- | ---RHO--- | --GAMO-- | ---BHN---
--EL.MOD-- | ---NU--- | --ALFA-- | ---CPS--- | ---GPL--- | ---EPS---
--T.MELT-- | --T.VAP-- | --H.FUS-- | --H.VAP-- | --ALFA--- | --BETA---
--ROPT---
-----

```

```

AL
ALUMINUM      5.380      1.340      2.712      2.130      120.0
 0.103E+08    0.35 0.240E-04    0.235      0.255      0.005
   660.0     2450.0      95.0     2450.0      5.0      5.0

```

2

```

A1
2XXX ALUM     5.350      1.340      2.800      2.000      120.0
 0.106E+08    0.33 0.209E-04    0.212      0.242      0.005
   640.0     2450.0      85.0     2450.0      5.0      5.0

```

2

```

A2
5XXX ALUM     5.310      1.340      2.670      2.000      84.0
 0.101E+08    0.33 0.225E-04    0.215      0.245      0.005
   641.0     2450.0      85.0     2450.0      5.0      5.0

```

2

```

A3
6XXX ALUM     5.380      1.340      2.700      2.000      93.0
 0.100E+08    0.33 0.233E-04    0.212      0.242      0.005
   652.0     2450.0      85.0     2450.0      5.0      5.0

```

2

```

A4
7XXX ALUM     5.290      1.340      2.810      2.000      150.0
 0.103E+08    0.33 0.221E-04    0.217      0.245      0.005
   636.0     2450.0      85.0     2450.0      5.0      5.0

```

2

```

BE
BERYLLIUM    7.975      1.124      1.820      1.160      120.0
 0.419E+08    0.08 0.140E-04    0.570      0.832      0.005
  1281.0     2884.0      260.0     8195.0      5.0      5.0

```

2

```

CD
CADMIUM      2.307      1.640      8.640      2.270      24.0
 0.672E+07    0.33 0.343E-04    0.058      0.063      0.005
   321.0     765.0      13.5     212.0      5.0      5.0

```

2

 CU
 COPPER 3.940 1.489 8.930 2.000 37.0
 0.190E+08 0.34 0.170E-04 0.097 0.114 0.005
 1083.0 2590.0 49.0 1150.0 5.0 5.0

2

 EP
 EPOXY 3.020 1.520 1.180 0.800 -1.0
 0.650E+06 0.50 0.500E-04 0.250 0.285 -1.0
 350.0 -1.0 -1.0 -1.0 -1.0 -1.0

2

 FE
 IRON 4.580 1.490 7.870 1.570 95.0
 0.290E+08 0.30 0.120E-04 0.120 0.150 0.005
 1539.0 3035.0 65.0 1591.0 5.0 5.0

2

 PB
 LEAD 2.030 1.470 11.340 2.770 7.0
 0.200E+07 0.45 0.293E-04 0.031 0.036 0.005
 327.0 1740.0 6.0 210.0 10.0 10.0

2

 LX
 LEXAN 2.750 1.480 1.180 0.860 37.0
 0.345E+06 0.50 0.650E-04 0.290 0.315 -1.0
 225.0 -1.0 -1.0 -1.0 -1.0 -1.0

2

 MO
 MOLYBDENUM 5.173 1.220 10.200 1.520 200.0
 0.460E+08 0.31 0.061E-04 0.079 0.104 0.005
 2610.0 5555.0 70.0 1242.0 5.0 5.0

2

 NI
 NICKEL 4.667 1.530 8.860 1.800 200.0
 0.330E+08 0.30 0.143E-04 0.130 0.157 0.005
 1454.0 2865.0 74.0 1523.0 5.0 5.0

2

 PT
 PLATINUM 3.680 1.500 21.370 2.940 70.0
 0.277E+08 0.39 0.110E-04 0.037 0.042 0.005
 1769.0 4349.0 26.0 632.0 10.0 10.0

2

S1
 304 STEEL 4.590 1.550 7.910 1.670 237.0
 0.284E+08 0.28 0.112E-04 0.110 0.125 0.005
 1425.0 3035.0 65.0 1590.0 5.0 5.0

2

S2
 430 STEEL 4.680 1.550 7.830 1.670 251.0
 0.299E+08 0.29 0.104E-04 0.110 0.125 0.005
 1470.0 3035.0 65.0 1590.0 5.0 5.0

2

S3
 4340 STEEL 4.570 1.550 7.830 1.670 290.0
 0.290E+08 0.30 0.112E-04 0.110 0.125 0.005
 1510.0 3070.0 65.0 1590.0 5.0 5.0

2

TA
 TANTALUM 3.374 1.201 16.650 1.690 200.0
 0.260E+08 0.35 0.065E-04 0.033 0.039 0.005
 2996.0 5425.0 38.0 1007.0 10.0 10.0

2

SN
 TIN 2.560 1.520 7.280 1.850 4.0
 0.603E+07 0.33 0.269E-04 0.058 0.062 0.005
 235.0 2450.0 14.0 580.0 10.0 10.0

2

TI
 TITANIUM 4.786 1.049 4.512 1.100 330.0
 0.180E+08 0.30 0.100E-04 0.150 0.167 0.005
 1676.0 3260.0 99.0 2182.0 5.0 5.0

2

W
 TUNGSTEN 4.150 1.237 19.170 1.480 400.0
 0.590E+08 0.30 0.040E-04 0.035 0.046 0.005
 3410.0 5900.0 53.0 1054.0 10.0 10.0

2

ZN
 ZINC 3.042 1.500 7.100 2.150 82.0
 0.108E+08 0.33 0.274E-04 0.100 0.115 0.005
 420.0 907.0 25.0 420.0 10.0 10.0

2

```

-----
AU
GOLD      3.060    1.570    19.240    3.100    33.0
 0.124E+08  0.42 0.161E-04  0.034    0.038    0.005
   1063.0   2960.0    16.0    413.0    10.0    10.0

```

2

```

-----
AG
SILVER    3.230    2.500    10.490    2.500    25.0
 0.120E+08  0.37 0.211E-04  0.062    0.071    0.005
   961.0    2210.0    25.0    554.0    10.0    10.0

```

2

```

-----
MG
MAGNESIUM 4.490    1.240    1.740    1.500    45.0
 0.640E+07  0.29 0.300E-04  0.295    0.336    0.005
   650.0    1110.0    88.0    1326.0    5.0    5.0

```

2

XX

2) Input File GPARAM:

2.0 1.0 0.5

APPENDIX C -- Sample Output File

HYPERVELOCITY IMPACT OF A COPPER PROJECTILE ON A ALUMINUM TARGET.

IMPACT VELOCITY ... V = 8.00 KM/S

PROJECTILE PROPERTIES ...

MAT = COPPER
CO = 3.940 KM/S (INPT)
CO = 3.909 KM/S (CALC)
K = 1.489
RHO = 8.930 GM/CU.CM.

TARGET PROPERTIES ...

MAT = ALUMINUM
CO = 5.380 KM/S (INPT)
CO = 5.394 KM/S (CALC)
K = 1.340
RHO = 2.712 GM/CU.CM.

***** TARGET MATERIAL RELEASE CALCULATION *****

TARGET PARTICLE VELOCITY ... UP = 5.379 KM/S
TARGET SHOCK WAVE SPEED US = 12.587 KM/S
HUGONIOT IMPACT PRESSURE ... PH = 183.607 GPA

PARAMETERS REQUIRED FOR CALCULATING TARGET MATERIAL RELEASE FROM SHOCKED STATE USING THE TILLOTSON EQUATION OF STATE:

TARG MATL ELASTIC MODULUS E = .7102E+11 N/SQ.M.
TARG MATL POISSON RATIO NU = .350
TARG MATL BULK MODULUS K = .7891E+11 N/SQ.M.
TARG MATL LIN. COEF. OF THERM. EXP. ... ALFA = .2400E-04 /DEG-C
TARG MATL SP HEAT (SOLID) CPS = .235 CAL/GM/DEG-C
TARG MATL SP HEAT (LIQUID) CPL = .255 CAL/GM/DEG-C
TARG MATL HUGON IMP PRESS (PA,MBAR) ... PH = .1836E+12, 1.813
TARG MATL HUGON IMPACT ENERGY EH = .1446E+08 JOULES/KG
TARG MATL SP VOL AT REST VO = .369 CU.CM./GM
TARG MATL SP VOL AT IMPACT V1 = .211 CU.CM./GM
TARG MATL AMB M-GRUN COEF (CAL,INP) ... GAMO = 2.129, 2.130
TARG MATL MELT TEMPERATURE TM = 660.00 DEG-C
TARG MATL VAPOR TEMPERATURE TV = 2450.00 DEG-C
TARG MATL HEAT OF FUSION HF = 95.00 CAL/GM
TARG MATL HEAT OF VAPORIZATION HV = 2450.00 CAL/GM
TARG MATL INICIPIENT MELT ENERGY IME = .6492E+06 JOULES/KG
TARG MATL INICIPIENT VAPOR ENERGY IVE = .2958E+07 JOULES/KG

ADDITIONAL PARAMETERS REQUIRED FOR CALCULATING MATERIAL RELEASE FROM SHOCKED STATE USING THE TILLOTSON EQUATION OF STATE:

AA = .7850E+11 N/SQ.M.
BB = .4831E+11 N/SQ.M.
A = .5000
B = 1.6292
ALF = 5.0000
BET = 5.0000
EOI = .6687E+07 JOULES/KG
EOM = 1.0000

EO - .6687E+07 JOULES/KG
 ES - .2958E+07 JOULES/KG
 HV - .1026E+08 JOULES/KG
 ESP - .1321E+08 JOULES/KG
 VS - .4170 CU.CM./GM
 EPS - .0050

END-STATE CALCULATION RESULTS USING THE TILLOTSON EOS ...

MATERIAL FIN SP VOL (VF)545 CU.CM./GM
 MATERIAL ENERGY AT IMPACT1446E+08 JOULES/KG
 MATERIAL ENERGY RECOVERED1155E+08 JOULES/KG
 WASTE HEAT GENERATED2917E+07 JOULES/KG
 ENERGY REQ, INCIPIENT MELT6492E+06 JOULES/KG
 ENERGY REQ, COMPLETE MELT1047E+07 JOULES/KG
 FXCESS ENERGY AVAILABLE1870E+07 JOULES/KG
 RESIDUAL MATERIAL TEMP 2412.285 DEG-C

PERCENT OF SHOCKED AND RELEASED MATERIAL ...

IN SOLID STATE00%
 IN MOLTEN FORM ... 100.00%
 IN VAPOR FORM00%

FREE SURF VEL (UP+UR) 11.631 KM/SEC
 FREE SURF VEL (2.0*UP) 10.757 KM/SEC

PROJECTILE DIAMETER 2.5400 CM
 TARG PLATE THICKNESS ... 1.2700 CM
 TARG PLATE HOLE DIA 10.1950 CM

MASS OF REMOVED TARG MATL 281.1638 GMS
 MASS OF UNSH TARGET MATL0000 GMS
 MASS OF SH AND REL TARG MATL ... 281.1638 GMS
 MASS OF S&R SOLID MATL0000 GMS
 MASS OF S&R LIQUID MATL 281.1638 GMS
 MASS OF S&R VAPOR MATL0000 GMS
 TOTAL SOLID MASS COMPONENT0000 GMS
 TOTAL NON-SOLID COMPONENT 281.1638 GMS

***** PROJECTILE MATERIAL RELEASE CALCULATION *****

PROJECTILE PARTICLE VELOCITY ... UP = 2.621 KM/S
 PROJECTILE SHOCK WAVE SPEED US = 7.843 KM/S
 HUGONIOT IMPACT PPESSURE PH = 183.607 GPA

PARAMETERS REQUIRED FOR CALCULATING PROJECTILE MATERIAL RELEASE FROM SHOCKED STATE USING THE TILLOTSON EQUATION OF STATE:

PROJ MATL ELASTIC MODULUS E = .1310E+12 N/SQ.M.
 PROJ MATL POISSON RATIO NU = .340
 PROJ MATL BULK MODULUS K = .1365E+12 N/SQ.M.
 PROJ MATL LIN. COEF. OF THERM. EXP. ... ALFA = .1700E-04 /DEG-C
 PROJ MATL SP HEAT (SOLID) CPS = .097 CAL/GM/DEG-C
 PROJ MATL SP HEAT (LIQUID) CPL = .114 CAL/GM/DEG-C
 PROJ MATL HUGON IMP PRESS (PA,MBAR) ... PH = .1836E+12, 1.813

PROJ MATL HUGON IMPACT ENERGY EH = .3436E+07 JOULES/KG
 PROJ MATL SP VOL AT REST VO = .112 CU.CM./GM
 PROJ MATL SP VOL AT IMPACT V1 = .075 CU.CM./GM
 PROJ MATL AMB M-GRUN COEF (CAL,INP) ... GAMO = 1.919, 2.000
 PROJ MATL MELT TEMPERATURE TM = 1083.00 DEG-C
 PROJ MATL VAPOR TEMPERATURE TV = 2590.00 DEG-C
 PROJ MATL HEAT OF FUSION HF = 49.00 CAL/GM
 PROJ MATL HEAT OF VAPORIZATION HV = 1150.00 CAL/GM
 PROJ MATL INICIPIENT MELT ENERGY IME = .4397E+06 JOULES/KG
 PROJ MATL INICIPIENT VAPOR ENERGY IVE = .1364E+07 JOULES/KG

ADDITIONAL PARAMETERS REQUIRED FOR CALCULATING MATERIAL RELEASE FROM SHOCKED STATE USING THE TILLOTSON EQUATION OF STATE:

AA = .1386E+12 N/SQ.M.
 BB = .1412E+12 N/SQ.M.
 A = .5000
 B = 1.4190
 ALF = 5.0000
 BET = 5.0000
 EOI = .7097E+07 JOULES/KG
 EOM = 1.0000
 EO = .7097E+07 JOULES/KG
 ES = .1364E+07 JOULES/KG
 HV = .4814E+07 JOULES/KG
 ESP = .6178E+07 JOULES/KG
 VS = .1267 CU.CM./GM
 EPS = .0050

END-STATE CALCULATION RESULTS USING THE TILLOTSON EOS ...

MATERIAL FIN SP VOL (VF)122 CU.CM./GM
 MATERIAL ENERGY AT IMPACT3436E+07 JOULES/KG
 MATERIAL ENERGY RECOVERED2722E+07 JOULES/KG
 WASTE HEAT GENERATED7139E+06 JOULES/KG
 ENERGY REQ, INCIPIENT MELT4397E+06 JOULES/KG
 ENERGY REQ, COMPLETE MELT6449E+06 JOULES/KG
 EXCESS ENERGY AVAILABLE6900E+05 JOULES/KG
 RESIDUAL MATERIAL TEMP 1227.600 DEG-C

PERCENT OF SHOCKED AND RELEASED MATERIAL ...

IN SOLID STATE00%
 IN MOLTEN FORM ... 100.00%
 IN VAPOR FORM00%

SHOCKED TARG MATL CO ... 11.3842 KM/S
 SHOCKED PROJ MATL CO ... 7.5770 KM/S
 PROJECTILE LENGTH 5.0800 CM
 PROJECTILE DIAMETER 2.5400 CM
 PROJECTILE MASS 229.8648 GMS

MASS OF UNSH PROJ MATERIAL 147.1135 GMS
 MASS OF SH AND REL PROJ MATL ... 82.7513 GMS
 MASS OF S&R SOLID MATL0000 GMS
 MASS OF S&R LIQUID MATL 82.7513 GMS

MASS OF S&R VAPOR MATL0000 GMS
TOTAL SOLID MASS COMPONENT 147.1135 GMS
TOTAL NON-SOLID COMPONENT 82.7513 GMS

FREE SURF VEL (UP+UR) 5.423 KM/SEC
FREE SURF VEL (2.0*UP) 5.243 KM/SEC

MASS DISTRIBUTION SUMMARY ...
PROJECTILE ... SOLID 147.11 GMS
 LIQUID ... 82.75 GMS
 VAPOR00 GMS
TARGET SOLID00 GMS
 LIQUID ... 281.16 GMS
 VAPOR00 GMS

DEBRIS CLOUD VELOCITY SUMMARY ...
REAR SURF VEL (VR) 2.577 KM/SEC
CENTER-OF-MASS VEL (VI) 3.598 KM/SEC
LEADING EDGE VEL (VL) 11.631 KM/SEC

DISTRIBUTION
(WL-TR-93-7028)

Defense Technical Information Center
Attn: DTIC-DDAC
Cameron Station
Alexandria VA 22304-6145
1

WL/MNOI (STINFO Facility)
203 W. Eglin Blvd., Ste 300
Eglin AFB FL 32542-6843
1

WL/MNSA (David M. Jerome)
101 W. Eglin Blvd., Ste 326
Eglin AFB FL 32542-6810
4